Title

Maximizing Power Output in Homogeneous Charge Compression Ignition (HCCI) Engines and Enabling Effective Control of Combustion Timing

Author

Saxena, Samveg

Publication Date

2011

Peer reviewed|Thesis/dissertation

Maximizing Power Output in Homogeneous Charge Compression Ignition (HCCI) Engines and Enabling Effective Control of Combustion Timing

By

Samveg Saxena

A dissertation submitted in partial satisfaction of the

requirements for the degree of

Doctor of Philosophy

in

Engineering – Mechanical Engineering

in the

Graduate Division

of the

University of California, Berkeley

Committee in charge:

Professor Robert W. Dibble, Chair
Professor Jyh-Yuan Chen
Professor Stephen Derenzo

Fall 2011

Abstract

Maximizing Power Output in Homogeneous Charge Compression Ignition (HCCI) Engines and Enabling Effective Control of Combustion Timing

by

Samveg Saxena

Doctor of Philosophy in Engineering – Mechanical Engineering

University of California, Berkeley

Professor Robert Dibble, Chair

Homogeneous Charge Compression Ignition (HCCI) engines are one of the most promising engine technologies for the future of energy conversion from clean, efficient combustion. HCCI engines allow high efficiency and lower CO_2 emission through the use of high compression ratios and the removal of intake throttle valves (like Diesel), and allow very low levels of urban pollutants like nitric oxide and soot (like Otto). These engines, however, are not without their challenges, such as low power density compared with other engine technologies, and a difficulty in controlling combustion timing.

This dissertation first addresses the power output limits. The particular strategies for enabling high power output investigated in this dissertation focus on avoiding five critical limits that either damage an engine, drastically reduce efficiency, or drastically increase emissions: 1) ringing limits, 2) peak in-cylinder pressure limits, 3) misfire limits, 4) low intake temperature limits, and 5) excessive emissions limits. The research shows that the key factors that enable high power output, sufficient for passenger vehicles, while simultaneously avoiding the five limits defined above are the use of: 1) high intake air pressures allowing improved power output, 2) highly delayed combustion timing to avoid ringing limits, and 3) using the highest possible equivalence ratio before encountering ringing limits. These results are revealed by conducting extensive experiments spanning a wide range of operating conditions on a multi-cylinder HCCI engine.

Second, this dissertation discusses strategies for effectively sensing combustion characteristics on a HCCI engine. For effective feedback control of HCCI combustion timing, a sensor is required to quantify when combustion occurs. Many laboratory engines use in-cylinder pressure sensors but these sensors are currently prohibitively expensive for wide-scale commercialization. Instead, ion sensors made from inexpensive sparkplugs are proposed for sensing combustion

timing. Ion sensing, however, is unreliable under certain HCCI conditions. The dissertation presents two strategies for improving the usefulness of ion sensors in HCCI engines: 1) the use of tiny fractions of metal-acetate fuel additives that expand the useful range of ion sensors, and 2) the use of ion sensors for detecting excessive ringing that must be avoided in HCCI engines. These two innovative research efforts make ion sensors viable for sensing combustion characteristics across the full range of HCCI operation, making them effective for use in engine control systems.

In summary, this Ph.D dissertation addresses two important technical challenges facing HCCI engines: power output limits, and difficulty in sensing combustion characteristics for control applications. The strategies proposed in this dissertation research bring HCCI engines closer to widespread commercialization allowing vehicles to operate with significantly higher efficiency and with cleaner emissions.

This dissertation is dedicated to my family, friends, colleagues

and mentors who have all provided tremendous support and advice.

Contents

Acknowledgements

I first acknowledge and thank my family for their tremendous support, love and encouragement throughout the years. Their hard work and guidance has been a tremendous source of motivation.

I also thank my friends and colleagues here at Berkeley who have made life as a graduate student well balanced. I am humbled by the smart people that surround me here at Berkeley, and the well-roundedness and outdoorsy-ness of my friends and colleagues have helped to ensure that my experience as a graduate student was simultaneously stimulating and fun.

I sincerely thank my advisor, Professor Robert Dibble. His wonderful guidance in research and his intriguing stories not only provided insightful knowledge, but also provided laughter when desperately needed. I also thank Professor Jyh-Yuan Chen for his guidance related to the theoretical aspects of combustion and his help with numerical modeling of combustion systems. Further, I thank Professor Stephen Derenzo for his advice on this dissertation, and for teaching me about the fundamentals of data acquisition which was used in setting up the experiments in this dissertation.

I also sincerely thank the undergraduate students I have mentored, and the visiting scholars I have worked with throughout my Ph.D studies. In particular, I thank Professor Ivan Bedoya from the University of Antioquia. The research relationship with Ivan has been one of the most productive and educational collaborations that I have ever had.

I also greatly appreciate the support of the technical staff in Hesse Hall, Scott, Mike, Pete and Alex. Their technical support and advice has been invaluable in keeping our engines running safely. I also thank MaryAnne Peters for her help in ensuring that all of our lab contracts are managed, that all of us graduate students are paid, and that all of the trinkets we need to carry out our research are ordered. Our lab would quickly grind to a halt without MaryAnne’s support.

I owe a special thanks to the Government of Canada through the Natural Sciences and Engineering Research Council (NSERC). The financial support provided through the Canada Graduate Scholarship and Postgraduate Scholarship provided 4 years of support during the pursuit of my Ph.D.

And finally, on a slightly humorous note, I thank coffee for helping me pull through at those key times when I had to push hard towards a deadline on little sleep.

Samveg Saxena

Tel: (510) 269-7260

UC Berkeley – Dissertation on improving HCCI power output e-mail: samveg@berkeley.edu

Education

PostDoctoral Research **Lawrence Berkeley National Laboratory**, beginning Jan. 2012
Environmental Energy Technologies Division, Exergy analysis of energy efficiency technologies

Ph.D **University of California at Berkeley**, Mechanical Engineering, Fall 2011
Dissertation title: Maximizing power output in homogeneous charge compression ignition (HCCI) engines and enabling effective control of combustion timing, Advisor: Prof. Robert Dibble

M.Sc. **University of California at Berkeley**, Mechanical Engineering, 2009

B.Eng **University of Ontario Institute of Technology,** Manufacturing Engineering, 2007

Accomplishments and Honors

NSERC PostGraduate Scholarship (Doctoral), 2009-2011
Award from the Natural Sciences and Engineering Research Council (NSERC) of Canada
Nationally-competitive award for distinguished students based on research potential

Anselmo John Macchi Graduate Fellowship (Doctoral), 2011
Institutional-level award at UC Berkeley recognizing academic and research excellence

NSERC Canada Graduate Scholarship (Masters), 2007-2009
Nationally-competitive award for distinguished students based on academic excellence & research potential

Outstanding Graduate Student Instructor Award (UC Berkeley), 2008
Berkeley's highest teaching honor for graduate students, recognizing overall effectiveness as an instructor, ability to promote critical thinking, ability to motivate students, and command of the subject area

Ontario Graduate Scholarship – Declined acceptance of award, 2007
Provincially-competitive award for distinguished students based on research potential

NSERC Industrial Undergraduate Student Research Award, 2006
Nationally-competitive award for distinguished students to conduct advanced research with industrial sponsors. Conducted R&D on new technologies for internal combustion engine lubrication systems

Millennium Excellence Award Recipient, 2005 - 2007
National award recognizing innovation, academic achievement, community involvement and leadership

Top 20 Under 20 Canada – Finalist, 2004
National awards program recognizing youth who demonstrate significant level of achievement, innovation and leadership and are under the age of 20.

Publications and conference presentations

Peer-reviewed publications:

1. **S. Saxena**, J-Y Chen, and R.W. Dibble, Increasing the signal-to-noise ratio of sparkplug ion sensors through addition of a potassium acetate fuel additive, Proceedings of the Combustion Institute, 33(2): 3081-3088, 2010, doi: 10.1016/j.proci.2010.07.046

2. **S. Saxena**, J-Y Chen, R.W. Dibble, Maximizing power output in an automotive scale multi-cylinder HCCI engine, SAE World Congress, SAE Paper 2011-01-0907, 2011, doi:10.4271/2011-01-0907

3. A. DeFilippo, **S. Saxena**, V.H. Rapp, Y. Ikeda, J-Y Chen, R.W. Dibble, Extending the lean flammability limit of gasoline using a microwave assisted sparkplug, SAE World Congress, SAE Paper 2011-01-0663, 2011, doi: 10.4271/2011-01-0663

4. I.D. Bedoya, **S. Saxena**, F.J. Cadavid, R.W. Dibble, M. Wissink, Experimental evaluation of strategies to increase the operation range of a biogas HCCI engine for power generation, Applied Energy, in Press, 2011
5. **S. Saxena**, J-Y Chen, R.W. Dibble, Characterization of HCCI ringing behavior using ion sensors, 2011 SAE Powertrains, Fuels and Lubricants meeting, SAE 2011-01-1777, 2011
6. I.D. Bedoya, **S. Saxena**, F.J. Cadavid, and R.W. Dibble, Exploring Strategies for Reducing High Inlet Temperature Requirements and Allowing Optimal Operating Conditions in a Biogas Fueled HCCI Engine for Power Generation, ASME IC Engine Conference, ICEF2011-60198, Accepted for publication in ASME Journal of Engineering for Gas Turbines and Power, 2011
7. I.D. Bedoya, **S. Saxena**, F.J. Cadavid, and R.W. Dibble, Numerical Analysis of the Effects of Biogas Composition in Combustion Parameters and Emissions in Biogas Fueled HCCI Engines for Power Generation, ASME IC Engine Conference, ICEF2011-60120, 2011
8. I.D. Bedoya, **S. Saxena**, F.J. Cadavid, R.W. Dibble, M. Wissink, Experimental study of biogas combustion characteristics and emissions in a HCCI engine for power generation, Energy Conversion and Management, 53(1): 154-162, 2011, doi: 10.1016/j.enconman.2011.08.016

Publications in review:

1. I.D. Bedoya, **S. Saxena**, S. Aceves, D. Flowers, F.J. Cadavid, and R.W. Dibble, A sequential chemical kinetics-CFD-chemical kinetics methodology to predict HCCI combustion and main emissions, for 2012 SAE World Congress, SAE Paper 12PFL-0840
2. **S. Saxena**, S. Schneider, and R.W. Dibble, Wet Ethanol in HCCI Engines with Exhaust Heat Recovery to Improve the Energy Balance of Ethanol Fuels, for Applied Energy Journal
3. V.H. Rapp, A. DeFilippo, **S. Saxena**, J-Y Chen, R.W. Dibble, A. Nishiyama, and Y. Ikeda, Extending lean operating limit of engines burning methane using a microwave-assisted sparkplug, for ASME Journal of Engineering for Gas Turbines and Power

Publications in Preparation:

1. **S. Saxena** and I.D. Bedoya, Physical Phenomena affecting Operating Limits for HCCI Engines & Strategies for Avoiding these Limits, invited submission in Progress in Energy & Combustion Science
2. **S. Saxena**, I.D. Bedoya, and R.W. Dibble, Pressure and Temperature Influence on the Equivalence Ratio Effects of Intermediate Temperature Heat Release in Gasoline-fueled HCCI engines
3. **S. Saxena**, J-Y Chen, and R.W. Dibble, Detailed Investigation of HCCI Heat Release Rates for Fuels with Acetate Additives
4. **S. Saxena**, D. Vuilleumier, C. Gotianun, and R.W. Dibble, Wet Ethanol Fueled HCCI Engines with Exhaust Heat Recovery for High Power Output, Low Ringing and Low NO_x

Invited Technical Talks:

1. HCCI Engines for Transportation & Power Generation in a Climate Constrained World
   a. Lawrence Berkeley National Laboratory, Berkeley, CA – Oct. 2011
   b. Argonne National Laboratory, Chicago, IL – Sept. 2011
   c. McMaster University, Hamilton, Canada – Jul. 2011
   d. University of Minnesota, Twin Cities, MN – Mar. 2011
   e. General Motors Research and Development, Detroit, MI – Jan. 2011

Conference Proceedings and Technical Talks:

1. S. Saxena, S. Schneider, M. Krieck, D. Vuilleumier, U. Maas, and R. Dibble, Investigation of wet ethanol combustion in a HCCI engine using an exhaust gas heat exchanger, Western States Section of the Combustion Institute, U.C. Riverside, Riverside, CA, Oct. 2011

2. S. Saxena, I.D. Bedoya, R.W. Dibble, and F.J. Cadavid, Exploring optimal operating conditions for stationary power generation from a biogas-fuelled HCCI engine, 2011 US National meeting of the Combustion Institute, Georgia Tech, Atlanta, GA, Mar. 2011
3. S. Saxena, M. Corvers, J-Y Chen, and R.W. Dibble, Detecting ringing in an HCCI engine using ion sensors, 2011 US National meeting of the Combustion Institute, Georgia Tech, Atlanta, GA, Mar. 2011
4. S. Saxena, I.D. Bedoya and R.W. Dibble, HCCI Progress at UC Berkeley with biogas and detecting ringing with ion sensors, Advanced Engine Combustion/HCCI Workgroup Meeting, Sandia National Laboratory, Livermore, CA, Feb, 2011
5. S. Saxena, A. DeFilippo, V.H. Rapp, R.W. Dibble, J-Y Chen, Y.Ikeda, Extending the Operating Regime of spark-ignited engines using a microwave assisted sparkplug (MWASP), Advanced Engine Combustion/HCCI Workgroup Meeting, USCAR, Southfield, MI, Sept. 2010
6. S. Saxena, V.H. Rapp, J-Y Chen, and R.W. Dibble, A Numerical Study of Ultra-high Efficiency Combustion of a Hydrogen-Oxygen-Argon Mixture in HCCI Engines, Combustion Institute Western States Section Meeting, Boulder, CO, Mar. 2010
7. S. Saxena, J-Y Chen, R.W. Dibble, Analysis of Experimental Boosted HCCI and New Results with Micro-wave spark plug ignition, Advanced Engine Combustion/HCCI Workgroup Meeting, Sandia National Laboratory, Livermore, CA, Feb. 2010
8. S. Saxena, J-Y Chen and R.W. Dibble, A Survey of Experimental HCCI Research at U.C. Berkeley, Australia National Combustion Symposium, Brisbane, Australia, Dec. 2009
9. S. Saxena, R.W. Dibble, Increasing signal-to-noise ratio of spark-plug ion sensors through addition of salt-based fuel additives, Combustion Institute Western States Section Meeting, Oct. 2009
10. S. Saxena, A. North, J-Y Chen, and R.W. Dibble, High Load, Boosted HCCI 4-cylinder operation; Enhanced ion signal by ppm additives; microwave assisted spark plugs, LTC University Consortium, Southfield, MI, Oct. 2009
11. S. Saxena, J.H. Mack, and R.W. Dibble, Increasing Indicated Mean Effective Pressure (IMEP) of HCCI Engines, Combustion Institute U.S. National Meeting, Ann Arbor, MI, May 2009
12. S. Saxena, J.H. Mack, N. Killingsworth, G. Bogin, R.W. Dibble and J-Y Chen, Boosted HCCI Operation of a Multi-Cylinder Engine: Experiments, Control and Modeling, Low Temperature Combustion (LTC) University Consortium Meeting, Sandia National Laboratory, Livermore, CA, Feb. 2009

Additional Research projects:

1. Effects of varied frequency of "skip-firing" upon a 3-way catalyst and tailpipe emissions – conducted at UC Berkeley Combustion Analysis Laboratory, with a startup corporate partner
2. Development of a passive two-stage vane pump for the oil pump of internal combustion engines – conducted at Magna Powertrain Engine Technologies Group
3. Development of a vortex generator to provide engine speed control of oil pumps in internal combustion engines – conducted at Magna Powertrain Engine Technologies Group

Professional Experience

Graduate Student Researcher, **UC Berkeley**, Combustion Analysis Laboratory, 2008-Present

Graduate Student Instructor, **UC Berkeley**, Department of Mechanical Engineering, 2007, 2008
Courses taught: Mechanical engineering laboratory for seniors, and thermodynamics class for juniors.
Recognized with UC Berkeley Outstanding Graduate Student Instructor Award.

Vehicle Systems Engineer, **Multimatic Technical Center**, Advanced Engineering Group, 2007
Responsible for design of a concept car, and prototyping of new automotive technology concepts

New Technology Engineer, **Magna Powertrain Engine Technologies Group**, 2006-2007
Responsible for calculations, design, testing and validation of new engine technology concepts

Editorial & Professional Development

1. Participant – 2011 Summer Institute for Preparing Future Faculty, UC Berkeley
2. Session Organizer – Kinetically Controlled CI (including HCCI), 2012 SAE World Congress
3. Session Organizer – Fuel and Additive Effects on CI Engines, 2012 SAE World Congress
4. Technical reviewer – 2011 ASME IC Engine Fall Technical Conference
5. Participant – 2011 Combustion Summer School, Princeton University
6. Technical reviewer – 2010 ASME IC Engine Fall Technical Conference
7. Technical reviewer – SAE Technical Conferences
8. Session moderator - 2010 Spring Meeting, Western States Section, Combustion Institute

Mentoring & Collaborative Research Experience

Visiting Scholars (Ph.D and PostDoctoral researchers):

1. D. Kozarac, University of Zagreb, Croatia, Study of biogas-fueled HCCI performance characteristics with negative valve overlap, 2011 (Fulbright Scholar)
2. I.D. Bedoya, University of Antioquia, Colombia, Study of biogas-fueled HCCI performance characteristics, 2010

Visiting Scholars (Masters):

1. M.S. Krieck, RWTH Aachen University, Germany, Study of wet ethanol, n-butanol and iso-butanol in HCCI engines, 2011
2. S. Schneider, Karlsruhe Institute of Technology, Germany, Study of wet ethanol in HCCI engines with exhaust heat recovery and elevated boost pressures, 2011
3. T. van Amstel, Eindhoven University of Technology, The Netherlands, Study of wet ethanol in HCCI engines with exhaust heat recovery and elevated boost pressure, 2011
4. M. Corvers, Eindhoven University of Technology, The Netherlands, Study of characterizing ringing in HCCI engines using ion sensors, 2010
5. J. Looijmans, Eindhoven Univeresity of Technology, The Netherlands, Study of improving Gasoline-fueled HCCI power output, 2008-2009

Undergraduate Students:

1. S. Lin, UC Berkeley, USA, Engine upgrades for HCCI engine studies, 2011
2. J. Tang, University of Queensland, Australia, Fuel injection upgrades for HCCI studies, 2011
3. D. Vuilleumier, UC Berkeley, USA, Study of wet ethanol in HCCI engines with exhaust heat recovery and elevated boost pressures, 2011
4. C. Gotianun, UC Berkeley, USA, Study of wet ethanol in HCCI engines with exhaust heat recovery and elevated boost pressures, 2011

Service Experience

Student Advocates for Graduate Education (SAGE), 2010-2011

Lobbied on Capitol Hill with staff-members of House Representatives and Senators as part of a team of student leaders from 10 top-tier public research Universities. Lobby issues focused on student indebtedness, taxation and immigration issues for International Graduate students

UC Berkeley Graduate Assembly & UC Berkeley Graduate Council, 2009-Present

Position: Graduate Council delegate (Elected)
Represented 10,000 Berkeley graduate students in issues affecting graduate academic affairs
Position: The Department of Mechanical Engineering delegate
Represented the Department in issues affecting graduate studies at U.C. Berkeley

International House Student Council, 2007-Present

Position: Chair, Vice-chair, Secretary, Communications Director
Elected from a student body of almost 600 students to improve quality of life at the UC Berkeley International House by advocating on issues affecting residents, organizing events, and overseeing allocation of approximately $22,000 budget per semester.
Position: Board of Directors Representative
Served as a student representative on a board of University, community, and business leaders which oversees the long-term plan of International House (including finances, endowments, admissions, etc.)

President and Founder of the DC-UOIT Solar Vehicle, 2003-2007

President & Founder of a team which will compete in the prestigious American Solar Challenge. Led a fundraising and community relations campaign that raised roughly $100,000.
Recognized in the Canadian House of Commons by a Member of Parliament for outstanding efforts in starting the team, shaping its vision, and bringing together local partners (March 24, 2005)

1 Introduction

The core motivation behind the research in this dissertation is the development of technologies that can lower the carbon dioxide emissions from transportation and power generation. The high efficiency aspect of homogeneous charge compression ignition (HCCI) engines makes them one attractive technology in achieving this goal. As a result, the key objective of this research is in addressing the challenges that prevent HCCI engines from becoming used more widely. With this goal in mind, two particular challenges of HCCI engines are addressed: 1) developing strategies to improve the power output from HCCI engines (Chapter 6 and 7), and 2) reducing the costs of using HCCI engines by developing low-cost ion sensors to detect combustion characteristics for controlling HCCI engines (chapter 8).

In the first objective, improving HCCI power output, experimental tests are conducted that explore a wide range of HCCI operating conditions. The experimental results are analyzed to understand the different limits on HCCI operation, how these limits intersect, and what conditions can lead to high power output, high efficiency and low emissions. Suggestions are made as to the best operating points for HCCI engines, and detailed operating characteristics are explored at the optimal operating points. Furthermore, the complications resulting from multi-cylinder operation at high power output conditions are discussed.

In the second objective, expanding the applicability of ion sensors for HCCI control, two topics are explored. The first is in extending the usefulness of ion sensors into low power output conditions by using fuel additives. The second is by developing a technique to use ion sensors instead of pressure sensors to characterize ringing (a phenomenon that must be avoided to prevent damage to HCCI engines).

Prior to discussing the results of this research, several chapters are dedicated to establishing the background necessary for understanding the results: chapter 2 introduces HCCI with its benefits, drawbacks and ideal applications and compares HCCI against spark-ignited and Diesel engines, chapter 3 explains the chemical reactions leading to autoignition in HCCI engines, chapter 4 provides an overview of prior research in HCCI engines, chapter 5 describes the experimental systems and data analysis techniques used in the research, and chapter 6 discusses the different limits that constrain HCCI operation.

2 Background

2.1 Introduction of HCCI

The discovery of HCCI is credited to Onishi et al. (1979) [1]. It is an alternative mode of operation for internal combustion engines that combines qualities of spark-ignited and Diesel engines. Similar with spark-ignited engines, HCCI premixes the fuel-in-air charge to create a homogeneous mixture. This is accomplished by either injecting the fuel in the intake manifold, or early in the intake stroke directly into the combustion chamber. Similar to Diesel engines, ignition in an HCCI engine occurs through high temperatures that are achieved by using a high compression ratio. As a result of combining the use of homogeneous fuel-in-air mixtures and compression ignition, the entire mixture ignites relatively uniformly resulting in rapid heat release [2]. The timing and duration of the autoignition event is controlled by chemical kinetics which predominantly depends on mixture temperature (discussed further in Chapter 3). As a result of the need for reducing the rapid rate of heat release, HCCI uses highly diluted mixtures, using either high concentrations of exhaust gas recirculation (EGR) or very lean equivalence ratios (between 0.2 to 0.55). The engine power output is controlled by varying the fuel-air equivalence ratio, and thus HCCI engines do not require intake throttling [3]. Given that the in-cylinder mixture is compression ignited and the mixture is typically too diluted for flame propagation to occur, sparkplugs are not typically used for ignition timing control.

2.2 Comparison of different engine types

A majority of automobile engines presently use four-stroke engines. Amongst these engines, two categories can be identified: spark-ignited (SI) and Diesel. The characteristics of these two styles of engines will be compared with HCCI in the following sections. Each of the four strokes in an engine is illustrated in Figure 2-1:

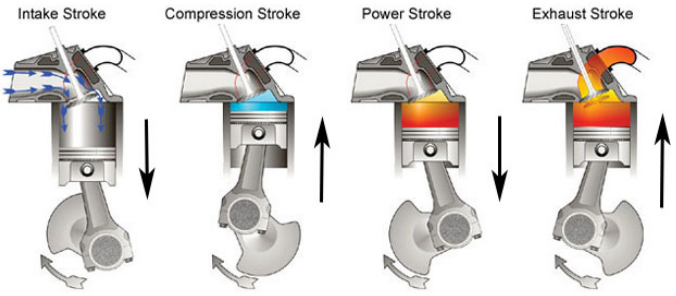

Figure 2-1 - Processes in a four-stroke engine
Source: [4]

Each of the four strokes illustrated in Figure 2-1 are explained here:

1. Intake stroke - the intake valve opens and the piston moves from top dead center (TDC) to bottom dead center (BDC) to inhale the fuel-in-air mixture.
2. Compression stroke - the intake valve closes and the piston moves up from BDC to TDC to compress the fuel-in-air mixture.

3. Power stroke – ignition of the fuel-in-air mixture causes high in-cylinder pressures forcing the piston to move from TDC to BDC producing useful work. This is often called the expansion stroke.
4. Exhaust stroke – The exhaust valve opens and the piston moves from BDC to TDC exhaling the burned gases from the combustion chamber.

One common tool for understanding the different operating and emissions characteristics of spark-ignited, Diesel and HCCI engines is by considering their operating ranges on a ϕ-temperature plot. Figure 2-2 shows such a plot and labels the regions for spark-ignited, Diesel and HCCI combustion, along with the different regions of soot and NO_x formation.

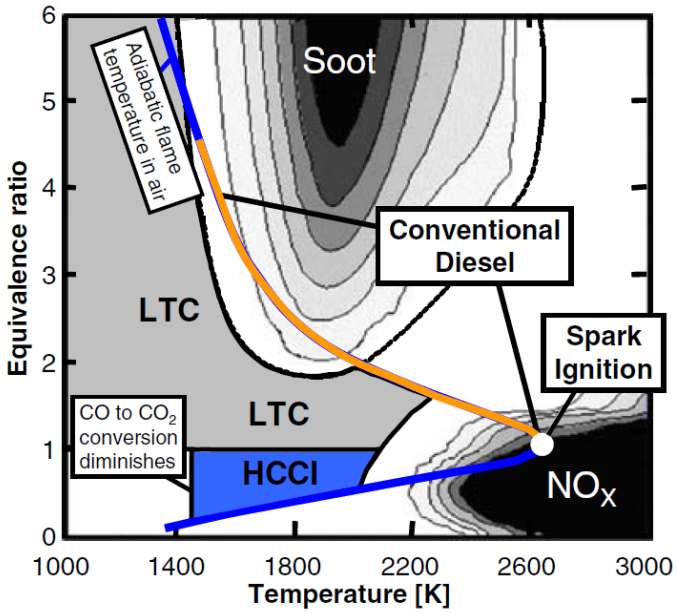

Figure 2-2 - ϕ-temperature graph showing the different regions for Diesel, spark-ignited and HCCI operation, and the different regions of soot and NO_x formation
Source: Dec, 2009 [5]

As shown in Figure 2-2, spark-ignited combustion occurs in a high temperature region near an equivalence ratio of 1, where high NO_x formation occurs. Diesel combustion begins at high equivalence ratios where soot formation occurs and transitions towards high temperature combustion where NO_x formation occurs. HCCI combustion occurs at leaner equivalence ratios and where sufficient charge dilution allows for lower temperatures; thus, HCCI avoids the regions of high soot and NO_x formation. In the next three sections, further details of each engine combustion technique will be discussed.

Sections 2.2.1 through 2.2.3 discuss the details of spark-ignited, Diesel and HCCI engines in depth, however a brief summary of the differences between these engine technologies is presented in Table 2-1:

	Spark-ignited	Diesel	HCCI
Fuel/air mixture type	Premixed	Non-premixed	Premixed
Ignition type	Spark-ignited	Compression ignited	Compression ignited
Power output control	Airflow control, with stoichiometric air-fuel ratio	Fuel flow control, with lean air-fuel ratio	Fuel flow control, with lean air-fuel ratio
Mechanism controlling fuel burning rate	Flame propagation speed	Time for fuel vaporization and mixing	Chemical kinetics
Emission characteristics	Cleaner with 3-way catalyst. Higher CO_2	Higher particulate matter, soot, NO_x (without aftertreatment). lower CO_2	Higher unburned hydrocarbons, CO. Lower NO_x, soot, particulates, and CO_2

Table 2-1 - Comparison of spark-ignited, Diesel and HCCI engine characteristics

2.2.1 Well-mixed spark ignition

Most automotive engines in North America are gasoline engines of the spark-ignited (SI) type. Typically these engines use the Otto-cycle (although other similar forms such as the Atkinson cycle also exist). Figure 2-3 shows a pressure vs. volume plot of the four thermodynamic processes in an ideal Otto cycle:

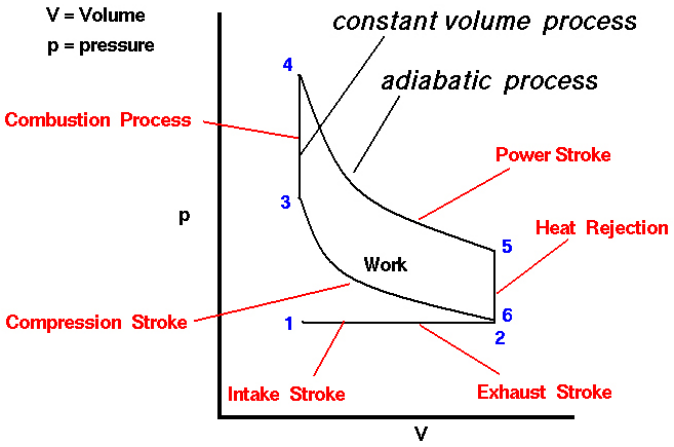

Figure 2-3 - PV Diagram of Ideal Otto-Cycle
Source: Nasa, Glenn Research Center [6]

Figure 2-3 shows the four thermodynamic processes of an ideal Otto-cycle, which are:

- 2→3: Isentropic compression – adiabatic and reversible compression of the fuel-in-air charge
- 3→4: Constant volume heat addition – combustion of the fuel-in-air mixture is approximated as an instantaneous and uniform ignition once the spark plug is fired
- 4→5: Isentropic expansion – adiabatic and reversible expansion of the product gases
- 5→6: Constant volume heat rejection – the excess enthalpy in the cylinder gases is released

In reality, combustion in an Otto-cycle four stroke engine does not take place according to the ideal cycle. The compression and expansion processes are not isentropic since heat transfer

through the cylinder walls, head and piston occurs. Additionally, the combustion process does not take place as a constant volume process since a small flame kernel is created by the spark, which gradually propagates outward towards the cylinder walls; during this flame propagation process the piston continues to move causing variation of the cylinder volume. Furthermore, the heat rejection process is also not a constant volume process. Finally, the ideal cycle does not capture the pumping work required for the intake and exhaust strokes.

The premixed nature of spark-ignited Otto-cycle engines allows for lower particulate matter and soot emissions. These engines typically operate with equivalence ratios near unity because of requirements by catalytic converters, which decrease emissions after combustion by reducing nitric oxides and oxidizing unburned hydrocarbons and carbon monoxide. Typical compression ratios for Otto-cycle engines range between 8:1 to 12:1 with most engines using about 9:1 [7], and this compression ratio has a significant impact upon Otto cycle thermal efficiency, $\eta_{th,Otto}$:

$$\eta_{th,Otto} = 1 - \frac{1}{CR^{\gamma-1}} \qquad \text{(Eq. 3.1)}$$

Thermal efficiency can therefore increased by increasing the compression ratio, CR, or the ratio of specific heats of the in-cylinder gases, γ. The ratio of specific heats is not easily subject to significant variation, so the only practical way of increasing thermal efficiency (at least in a thermodynamic sense) is through higher compression ratios. The compression ratio, however, is limited by the onset of knocking which occurs because of compression heating of unburned gases. This excessive compression heating causes undesired auto-ignition to occur ahead of a propagating flame front [7]. The undesired auto-ignition of these end gases causes rapid rates of pressure rise and strong in-cylinder pressure waves that can damage an engine over time.

Given that the equivalence ratio is fixed near 1.0, spark-ignited engines control the power output by varying the amount of intake air. Lower power output is achieved by throttling the intake air, and higher output is achieved by fully opening the intake throttle or by providing boosted intake pressures using a turbocharger or supercharger.

In-cylinder pressure traces of spark-ignited engine operation show that there is a high degree of cycle-to-cycle variations. This phenomena is where some cycles will have higher peak pressures and higher pressure rise rates compared to others. This behavior is caused by variations in turbulence from cycle to cycle, inhomogeneities in the fuel-in-air mixture, uneven presence of exhaust gas residuals, localized hot spots, or variations in the spark plasma. Studies have estimated that these cycle-to-cycle variations can reduce fuel economy by 6-10% [7].

Harmful pre-catalyst emissions from spark-ignited engines typically include high amounts of hydrocarbons (HC) and oxides of Nitrogen (NO_x) in the range of 500-1000 ppm. Carbon monoxide emissions are in the range of fractions of a volume percent, ie. 0.68 vol-% [8]. The high NO_x emissions are caused by high peak flame temperatures (in excess of 1800 K) behind the premixed flame front, which provides sufficient energy for breaking the strong triple bond in N_2 molecules. The high emissions of unburned hydrocarbons and carbon monoxide is due to fuel becoming trapped in the crevices during the compression stroke, then being released without burning completely in the exhaust stroke. An important feature of spark-ignited engines is that they have very low emissions of particulate matter compared to Diesel engines.

A method of significantly reducing harmful emissions from an spark-ignited engine is to include a three-way catalyst. This device simultaneously performs three tasks to reduce overall harmful emissions:

1. Reducing NO_x into N_2 and O_2
2. Oxidizing CO to CO_2
3. Oxidizing unburned hydrocarbons to CO_2 and H_2O

[8, p.180-181]

An emerging technology for spark-ignited engines is the use of fuel injection directly into the combustion chamber rather than into the intake manifolds. Spray-guided gasoline direct injection (GDI) can allow for higher efficiency because the fuel can be kept in the central region of the combustion chamber to prevent efficiency losses from heat transfer through the cylinder walls and piston, and also prevent fuel from being trapped in the crevices. Furthermore, direct injection of the fuel into the cylinder causes charge cooling which enables the use of higher compression ratios [9].

2.2.2 Stratified charge compression ignition - Diesel

In Diesel engines only air is present in the cylinder during the intake and compression strokes and fuel is injected at high pressures late in the compression stroke. As a result, higher compression ratios can be achieved and ignition occurs relatively quickly as the fuel is injected into the cylinder. Figure 2-4 shows a pressure vs. volume plot of the four thermodynamic processes in an ideal Diesel cycle:

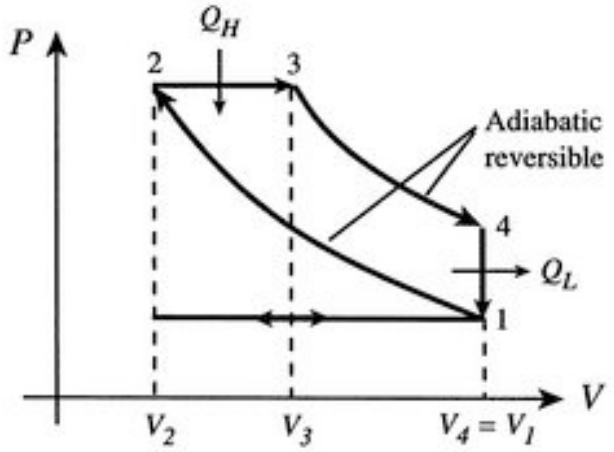

Figure 2-4 - PV Diagram of Ideal Diesel Cycle
Source: MIT [10]

The four processes in an ideal Diesel cycle, depicted in Figure 2-4, are:

- 1→2: Isentropic compression – adiabatic and reversible compression of air
- 2→3: Constant pressure heat addition – non-premixed combustion of the fuel as it is injected into highly compressed air
- 3→4: Isentropic expansion – adiabatic and reversible expansion of the product gases
- 4→1: Constant volume heat rejection – the excess enthalpy of the cylinder gases is released

Combustion in an actual Diesel engine deviates from the ideal cycle in several ways. First, the compression and expansion processes are not isentropic since there is heat transfer between the cylinder gases and the cylinder walls, head and piston. Additionally the combustion process is not a truly constant pressure process since that would require precise control of heat release rates matched with the cylinder expansion rate. Furthermore, the heat rejection is not actually a constant volume process. Finally, the ideal process does not capture the pumping work required for the intake and exhaust strokes.

Diesel engines are particularly attractive because of their ability for attaining higher thermal efficiencies. Once the fuel is injected, and after a small delay for mixing, ignition takes place due to high compression and thus much leaner equivalence ratios can be achieved in comparison with spark-ignited engines. Diesel engines are not constrained to operation near ϕ=1, because they typically do not use three-way catalysts. This allows for higher efficiency with the removal of a throttle valve since power output can be controlled by varying the amount of fuel injected into the cylinder. Since only air is present in the compression stroke, higher compression ratios, typically between 12:1 to 24:1 [7], can be achieved. This allows for higher thermal efficiency, $\eta_{\text{th,Diesel}}$, which is expressed as:

$$\eta_{\text{th,Diesel}} = 1 - \frac{1}{\text{CR}^{\gamma-1}}\left[\frac{r_c^{\gamma}-1}{\gamma\left(r_c-1\right)}\right] \qquad \text{(Eq. 3.2)}$$

In Eq. 3.2, r_c is the cutoff ratio which is the ratio of cylinder volumes after and before the combustion process.

Maximum engine speeds in Diesel engines are lower because the combustion process is slower. This slower combustion is caused by the time delay from evaporation and mixing of the fuel following injection into the cylinder gases. These lower engine speeds also limit the power output since power is the product of torque and speed.

Power output in Diesel engines is controlled by varying the air-fuel ratio, while staying at an overall fuel lean ratio. The air-fuel ratio can be changed through fuel injection control, by injecting more or less fuel, or by changing the amount of air entering the cylinder through super or turbo charging. The latter strategy, increasing the airflow, does not actually enable higher power output on its own; however, the introduction of more air allows more fuel to be introduced. Diesel engines typically do not use intake throttling, and thus do not suffer from the pumping efficiency losses as in spark-ignited engines.

The high compression ratio, and removal of an intake throttle allows Diesel engines to achieve high efficiency (on the order of 15% higher than typical spark-ignited engines [11, p.123]). This higher efficiency allows for lower carbon dioxide emissions, which is beneficial in slowing the effects of global warming. The non-premixed nature of Diesel engines, however, causes higher emissions of other harmful products, such as soot, particulate matters, and nitric oxides. Soot and particulate matter emissions are higher in Diesel engines because fuel molecules (and their partially-burned constituents) do not have sufficient time to find oxygen to complete the oxidation process. Nitric oxide emissions are higher in Diesel because high temperatures, above 1800 K, are achieved in the core burning region which causes the strong triple-bond in nitrogen molecules to be broken.

The high levels of harmful soot, particulate matter and nitric oxide emissions from Diesel engines require the use of aftertreatment technologies, particularly to meet increasingly stringent emissions regulations. Diesel engines, however, cannot use a three-way-catalyst as with spark-ignited engines because they operate with an overall lean fuel-air equivalence ratio. As a result, more expensive aftertreatment technologies must be used, and these technologies can sometimes be as expensive as the Diesel engine itself, thereby doubling the cost of a vehicle's power generation system. Aftertreatment options for Diesel engines include [12]:

1. Oxidation catalysts which remove unburned hydrocarbons
2. Selective catalytic reduction (SCR), which injects Urea (also known as Diesel exhaust fluid) into the exhaust stream to reduce NO_x
3. Lean NO_x traps to remove nitric oxide
4. Diesel particulate filters to trap and periodically burn off soot emissions through a high temperature regeneration process

Current areas of research in Diesel engines include strategies for reducing emissions and understanding the effects of emerging fuels on Diesel processes. Extensive experimental and numerical studies are being conducted to understand the physics of high pressure sprays to develop strategies to lower the vaporization and mixing time of fuel in high pressure air (enabling lower soot emissions) [13]. Low temperature combustion (LTC) is an active area of research, where early injection and leaner mixtures are used to promote fuel-air mixing and lower peak temperatures to avoid nitric oxide formation. The use of high octane fuels (such as gasoline with lubricity additives), is being explored in Diesel engines. Since high octane fuels have a higher resistance to autoignition, they allow more time for fuel-air mixing prior to the occurrence of autoignition, thereby lowering the soot and particulate matter emissions. Extensive research is underway to understand the effects of alternative and renewable fuels in Diesel engines. Biodiesel, for example, is one fuel being extensively explored in Diesel engines because it can be produced renewably. Emerging research, however, has shown that there are higher nitric oxide emissions when using a Diesel engine with oxygenated alternative fuels like biodiesel.

2.2.3 Homogeneous charge compression ignition (HCCI)

HCCI engines combine properties of both spark-ignited and Diesel engines. Similar with spark-ignited engines, HCCI uses a premixed fuel-air charge, and similar with Diesel engines the fuel-air mixture is compression ignited. This allows HCCI to combine the premixed cleaner burning (lower particulate matter and lower soot) aspect of spark-ignited engines with the high efficiency compression-ignited aspect of Diesel engines. In HCCI, the combustion process and the burn rate are controlled by chemical kinetics (the rate at which individual chemical reactions proceed), and thus high compression ratios are used to elevate the fuel-air temperature to levels at which the chemical reactions proceed quickly enough to produce autoignition.

HCCI follows a thermodynamic process that is even closer to the ideal Otto cycle (shown in Figure 2-3) than spark-ignited engines. The fundamental difference between spark-ignited and HCCI is that in spark-ignited engines the burn rate is controlled by a gradual flame propagation process, while in HCCI the burn rate is controlled by the fast chemical kinetics of an autoignition

process. As a result, the heat addition thermodynamic process takes place under conditions that are much closer to a constant volume process that would be approximated in an ideal Otto cycle. The rapid release of heat from the fast burning process in HCCI is also the root cause of power output limitations within HCCI engines (one of the topics addressed in the research presented in this dissertation). Excessive rates of heat release (and the accompanying excessive pressure rise rates) can damage an engine over time, and thus steps must be taken to avoid these harmful conditions. One approach to limiting the maximum heat release rates is by using charge dilution, through lower fuel-air equivalence ratios, or with exhaust gas recirculation. Although HCCI combines the clean burning and high efficiency aspects of spark-ignited and Diesel, this charge dilution causes power output from HCCI engines to be lower than comparable spark-ignited or Diesel engines.

HCCI engines typically operate at compression ratios higher than spark-ignited engines. Depending on the intake conditions and the fuel type, HCCI compression ratios can range from 14:1 [14,15,16] to 22:1 [17,18], however lower compression ratios can be used in spark-assisted HCCI implementations. Fuel-air equivalence ratios in HCCI range between 0.20 and 0.55 for implementations without exhaust gas recirculation [17], but can go as high as 1.0 (stoichiometric) for implementations that use extensive dilution with exhaust gas recirculation [14].

Given that the HCCI engine can be approximated with the Otto cycle, the thermal efficiency limits can be estimated using the Otto cycle efficiency relationship in Eq. 3.1. The higher compression ratios of HCCI compared with spark-ignited engines is one reason for their ability to achieve higher thermal efficiencies (similar to Diesel). Another factor contributing to the high efficiency of HCCI is that the intake air is not throttled for power output control. As a result, HCCI does not suffer from the throttling losses that affect part-load operating conditions in spark-ignited engines. The efficiency limits for HCCI engines are discussed in Chapter 7 alongside the power output limits.

As in Diesel, power output in HCCI is controlled by varying the fuel-air equivalence ratio, while typically staying at an overall fuel lean ratio. The air-fuel ratio can be changed through fuel injection control, by injecting more or less fuel, or by changing the amount of air entering the cylinder through super or turbo charging. The latter strategy, increasing the airflow, does not actually enable higher power output on its own, however the introduction of more air allows more fuel to be introduced. While it is not typical for Diesel engines to reach stoichiometric fuel-air ratios due to excessive soot emissions, HCCI can accommodate equivalence ratios up to stoichiometric provided that sufficient EGR is used to prevent excessive heat release rates.

Two significant challenges for HCCI engines are effectively controlling combustion timing, and improving the power output. These challenges are addressed as part of the research presented in this dissertation. Combustion timing is difficult to control in HCCI engines because there is no direct method for initiating the combustion process. Sparkplugs, as in spark-ignited engines, are ineffective because of the diluted fuel-air mixtures which are below the limits of flame propagation. Given that the fuel is typically premixed in HCCI, fuel injection timing cannot be used as a means for controlling the combustion timing as in Diesel. As a result of these limitations, precise control of intake conditions must be used to determine the temperature and

pressure of the fuel-air mixture near top-dead center to have autoignition occur at the correct time. Aside from lower power output and difficulty in controlling combustion timing, HCCI can also be difficult to cold start when compared with other engine technologies.

The high levels of charge dilution typical in HCCI also cause lower in-cylinder temperatures compared with spark-ignited or Diesel engines, which is important in determining the emissions characteristics of HCCI engines. In-cylinder temperatures are typically sufficiently low to avoid significant nitric oxide formation, and the premixed nature of HCCI allows very low soot and particulate matter emissions. The low in-cylinder temperatures, however, also cause higher emissions of unburned hydrocarbons and carbon monoxide. Detailed plots of the emissions characteristics in HCCI are shown in Chapter 7. One principle benefit from the high-efficiency operation of HCCI is that carbon dioxide emissions are lower than spark-ignited engines.

Aftertreatment technologies can be used to remove unburned hydrocarbon and carbon monoxide emissions. Oxidation catalysts are one promising technology in this effort, however research is required to ensure that sufficiently high temperatures are present in the exhaust stream from an HCCI engine for an oxidation catalyst to operate with high conversion efficiencies. One approach is to keep the HCCI engine at conditions where high exhaust temperatures occur, however there is also active research in finding catalytic materials that have lower light-off temperatures.

Current areas of research in HCCI engines focus on several challenges, including: 1) expanding the power output limits for HCCI, 2) effectively controlling HCCI engines on a cycle-to-cycle basis, 3) effectively starting an HCCI engine, or transitioning into HCCI mode, and 4) exploring the use of alternative fuels in HCCI. The first challenge, improving HCCI power output, is the focus of Chapter 7. For improving HCCI power output, the focus is on techniques for allowing more gradual heat release. National laboratories, universities and industry laboratories are all exploring a variety of strategies for reducing the maximum heat release rate, including the use of delayed combustion timing and charge dilution [14,17,19,20], thermal stratifications [19], charge stratifications [21], and mixtures of different fuel types [22,23]. On effectively controlling combustion timing, one particularly effective strategy being explored is the use of direct injection during a negative valve overlap compression period to reformulate different amounts of gasoline fuels to produce the reactivity levels necessary to control combustion timing on a cycle-by-cycle basis [24]. On effectively starting and transition into HCCI operating modes, the current strategy of choice for automotive applications is starting an engine in spark-ignited or Diesel mode, and transitioning into a low-temperature combustion (or HCCI) operating mode. Finally, alternative and renewable fuels are continuously being explored. HCCI has been shown to be highly advantageous particularly for power generation applications which use gaseous biofuels, such as biogas [18,25,26,27].

2.3 Ideal applications of HCCI engines

The most common applications of engines are for transportation and power generation. In transportation, engines provide mobile power for cars, trucks, buses, trains, ships and small aircraft. Although the HCCI engine provides a clean and efficient alternative to spark-ignited and Diesel engines, its historical drawbacks of lower power output and difficulty in controlling

combustion timing have not allowed it to become widely accepted yet. Immerging research has revealed innovative techniques to overcome the control and power output issues, yet further research is still necessary to develop production versions of these technologies. As a result, this section will discuss applications for HCCI engines that can utilize the clean and high efficiency aspects of the HCCI engine in conditions that require fairly transient operation over a constrained load regime.

In a personal transportation context, two immerging technologies can allow wide market penetration of HCCI engines. The first is dual-mode engines which operate as HCCI engines for lower and medium load regions, and then as traditional Diesel or spark-ignited engines for high load regions. Simulations of a SI-HCCI engine in the EPA urban and highway drive cycles have shown that this dual-mode approach can allow a 17% fuel economy improvement over a conventional SI engine [28]. The second approach is using HCCI engines within a hybrid-electric powertrain. In this second approach, the hybrid powertrain can absorb many of the transient and high load requirements upon an engine, making HCCI engines the perfect fit for this approach. Recent research has shown that combining the above strategies of using SI-HCCI engines within a mild hybrid powertrain can enable a 35% fuel efficiency improvement over a traditional spark-ignited engine [28], and a 6 to 12% fuel efficiency improvement over a mild hybrid powertrain using a high efficiency Atkinson spark-ignited cycle [29].

In a locomotive application, Diesel-electric powertrains are already being used [30] to combine the high efficiency aspect of Diesel engines with the high torque (at low speeds) aspect of electric motors. Although Diesel engines provide high efficiency similar to HCCI engines, the HCCI engine applied to locomotive applications can significantly reduce the need for expensive aftertreatment technologies. An HCCI engine in a locomotive application can use simple oxidation catalysts to remove harmful unburned hydrocarbons and carbon monoxide, while a Diesel engine also requires expensive aftertreatment technologies to remove nitric oxides (such as selective catalytic reduction, or lean NO_x traps).

In power generation applications, the power density of an engine is not nearly as important as it is in transportation applications. HCCI engines can be particularly advantageous in this context as they provide higher efficiency than spark-ignited engines, cleaner emissions than a Diesel engine (without the need for expensive aftertreatment technologies), and they are significantly less expensive than gas turbines. In a power generation context, there are very few transients compared with transportation applications (for example, for a 60 Hz power grid, the engine can remain at a constant engine speed of 1800 RPM), thus making HCCI engines even more attractive. Several recent studies have demonstrated effective strategies for using renewable fuels, like biogas, for power generation within an HCCI engine [18,25,26,27].

3 Hydrocarbon oxidation in an HCCI engine

3.1 Global reactions and combustion stoichiometry

The global reaction for the oxidation of a fuel with air can be expressed as:

$$Fuel + x\left(O_2 + 3.76N_2\right) \rightarrow yCO_2 + zH_2O \qquad \text{(Eq. 3.3)}$$

where (O_2+3.76N_2) represents air, which consists roughly of 21% Oxygen and 79% Nitrogen. The coefficients x, y, and z depend on the particular fuel and the fuel-air equivalence ratio of the reaction. The equivalence ratio is defined as

$$\phi = \frac{m_{fuel} / m_{air}}{\left(m_{fuel} / m_{air}\right)_{stoich}} = \frac{1}{\lambda} \qquad \text{(Eq. 3.4)}$$

where the denominator corresponds to the stoichiometric ratio of fuel and air, when the right proportion of both are available to completely consume all fuel and oxygen molecules. ϕ=1 corresponds to a stoichiometric ratio, ϕ<1 is lean (excess air), and ϕ>1 is rich (excess fuel). In cases of lean combustion, Eq. 3.3 must also include unconsumed O_2 as a product on the right-hand-side of the equation. The stoichiometric air-fuel ratio (inverse of the denominator in Eq.3.4) for several common fuels is listed in Table 3-1 [31]:

Table 3-1 - Stoichiometric air-fuel ratios (by mass) for common fuels

Fuel	AFR_{stoich}
Methane	17.2
Propane	15.7
Butane	15.5
Gasoline	14.5-14.7
Ethanol	9.0

3.2 Elementary reactions and reaction mechanisms

The global reaction for fuel oxidation shown in Eq. 3.3 is a significant simplification compared with the reaction pathways that are actually followed in a combustion process. In reality, the oxidation of large hydrocarbon fuel molecules proceeds as steps consisting of thousands of individual reactions with many intermediate species produced along the way. Each of the individual reactions is called an elementary reaction and these can be categorized into four fundamental types of reactions: initiation, propagation, branching and termination [31,32]. The four types of reactions are classified on the basis of whether they create, sustain, increase or decrease the number of unstable radical species during the reaction.

Initiation reactions generate unstable radical species from the decomposition of stable species, for example:

$$CH_4 + O_2 \rightarrow CH_3\bullet + HO_2\bullet \quad \text{(Eq. 3.5)}$$

Propagation reactions produce the same number of radical species in the products as the number of radical species entering as reactants, thus there is no change in the radical concentration. An example of a propagation reaction is:

$$CH_4 + OH\bullet \rightarrow CH_3\bullet + H_2O \quad \text{(Eq. 3.6)}$$

Branching reactions result in more radical species in the products as compared with the number that entered as reactants, for example:

$$CH_4 + O\bullet \rightarrow CH_3\bullet + OH\bullet \quad \text{(Eq. 3.7)}$$

Finally, termination reactions are where radicals are recombined to form stable species, for example:

$$H\bullet + OH\bullet + M \rightarrow H_2O + M \quad \text{(Eq. 3.8)}$$

An additional classification on reaction types can be made based on the number of reactant species that take part in the reaction. For example, Eq.3.5 through Eq. 3.7 are examples of 2-body reactions, while Eq. 3.8 is an example of a three-body reaction.

The reaction rate of each elementary reaction (such as the one shown in Eq. 3.9) can be modeled using an empirical rate formulation shown in Eq. 3.10:

$$aA + bB \rightarrow cC + dD \quad \text{(Eq. 3.9)}$$

$$\frac{d[C]}{dt} = ck_f [A]^a [B]^b \quad \text{(Eq. 3.10)}$$

The terms in square brackets in 3.10 correspond to the molecular concentration of each species. The term k_f represents the forward reaction rate, which can be modeled using the Arrhenius form shown in Eq. 3.11:

$$k_f = k_0 e^{-E/RT} \quad \text{(Eq. 3.11)}$$

In Eq. 3.11, the term k_0 is the pre-exponential factor, E is the activation energy for the reaction, R is the gas constant, and T is the gas temperature. The pre-exponential factor and activation energy for a given reaction can be measured in experiments (such as in a shock tube, rapid compression machine, or flow reactor), or predicted from theory using Ab-Initio calculations.

A complete chemical mechanism for a given fuel will include reaction kinetic information (such as pre-exponential factors and activation energies) for thousands of reactions. To perform useful calculations with these mechanisms, physical properties for each chemical species must also be provided, and a computational solver must be constructed to solve all of the individual differential equations for each species, and keep track of individual species concentrations and the overall pressure and temperature of the gas mixture.

3.3 Reaction pathways for single-stage and two-stage ignition fuels

Given that the fuel-air mixture in an HCCI engine is generally well-mixed prior to the onset of combustion, the fuel chemistry plays a very important role in determining combustion characteristics (more than in spark-ignited or Diesel engines, where flame propagation or spray and vaporization processes also play an important role). Different fuels have different paths for oxidation, and as a result different fuels can be behave drastically differently under the same conditions in an HCCI engine. Given that the chemical kinetics plays such an important role in HCCI engine performance, this section is dedicated to describing the reaction pathways followed by different fuels during their oxidation process in an HCCI engine.

Fuels for HCCI can generally be characterized based on whether they display single- or two-stage ignition behavior. Generally, fuels with lower octane ratings such as n-heptane, Diesel, PRF80, and dimethyl ether (DME) display two-stage ignition while fuels with higher octane ratings such as ethanol display a single-stage ignition. The difference in ignition behavior in an HCCI engine between a single- and two-stage ignition fuel is demonstrated in Figure 3-1.

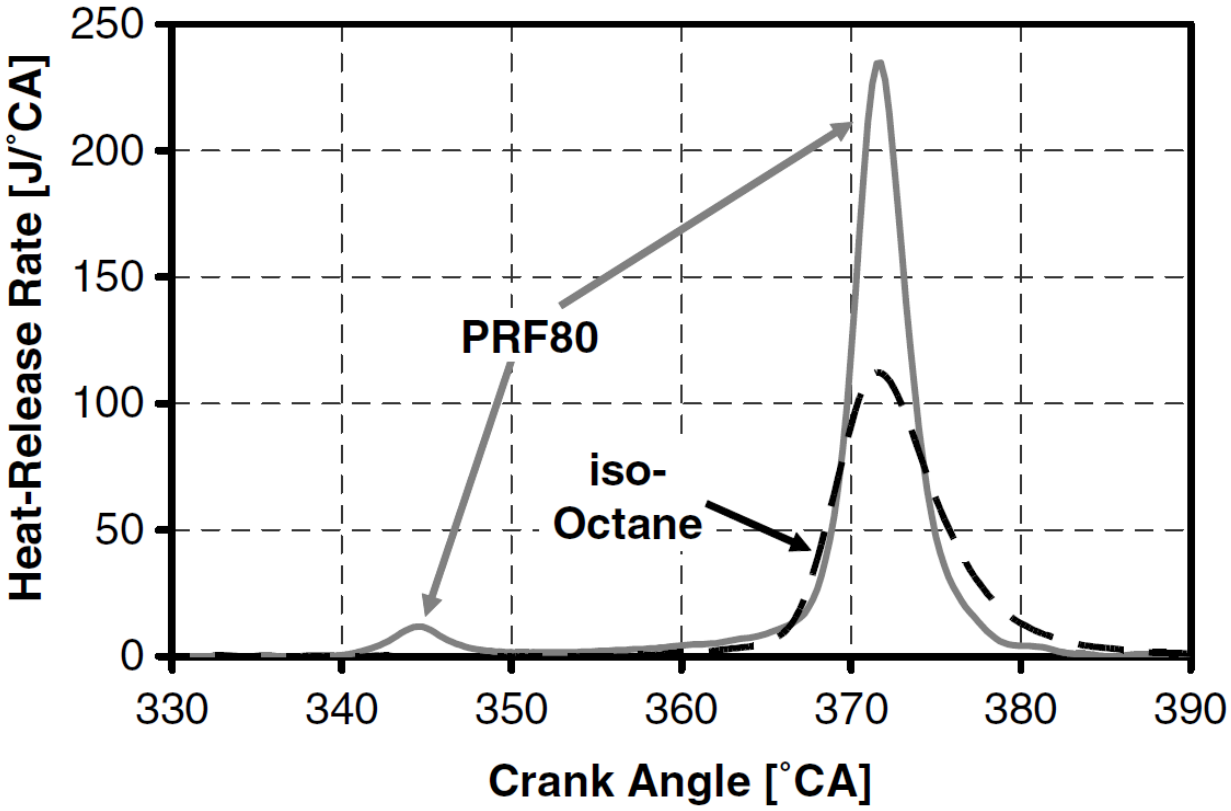

Figure 3-1 - Heat release rate from an HCCI engine (TDC=360°) using two different fuels, PRF80 which exhibits two-stage ignition, and iso-octane which exhibits a single-stage ignition
Source: Sjöberg and Dec, 2007 [43]

Two-stage ignition fuels like PRF80 (which is a blend of 80% iso-octane, and 20% n-heptane by volume) exhibit a small amount of heat release at temperatures which are lower than the hot ignition temperature zone (above 1000 K). This low temperature heat release (LTHR) causes a

fraction of the fuel to be partially oxidized at temperatures below 850 K. This LTHR can cause a temperature rise of between 10-20 K in the fuel-air mixture within the engine [33]. LTHR can cause the hot ignition (shown near 375 CAD in Figure 3-1) to occur earlier, or it can cause the requirement of lower intake temperatures for achieving hot ignition at a comparable timing as with a fuel showing single-stage ignition.

3.3.1 Heat release at low temperatures

Reactions for a straight-chained alkane will be used in illustrating the reaction pathways followed by a fuel undergoing LTHR, however similar processes are followed by many fuels which exhibit two-stage ignition behavior. At temperatures below 1000 K, the primary reaction paths for heat release begin with hydrogen abstraction from the fuel molecules:

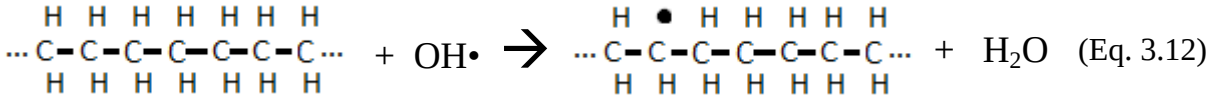

(Eq. 3.12)

At temperatures below 1000 K, the alkyl radicals (such as the one shown in the products in Eq. 3.12) can combine with oxygen molecules to produce an alkylperoxy radical:

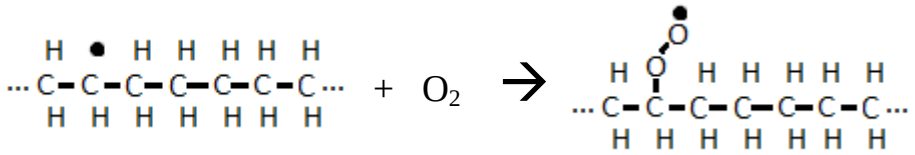

(Eq. 3.13)

The available bonding site on the outermost oxygen atom in the alkylperoxy radical (shown as a product in Eq. 3.13) can then reach over and bond with a nearby hydrogen atom as part of an alkylperoxy radical isomerization reaction. The bond between the hydrogen atom and its attached carbon atom will break to leave an open reaction site on the main carbon chain. There are several possibilities for which hydrogen atom is taken by the oxygen atom, and these different possibilities can be characterized by the intermediate transition state ring that is formed during the isomerization process. If the oxygen atom takes the closest hydrogen atom, a 5-member ring is formed (two carbon, two oxygen and a hydrogen atom). For each successively further hydrogen atom, a larger transition ring is formed. Several of these transition state rings are illustrated in Figure 3-2:

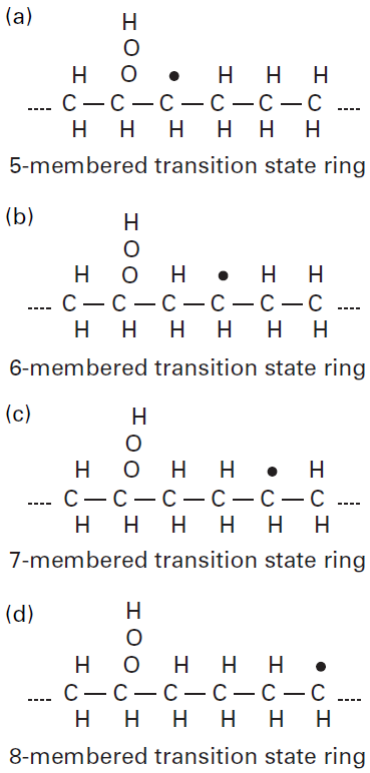

Figure 3-2 - Possible alkylperoxy radical isomerization sites, illustrating the different sizes of transition state rings
Source: Westbrook, Pitz and Curran, 2007 [33]

Once an isomerized alkylperoxy radical is formed, several possibilities exist for the next reaction. One possibility is that the oxygen-oxygen bond can be broken to produce an OH radical as illustrated in Eq. 3.14:

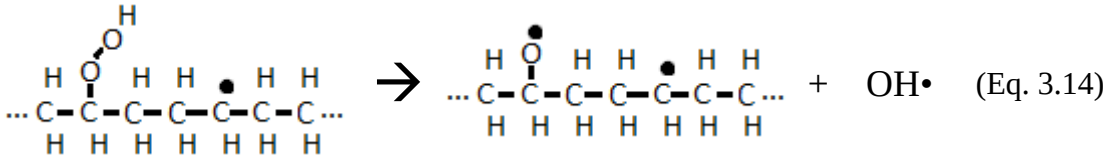

(Eq. 3.14)

Alternatively, a similar reaction as in Eq. 3.13 can occur, where another oxygen molecule bonds with the open reaction site on a carbon atom located on the main hydrocarbon chain. This process is illustrated for a 7-member transition state ring in Figure 3-3:

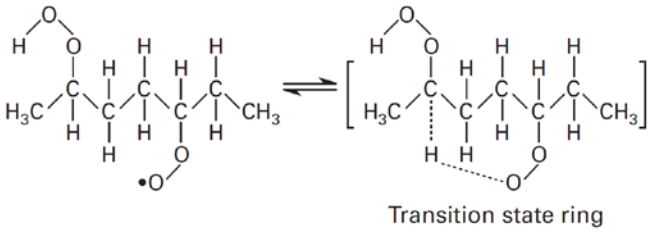

Figure 3-3 - Second isomerization reaction illustrated for a 7-member transition state ring
Source: Westbrook, Pitz and Curran, 2007 [33]

The molecule undergoing a second isomerization reaction (as illustrated in Figure 3-3) can react in a branching reaction to release three radicals, two OH radicals, and the hydrocarbon molecule with open O sites. This set of reactions which finally leads to the branching reaction producing two OH radicals is responsible for the rapid heat release observed in the low temperature zone (less than 1000 K). The other reaction paths (for example Eq. 3.14) which only release one OH radical are propagation reactions, and thus do not have a net effect on the radical concentration.

The reaction of alkyl radicals with oxygen molecules (as in Eq. 3.13, or the reaction preceding the one shown in Figure 3-3) are highly temperature and pressure dependent. With higher temperatures, the equilibria of these reactions shifts towards the reactants, and by roughly 850 K the addition of O_2 to the alkyl radicals is almost completely extinguished [33]. As a result of the equilibria shifting towards the reactants, with higher temperatures the rate of heat release for the LTHR reactions is reduced. This causes a region that is characterized by a phenomena called the negative temperature coefficient (NTC), where higher temperatures actually cause lower reaction rates. In Figure 3-1, this NTC region is observed for PRF80 between 345 and 350 CAD.

Above 850 K, very little heat release occurs until the intermediate and high temperature regimes are encountered above 1000 K. As a result, the majority of heating between 850 and 1000 K comes from piston work during the compression stroke.

3.3.2 Heat release at intermediate and high temperatures

Above 850 K the main reactions involving the fuel molecules are H-atom abstraction by OH (illustrated in Eq. 3.12) or HO_2. Abstraction with HO_2 causes the production of hydrogen peroxide (H_2O_2) which gradually increases in concentration until the mixture reaches an intermediate temperature of approximately 1000 K. Above 1000 K, the strong oxygen-oxygen bond in H_2O_2 breaks more readily causing the reaction in Eq. 3.15 [33], which rapidly releases a large amount of OH radicals.

$$H_2O_2 \rightarrow OH\bullet + OH\bullet \qquad \text{(Eq. 3.15)}$$

As a result of Eq. 3.15 which proceeds more quickly above 1000 K, the previously stable hydrogen peroxide molecules act as a sudden source of OH radicals which consume the fuel molecules more quickly leading to rapid heat release. The breakdown of hydrogen peroxide into OH radicals and their subsequent reactions causes increasing temperature which further accelerates the breakdown of hydrogen peroxide. This leads to an auto-ignition event that increases the temperature to above 1200 K where hot ignition takes over through the branching reaction of Eq. 3.16 [32,33]:

$$H\bullet + O_2 \rightarrow O\bullet + OH\bullet \qquad \text{(Eq. 3.16)}$$

An interesting side effect from the importance of the hydrogen peroxide branching reaction (Eq. 3.15) is that the intermediate and hot ignition temperatures are relatively independent of the fuel type. Almost uniformly, the intermediate ignition takes place when hydrogen peroxide breaks down near 1000 K, and the hot ignition takes place near 1200 K when Eq. 3.16 dominates.

3.3.3 Characteristics of single- and two-stage ignition fuels

The hydrogen abstraction and isomerization reactions shown in Eq. 3.12 and Figure 3-2 are critical in the low temperature heat release process (the first stage in two-stage ignition). Thus fuels that are more conducive to these reactions show a higher tendency of exhibiting two-stage ignition behavior. The ease with which hydrogen abstraction and isomerization can occur are related to the molecular structure of the fuel molecule, and the type of carbon-hydrogen bond that is to be broken.

Chemical bonds between carbon and hydrogen in a hydrocarbon fuel can be characterized by primary, secondary or tertiary bond strengths which depend on the neighboring environments of the carbon atom. As illustrated in Figure 3-4, primary carbon-hydrogen bonds are where the carbon atom is bonded to only one other carbon atom. A secondary carbon-hydrogen bond is one where the carbon atom is bonded to two other carbons, and a tertiary is where the carbon atom is bonded to three other carbons. Primary carbon-hydrogen bonds are the strongest and thus they have the highest activation energy to prevent hydrogen abstraction [34]. As a result of the relative bond strengths for carbon-hydrogen bonds, a fuel molecule which has more secondary carbon-hydrogen bonds (such as a straight-chained alkane) is more likely to allow the abstraction reactions which lead to low temperature heat release.

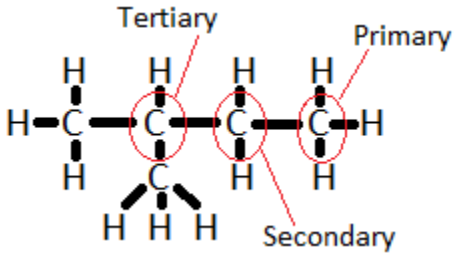

Figure 3-4 - 2-methylbutane molecule illustrating locations of primary, secondary and tertiary carbon atoms

The isomerization reaction illustrated in Figure 3-2 occurs when the O_2 chain which has bonded to an initially abstracted site reaches around to remove a hydrogen atom from another site. Due to the relative bond strengths, this hydrogen removal occurs more easily by breaking a secondary carbon-hydrogen bond as compared to a primary. Furthermore, the O_2 chain reaching to abstract hydrogen occurs more easily in long straight chain molecules because of the long chain length and flexibility of the molecule [35].

Long straight chained alkanes such as n-heptane (C_7H_{16}) are more conducive to low temperature heat release than branched alkanes such as iso-octane (C_8H_{18}). This is because of the higher number of secondary bonds, the longer chain length, and greater internal flexibility. It is for this reason that primary reference fuels with greater n-heptane content (and thus lower octane rating) tend to display a greater extent of low temperature heat release.

Using this knowledge of bond strengths and molecular structure we can analyze different fuel molecules. N-heptane, as already discussed, displays a great deal of low temperature heat release because of its large number of secondary bonds, its longer chain length, and its greater internal

flexibility for isomerization reactions. Iso-octane displays very little low temperature heat release because its branched structure creates more primary bonds making the initial hydrogen abstraction difficult. Ethanol also displays very little low temperature heat release because it has few secondary carbon-hydrogen bonds and it has a very short chain length.

3.4 Gasoline fuel in HCCI engines

The above sections discussed heat release characteristics in single- and two-stage ignition fuels, and the chemical reactions that cause heat release. The majority of the research in this dissertation is carried out with gasoline fuel, thus a brief discussion of heat release for gasoline HCCI is in order. Table 3-2 lists the fuel properties for a typical gasoline fuel:

Table 3-2 - Fuel properties for typical gasoline fuel [7]

RON	95.4
MON	85.6
Energy content, MJ/kg	43.5
Density at 15°C, kg/L	0.738
Initial boiling point, °C	28
Final boiling point, °C	198.5
Normal paraffins, %Vol	10.8
Iso paraffins, %Vol	43.4
Total paraffins, %Vol	54.2
Naphthenes, %Vol	2.9
Olefins, %Vol	8.6
Aromatics, %Vol	33.6
Avg molecular formula	
C	6.64
H	12.11
Stoichiometric AFR	14.53 to 14.70

Under the majority of conditions, gasoline behaves as a single-stage ignition fuel with limited heat release prior to hot ignition. At HCCI conditions where low intake temperature is used however, for example with low engine speeds (below 900 RPM) or high intake pressures, gasoline begins to display low temperature heat release [14,16,20].

At elevated intake pressures, gasoline also displays an intermediate temperature heat release (ITHR). In Chapter 7 of this dissertation, the use of highly delayed combustion timings and high intake pressures are discussed as methods for allowing increased HCCI power output. The ITHR behavior of gasoline is critical for allowing delayed combustion timing since it counteracts the cooling effect from piston expansion after TDC. This ITHR behavior increases with lower intake temperatures and with higher intake pressures up to a maximum at 1.8 bar (absolute). Intake pressure has a more dominant effect upon ITHR than intake temperature [14,16,20]. The chemical reactions contributing to ITHR, the pressure dependence of ITHR and its saturation behavior at a maximum of 1.8 bar are up to this point not well understood [16].

4 Present research in HCCI

Previous research has identified the key factors affecting combustion characteristics in HCCI including power output, and the different factors that limit the maximum achievable power output. Power output (IMEP, for example) in HCCI is affected by boost pressure, equivalence ratio, combustion timing, compression ratio, peak temperatures, heat loss, EGR, fuel type (and the extent of occurrence of low temperature chemistry), engine speed and other factors. Maximum power output is limited by excessive combustion noise (ringing), peak in-cylinder pressure limits, misfire, excessive NO_x emission, and a loss of controllability if intake temperature requirements become too low [36,37]. In recent years, research efforts have revealed different strategies that can enable higher power output in HCCI engines while staying within the prescribed limits of operation.

4.1 Extending the high load limits of HCCI

Many past studies have focused on maintaining acceptable levels of ringing while enabling higher power output. Although excessive ringing can be heard at audible frequencies, a useful empirical relationship was developed by Eng which classifies ringing intensity in HCCI engines [36]. In his work, Eng showed that ringing is strongly correlated with excessive rates of pressure rise, while peak temperature and pressure also play a role. Recent studies have focused on a variety of strategies for reducing the peak rate of pressure rise. Two particular strategies are in the use of delayed combustion timing for reducing peak pressure rise rates, and the use of thermal and mixture stratifications to cause more gradual heat release.

4.1.1 Delayed combustion timings for reducing peak heat release rates

Delayed combustion timing has been proven as one of the most effective tools for reduction of pressure rise and heat release rates. Sjöberg et al. [19] compared the effects of enhanced natural thermal stratifications (by enhancing heat transfer) versus the use of delayed combustion timing, and concluded that delayed combustion timing is most effective at reducing peak heat release rates because of lower combustion temperatures, lower pressure rise rates because of faster piston expansion, and enhanced natural thermal stratification around TDC. The downsides of highly delayed combustion timing, however, are that it causes lower efficiency with excessive delays in combustion timing, it can cause less stable combustion (or complete misfire), and can require intake temperatures that are below ambient temperatures.

Delayed combustion timing is useful in reducing ringing because the faster piston expansion at later combustion timings causes greater rates of pressure decrease, thereby counteracting the high pressure rise from a uniform autoignition event. Figure 4-1 shows the in-cylinder pressure and pressure rise rate for a naturally aspirated motored condition. The pressure rise rate from Figure 4-1 shows that when combustion is delayed after top dead center, the rate of pressure decrease is higher with later crank angle degrees, with a minimum occurring near 11 CAD ATDC.

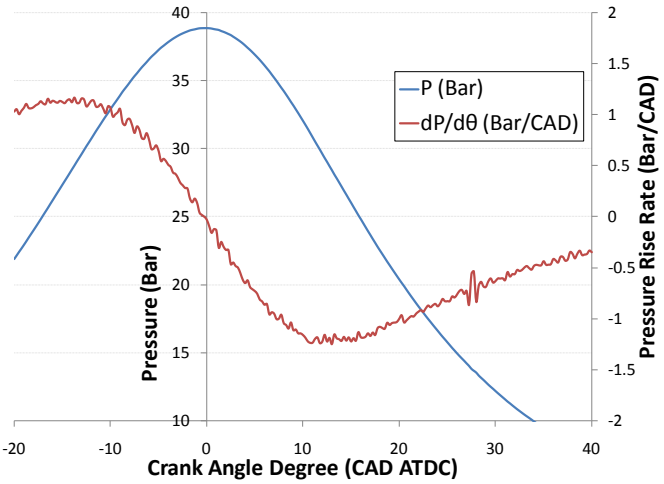

Figure 4-1 - Motored Pressure and Pressure Rise Rate for Naturally Aspirated Conditions

The control of intake temperature has been shown as one highly effective means of controlling combustion timing for different equivalence ratios, engine speeds and intake pressures [14,20,24,37,38,39,40]. Higher intake temperatures generally cause advanced combustion timings, while reduced intake temperatures delay timing. Fuel chemistry (particularly whether the fuel is a single-stage or two-stage ignition fuel) also plays an important role in determining heat release rates and the extent with which combustion timing can be delayed. Tanaka et al. [41] showed that straight chained hydrocarbon fuels with $–CH_2-CH_2-CH_2-$ structures more readily show two-stage ignition behavior and shorter ignition delay times. In their work, they identified means of independently controlling the burn rate and the ignition delay that a particular fuel would exhibit in HCCI conditions. Several important studies by Sjöberg and Dec [14,15,38,42,43] have revealed specific strategies that can be employed for enabling delayed combustion timing for single-stage and two-stage ignition fuels. Specifically, for highly delayed combustion near the point of misfire, combustion stability is highly sensitive to random fluctuations in charge temperature, and higher temperature rise rates just before hot ignition have been shown effective in dampening the effects of these temperature fluctuations [43]. With increasingly delayed combustion, the temperature rise rates before hot ignition are lowered because of faster piston expansion. Two-stage ignition fuels such as PRF80, however, have been demonstrated in maintaining higher temperature rise rates because of higher reactivity just before hot ignition.

Numerous studies, including early research from Christensen, et al., have shown that boost pressure allows higher power output before the onset of excessive ringing is encountered [14,20,36,42,44,45,46,47]. In their research, Christensen et al. [44] showed fuel dependencies on maximum IMEP, showing 14 bar maximum net IMEP for natural gas and 9.7 bar net IMEP for iso-octane. Subsequent studies [14,45,48] have also shown that EGR provides an effective means of enabling higher power output by smoothing heat release and pressure rise rates through dilution and enabling further delayed combustion timings.

Many of the results discussed above were combined in a single-cylinder gasoline-fueled study by Dec and Yang [14]. In their study, intake temperature was decreased as boost pressures increased allowing delayed combustion timings, however beyond P_{in}=180 kPa abs the intake temperature levels required for maintaining delayed combustion timing were lower than expected

temperatures out of a turbocharger's compressor. Beyond this level of boost pressure, increasing EGR fractions were used in maintaining delayed combustion timing (as late as 19 CAD ATDC). Using this strategy, a gross IMEP of 16.34 bar was found at P_{in}=3.25 bar abs, with a stoichiometric equivalence ratio, and 60% EGR. This high power operating point was demonstrated with little ringing, high overall efficiency, good combustion stability and very low levels of NO_x. In this study, it was found that a key factor in enabling highly delayed combustion timings was in keeping bulk gas temperatures rising despite high rates of piston expansion through ITHR reactions which are enhanced by increased boost pressures. These ITHR reactions could be increased up to boost pressures of 180 kPa.

4.1.2 Thermal and mixture stratification for reducing peak heat release rates

Another strategy in reducing the peak heat release rate to avoid excessive ringing is by intentionally creating thermal or mixture stratifications to enable sequential (rather than uniform) autoignition throughout the fuel-air mixture.

Thermal stratifications naturally occur in engines because of the inhalation of charge with non-uniform temperature, and non-uniform heat transfer during the intake and compression stroke. These temperature gradients cause different rates of chemical reaction throughout the charge and can cause sequential autoignition which is useful in lowering the maximum heat release rate. A multi-zone model coupled with CFD analysis [49,50,51] can be used to study thermal stratifications and its effects on enabling more gradual heat release. Figure 4-2 shows the temperature distribution computed using CFD analysis and divided into 40 temperature zones near the end of the compression stroke [51].

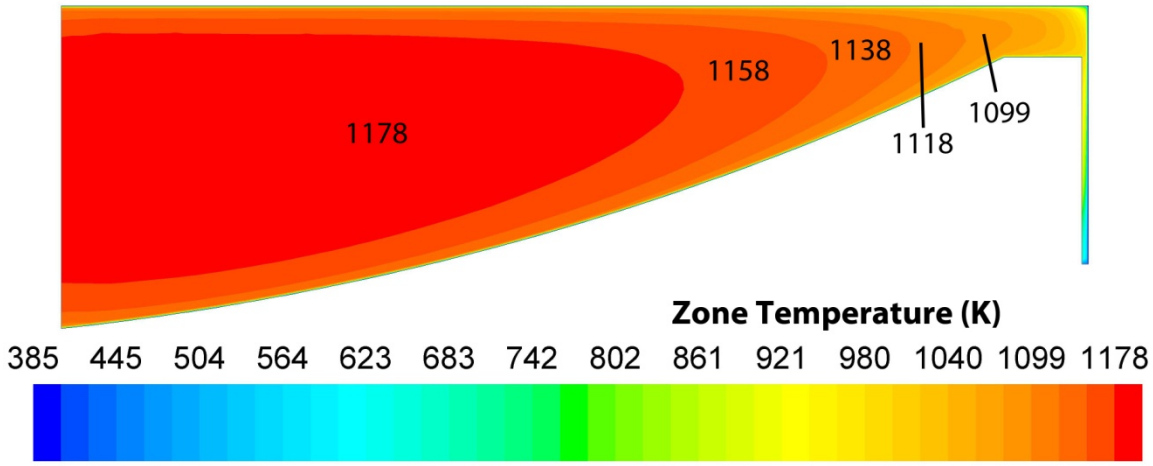

Figure 4-2 - Thermal stratifications in a 40-zone model at 3 CAD bTDC show that core region is the hottest. Intake conditions P_{in}=2 bar abs, T_{in}=438 K, ϕ=0.29, for biogas fuel (60% CH_4, 40% CO_2) Source: Bedoya, Saxena, Aceves, Flowers, Dibble, 2012 [51]

As Figure 4-2 shows, the core fluid region near the center of the combustion chamber is the hottest and the fuel-air mixture gets progressively cooler near the boundaries and in the crevices. These temperature gradients naturally occur as a result of heat loss to the cylinder walls, head and piston during the compression stroke. In determining the effects of these thermal stratifications upon the overall heat release rate, it is important to consider the amount of mass

present within each simulated zone. The hottest zone will ignite first with subsequent ignition occurring in colder zones, however as seen in Figure 4-2, the largest volume (and therefore the most mass) is encompassed within the hottest zone. Figure 4-3 shows the zone temperature and zone mass fraction for the 10 hottest zones for simulations using a 40-, 20- and 10-zone model [51].

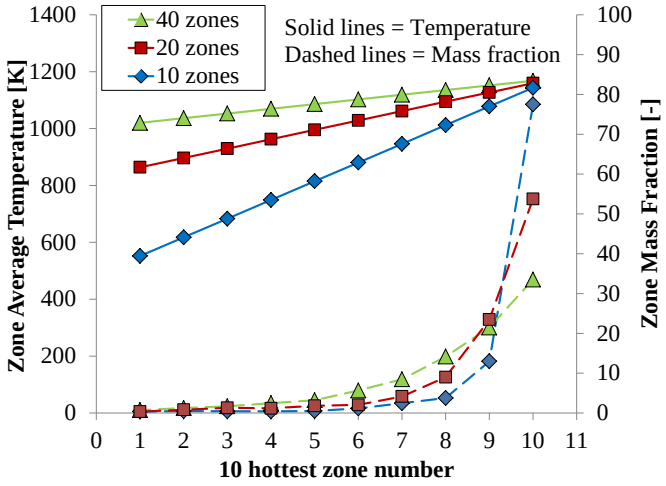

Figure 4-3 - Zone temperature and mass fraction for multi-zone model with 10, 20 and 40 zones at 3 CAD bTDC
Source: Bedoya, Saxena, Aceves, Flowers, Dibble, 2012 [51]

As shown in Figure 4-3, more mass is present in the hotter zones for HCCI engines. It is interesting to note that a larger number of zones in a simulation allows better resolution of the thermal stratifications and the mass present in each zone. Figure 4-4 shows the temperature profile of the 10 hottest zones in a 40-zone model [51].

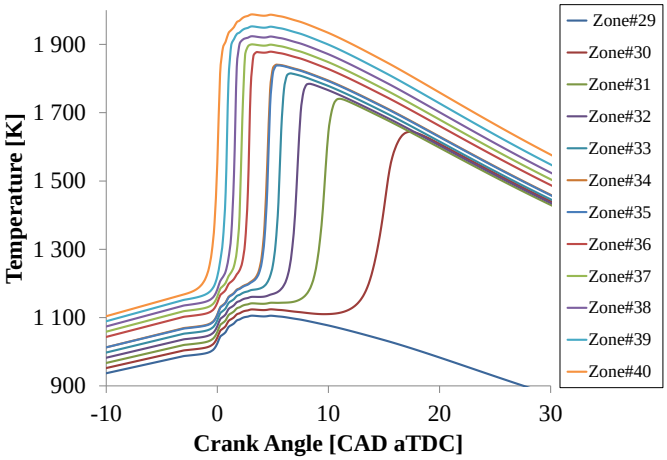

Figure 4-4 - Crank angle resolved zone temperature showing sequential autoignition with hottest zones igniting first
Source: Bedoya, Saxena, Aceves, Flowers, Dibble, 2012 [51]

As illustrated in Figure 4-4, sequential autoignition occurs, with the hottest zones igniting first. Since more mass is present in the hotter zones (Figure 4-3), more heat will be released when earlier ignition occurs in the hot zones. Thus, these hotter zones have the largest impact on

determining the maximum heat release and maximum pressure rise rate that influence the ringing intensity. As a result of this sequential autoignition, any strategy that enhances the thermal stratifications should be effective at also lowering the ringing intensity. This strategy has been explored in experimental studies, and at least three strategies can be used to artificially enhance the thermal stratifications: 1) increasing the heat transfer to the walls by using lower engine coolant temperatures [19], 2) increasing the heat transfer to the walls through more in-cylinder turbulence, with higher swirl for example [19], and 3) using charge cooling from vaporization by using direct fuel injection at delayed injection timings [37].

The first two strategies of promoting thermal stratifications through enhanced heat transfer to the walls was demonstrated as being effective in lowering the maximum heat release rates and ringing intensities. The higher rates of heat loss, however, also resulted in lower power output and worse fuel economy. When the fueling rate was increased to compensate for the lower power output, the benefits of enhanced thermal stratifications were lost [19]. The use of vaporization charge cooling from direct injection is less effective in lowering the peak heat release rates for fuels with single-stage ignition. However, the mixture stratifications that arise from direct injection can potentially play a much larger role in lowering the maximum heat release rate.

The use of mixture stratification is commonly referred to as partial fuel stratification (PFS). Under PFS, a majority of the fuel is injected in the intake manifold to allow premixing, while a small amount of fuel is directly injected into the cylinder to create areas of stratified charge. The effectiveness of PFS in lowering heat release rates and ringing intensity is highly dependent on a fuel property known as ϕ-sensitivity. Fuels with high ϕ-sensitivity allow earlier combustion at higher equivalence ratios, and thus sequential ignition can be achieved using mixture composition gradients through the use of direct fuel injection [15,21,52,53]. Fuels exhibiting two-stage ignition are more ϕ-sensitive and allow lower peak heat release rates with PFS, while fuels exhibiting single-stage ignition are not ϕ-sensitive and result in higher peak heat release rates and more NO_x emissions when using PFS. For ϕ-sensitive fuels, the use of direct injection fraction and direct injection timing can be used as control parameters for controlling the extent of fuel stratification and tailoring the heat release rate under particular operating conditions.

For fuels with two-stage ignition, PFS allows lower peak pressure rise rates (and lower ringing intensities). This occurs because regions with higher localized equivalence ratio tend to ignite earlier with subsequent ignitions occurring in regions with lower localized equivalence ratio [15]. It has been shown that the overall fuel reactivity, rather than the exact fuel composition determines the ϕ-sensitivity of a given fuel and therefore also determines its performance with PFS [21]. Fuels containing molecules with $-CH_2-CH_2-CH_2-$ chains, which allow 6-member low strain C-C-C-O-O-H rings (see Section 3.3) tend to display two-stage ignition and are more ϕ-sensitive [41]. The ϕ-sensitivity of fuels is not highly sensitive to engine speed, thus PFS can be used successfully over a wide range of engine speeds, however ϕ-sensitivity does depend on the intake temperature and intake pressure [21].

PFS for fuels displaying two-stage ignition and high ϕ-sensitivity has been shown as being effective in preventing excessive ringing to allow higher power output from HCCI engines. Since PFS reduces the extent of ringing, less combustion timing delay is needed for preventing ringing, and thus PFS also allows for improved fuel economy (roughly 2 to 2.5% fuel economy

improvement). The ability of using PFS with gasoline fuel has been a recent subject of study, and at naturally aspirated conditions PFS is ineffective for reducing ringing since gasoline is not highly ϕ-sensitive at these operating conditions [52]. Interestingly, as the intake pressure is increased in gasoline HCCI engines (i.e. beyond 1.8 bar absolute), gasoline becomes highly ϕ-sensitive since more intermediate temperature heat release (ITHR) reactions occur [14,16,20,52]. Thus, at high power output conditions which utilize high boost pressure, PFS can be used to reduce ringing and allow higher efficiency.

Although PFS has been shown to be effective for highly ϕ-sensitive fuels with two-stage ignition, there are two limits which constrain the operating limits of PFS. First, when overly delayed direct injection timing is used to facilitate PFS, separate ignition events can occur between the premixed charge and the direct injected charge. Under these conditions, the maximum pressure rise rate of the premixed charge ignition will constrain the operating limits. Second, when too high a direct injected fuel fraction is used to facilitate PFS, the heat release rate of the direct injected portion can be too high [53].

4.2 Control strategies

High power output in HCCI engines is enabled by combining the results of the studies discussed above. The highest power operating points for gasoline HCCI exist near the limits of misfire, ringing, maximum allowable in-cylinder pressure and loss of controllability from low intake temperatures. The balance between the ringing and misfire (or unstable combustion) limits requires precise control for maintaining a stable operating point. Sjöberg et al. [19] showed that at high equivalence ratios ($\phi>0.44$ in their study) simply maintaining constant intake temperature is insufficient for maintaining fixed combustion timing. This occurs because brief disturbances in combustion timing cause large changes in the cylinder wall temperature. These changes in wall temperature amplify the original combustion timing disturbance, causing the requirement of very fast response closed-loop control.

In a multi-cylinder context, the control challenge is amplified even further since individual cylinders can affect the conditions in their neighboring cylinders. As a result, instabilities in one cylinder can be transmitted (or amplified) in adjacent cylinders. Hyvönen et al. [54] identified further complications for multi-cylinder HCCI since each cylinder has different gas exchange behavior, compression ratio, heat transfer, fuel supply and intake temperature. In their study, the relative effect of these different multi-cylinder factors upon combustion timing was identified. Three specific cylinder balancing strategies were explored: 1) the use of even intake temperature between cylinders, 2) closed-loop combustion timing control with individual cylinder control of intake temperature, and 3) closed-loop control of combustion timing using individual cylinder control of fuel amount. The first strategy was ineffective at balancing combustion timing between cylinders. The third strategy allowed effective control of combustion phasing between cylinders, however uneven power output was seen across the different cylinders. The second strategy, using individual control of intake temperature, was shown as the most effective since it provided good balancing of both combustion timing and power output between cylinders.

The use of individual control of intake temperature across cylinders has been extensively used in previous research [40,55,56,57], and this technique is commonly called thermal management. As

shown in the Hyvönen et al. study [54], thermal management is effective at balancing combustion phasing between cylinders, however it has two significant challenges: 1) slow response, and 2) intake temperatures for sufficiently delayed combustion timing at high power output conditions for gasoline are below ambient temperatures. The first problem can be partially remedied by controlling the relative flow of intake air through heaters (or exhaust gas heat exchangers) versus through non-heated paths allowing more rapid response for changes in intake temperature. The second problem can be offset by using variable compression ratios, or variable valve actuation which allows expansion of the intake temperature range for different boost pressure conditions. This strategy has been demonstrated in conjunction with thermal management in several studies [40,54,57].

Aside from thermal management, fuel stratification using multiple in-cylinder injection events [58,59] and the use of spark-assistance in HCCI has also allowed for multi-cylinder control [24]. One effective example of this strategy is where some gasoline is directly injected into the cylinder during a NVO compression event to reform the gasoline into a more reactive mixture. The remaining fuel is then directly injected during the intake stroke. By controlling the relative amount of fuel injected in the NVO versus the intake stroke, the overall mixture reactivity can be varied to control the combustion timing on a cycle-by-cycle basis [24].

4.3 Modeling

Accurate numerical models are useful in providing further insight into the interaction of physical phenomena that are difficult to isolate in engine experiments. This section provides a brief overview of different approaches to simulating HCCI engine operation.

Early studies investigating HCCI [60] demonstrated the importance of calculating detailed chemical kinetics to predict the combustion properties in these engines. Calculation of detailed chemical kinetics (particularly for complex fuels like gasoline) requires a great deal of computing time. The calculation of detailed fluid dynamics simultaneously with detailed chemical kinetics can be prohibitively time consuming. One common simplifying assumption to reduce the computing time is to ignore the fluid dynamics and assume that the combustion chamber is a perfectly homogenous volume. This approach, called a single zone model, has been shown to be effective in predicting ignition timing when the pressure, temperature and mixture composition are known. The single zone model, however, tends to over predict the peak pressure rise rate (and thus also the ringing intensity) and is inaccurate in predicting emissions.

In reality, the ignition event in HCCI occurs at multiple points throughout the charge with slight time differences between each ignition event. The single-zone model is unable to capture these subtle differences in spatial ignition times and one approach to improving the model is to introduce several different zones. A multi-zone model treats several different regions within the combustion chamber as distinct reactors, each having of its own temperature and mixture composition [49]. For these models, it is common to only model the effects of mechanical work between zones and neglect the effects of heat transfer, mixing and diffusion between zones. Neglecting these effects is a valid assumption because during the combustion event the chemical time is typically much shorter than the time scale of mixing and heat transfer between zones [61]. Although not perfect, the multi-zone models are more accurate at predicting the peak pressure rise rate and emissions than single-zone models. Peak pressure rise rate calculations are

improved because the ignition event proceeds sequentially throughout several zones, and emissions results are improved since several zones are typically dedicated to the colder boundary and crevice regions where HC and CO emissions originate.

Studies [62,63] have shown that fluid dynamic effects, such as turbulence and mixing, must be included with the chemical kinetic calculations to improve the prediction of ignition timing and also the prediction of peak pressure rise rates. These turbulence and mixing effects are important during the compression stroke, however they are less important during the combustion duration (discussed in the previous paragraph). Thus, coupling a CFD model with a multi-zone model allows more accurate simulations since this approach successfully estimates the thermal stratifications that arise because of heat loss during the compression stroke [50]. Prior to the ignition event, the temperature profiles for each zone are specified within a multi-zone chemical kinetic model which continues the simulations throughout the combustion process and through the expansion stroke. This approach is even more accurate than the multi-zone model at predicting the ignition timing and produces more accurate peak pressure rise rates. The two major disadvantages of this approach are that 1) it can be difficult to determine the energy switch angle when chemical kinetic calculations should be activated, and 2) it is very time consuming to use this approach to simulate engine conditions spanning a wide range of operating conditions.

To take advantage of the benefits of the coupled CFD and multi-zone chemical kinetics methodology while avoiding the two drawbacks, another approach is proposed which sequentially couples chemical kinetics-CFD-chemical kinetics [51]. This approach proceeds in three steps: 1) a 1-zone chemical kinetic model is used to determine either the intake conditions at IVC to achieve a desired ignition timing or the ignition timing corresponding with given IVC conditions, 2) these initial conditions are used as input parameters in a CFD model to calculate the charge temperature profile and mass distribution prior to autoignition, and 3) the temperature profile and mass distribution are fed into a multi-zone chemical kinetic model to determine the main combustion characteristics. This three-step methodology has two main advantages over the CFD-chemical kinetics approach discussed in the last paragraph. First, the use of a 1-zone model prior to detailed calculations allows determination of practical operating limits based on the ignition timing for given intake charge conditions. For instance, the 1-zone model can be used quickly to eliminate cases that would result in excessive ringing or misfire before having to run the time consuming CFD and multi-zone chemical kinetic calculations. Second, the 1-zone model allows accurate determination of the energy switch crank angle by providing a good estimate of the ignition timing. Overall, this three-step methodology allows for all the benefits of the coupled CFD-chemical kinetic model while simultaneously reducing the computing time required for running a large number of simulated cases.

5 Experimental setup and data analysis

5.1 Overall engine specifications

A four-cylinder 1.9L Volkswagen TDI engine is used for this study. The engine includes significant modifications to enable and enhance HCCI combustion, including:

1. The original deep-bowl pistons on the Volkswagen TDI engine are replaced with relatively flat pistons to reduce heat transfer.
2. The glow plug holes are remachined to accommodate standard 10 mm spark plugs that serve as ion sensors.
3. In-cylinder quartz piezoelectric pressure transducers are installed in the Diesel fuel injector ports.
4. Port fuel injectors are installed in a custom intake manifold, and the fuel injection is controlled using a custom injection control system constructed with solid-state relays and control signals generated from a National Instruments/Labview system.
5. The stock turbocharger is removed, and an external 100 HP compressor with 6 m^3 surge tank is used to provide intake air at boosted pressure.

Table 5-1 presents the overall engine specifications, and Figure 5-1 shows the intake and exhaust valve profiles:

Configuration	Inline 4 cylinder
Firing order	1-3-4-2
Displacement	1.9 L
Compression ratio	17.0 : 1
Bore	79.5 mm
Stroke	95.5 mm
Connecting rod length	144.0 mm
Valves (intake, exhaust)	1, 1
Valve Overlap	3 degrees
Valve lift (intake, exhaust)	1.0 cm
Engine speed	1800 +/- 5 RPM
Volume BDC	504.72 cm^3
Volume TDC	29.69 cm^3

Table 5-1 - List of engine specifications

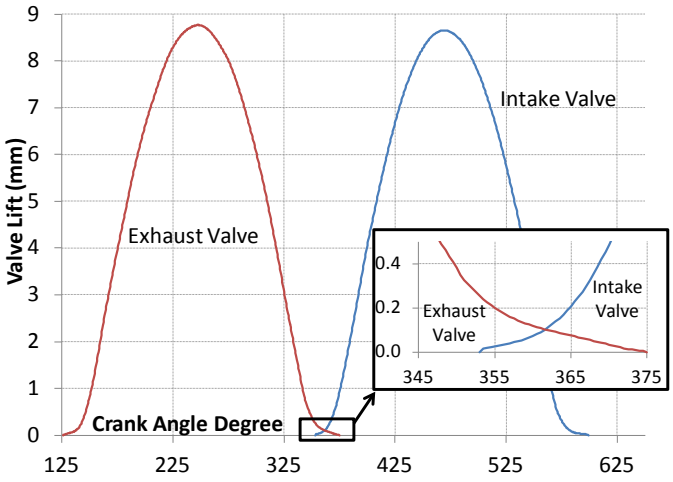

Figure 5-1 - Valve lift profiles for experimental engine

In order to control engine speed, a direct coupling driveshaft (no transmission) connects the engine to an AC motor/generator. For this study, the motor/generator does not include a variable frequency drive and therefore the engine speed is locked to 1800±5 RPM regardless of whether the engine is firing or motoring.

The overall engine configuration is shown in Figure 5-2 with the location of different sensors and actuators:

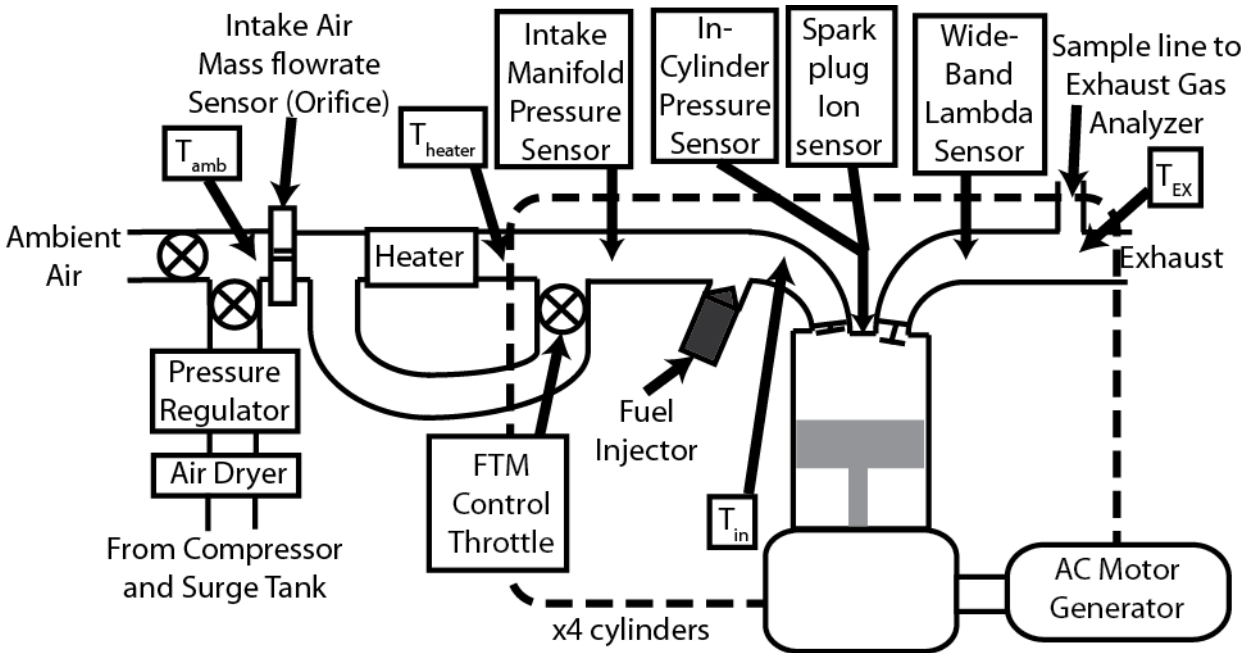

Figure 5-2 - Schematic of engine and supporting systems

5.2 Data analysis

5.2.1 Pressure-based computations

In-cylinder pressure is monitored using AVL QH33D water-cooled quartz pressure-transducers connected to the Labview data acquisition system through a Stanford Research Systems charge amplifier. The pressure measurements are triggered using a TTL signal with 4 pulses per crank angle degree from an encoder fitted to the engine crankshaft. Thus, for each thermodynamic cycle (2 crankshaft revolutions), 2880 in-cylinder pressure measurements are captured per cylinder. This pressure data is used to compute many engine operating parameters such as in-cylinder temperature, heat release rates, CA50, and ringing intensities, and the discussions below will show how each of these parameters are calculated. Prior to calculating combustion parameters using in-cylinder pressure data a filtering algorithm using the Savitzky-Golay least-squares polynomial fitting procedure [64] is applied. The average filtered pressure from 300 consecutive thermodynamic cycles is then taken to generate a single pressure trace which is used in the remainder of the analysis.

The heat release rate is calculated using Eq. 4.1 from the filtered and averaged pressure data:

$$\frac{dQ}{d\theta} = \frac{\gamma}{\gamma - 1} P \frac{dV}{d\theta} + \frac{1}{\gamma - 1} V \frac{dP}{d\theta} \qquad \text{(Eq. 4.1)}$$

In Eq. 4.1, Q represents the heat release, γ is the specific heat ratio (c_p/c_v), P is the in-cylinder pressure, and V is the cylinder volume. It is important to note that the calculated heat release rate includes both heat release from chemical reactions and heat loss through the cylinder head, walls,

and piston. Separating the chemical heat release from the heat loss would require further calculations and heat transfer modeling.

The cylinder volume is calculated for each crank-angle position from the slider-crank relationship in Eq. 4.2:

$$V(\theta) = V_c + \frac{\pi \cdot \text{bore}^2}{4}\left[\text{conrod} + \frac{\text{stroke}}{2} - \left\{\frac{\text{stroke}}{2}\cdot\cos(\theta) + \sqrt{\text{conrod}^2 - \left(\frac{\text{stroke}}{2}\sin(\theta)\right)^2}\right\}\right] \quad \text{(Eq. 4.2)}$$

Where V_c is the clearance volume at TDC, defined as:

$$V_c = \frac{\pi \cdot \text{bore}^2}{4 \cdot \text{stroke} \cdot (CR - 1)} \quad \text{(Eq. 4.3)}$$

And CR is the compression ratio, defined as:

$$CR = \frac{V_{BDC}}{V_{TDC}} \quad \text{(Eq. 4.4)}$$

For the Volkswagen TDI engine with modified piston used in this research, the compression ratio is 17.

The heat release rate calculation in Eq. 4.1 also requires the specific heat ratio, γ. This is calculated using a fitting algorithm on the compression and expansion portions (excluding where heat release occurs) of the cycle. The following equation is fit to in-cylinder pressure data, where γ is the fitting parameter:

$$PV^{\gamma} = \text{constant} \quad \text{(Eq. 4.5)}$$

The calculated heat release rate (in Eq. 4.1) can then be integrated to determine the cumulative heat release:

$$Q_i = \sum_{-180^\circ}^{i} \frac{dQ}{d\theta}_i \cdot d\theta \quad \text{(Eq. 4.6)}$$

where Q_i is the cumulative heat release up until crank angle i. Using the cumulative heat release calculated from Eq. 4.6, the burn duration and the crank angle of 50% heat release (CA50) can also be calculated. As shown in Figure 5-3, the crank angle for 0% burn (CA0) is taken as the local minimum in heat release just prior to the hot ignition. The crank angle for 100% burn (CA100) is taken as the overall maximum heat release. By interpolating between CA0 and CA100, all other values of interest can be determined, including the CA50 which is used in the feedback control of combustion timing.

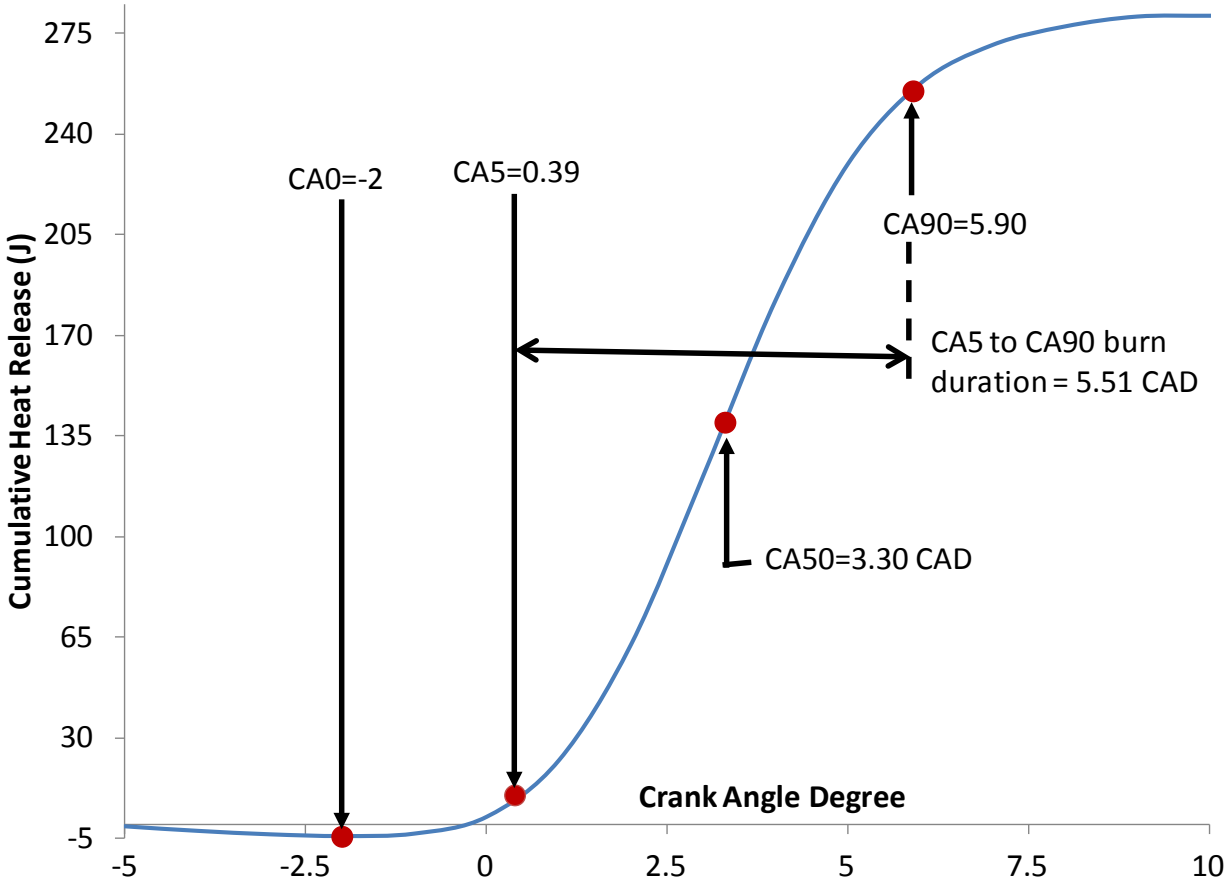

Figure 5-3 – Sample of crank angle positions for different extents of burn

Using the in-cylinder pressure measurements, estimates of the mass averaged in-cylinder gas temperature can also be found. Ideal gas law is used in estimating the gas temperature:

$$T = \frac{P \cdot V}{m_{\text{inducted}} \cdot R} \qquad \text{(Eq. 4.7)}$$

where P is the measured in-cylinder pressure, V is the calculated volume (from Eq. 4.2), m_{inducted} is inducted mass (fuel and air), and R is the gas constant. The gas constant, R, is calculated as:

$$R = \frac{R_u}{M} \qquad \text{(Eq. 4.8)}$$

where R_u is the universal gas constant, and M is the average molecular weight of the in-cylinder gases. M is set to a value for the air-fuel mixture prior to the ignition event, and then transitions from a value for the reactants to a value for the burned gases during the burn duration. The rate of this transition from a value for reactants to products is determined from the CA0 to CA100 cumulative heat release. The value of M for burned gases considers the overall equivalence ratio to determine the amount of carbon dioxide, water and oxygen in the exhaust, but it neglects trace emissions such as unburned hydrocarbons, carbon monoxide and nitric oxides. The procedure for

calculating M is demonstrated in Eq. 4.12, while the unburned and burned average molecular weights are calculated using Eq. 4.10 and Eq. 4.11. Eq. 4.9 shows a balanced chemical equation for lean burning hydrocarbons, from which Eq. 4.10 and Eq. 4.11 are derived.

$$C_\alpha H_\beta + \frac{1}{\phi}\left(\alpha + \frac{\beta}{4}\right)\left(O_2 + 3.76N_2\right) \rightarrow \alpha CO_2 + \frac{\beta}{2}H_2O + \frac{3.76}{\phi}\left(\alpha + \frac{\beta}{4}\right)N_2 + \left(\alpha + \frac{\beta}{4}\right)\left(\frac{1}{\phi} - 1\right)O_2 \quad \text{(Eq. 4.9)}$$

$$M_{unburned} = x_{C_\alpha H_\beta} M_{C_\alpha H_\beta} + x_{O_2} M_{O_2} + x_{N_2} M_{N_2} \quad \text{(Eq. 4.10)}$$

$$M_{unburned} = x_{CO_2} M_{CO_2} + x_{H_2O} M_{H_2O} + x_{O_2} M_{O_2} + x_{N_2} M_{N_2} \quad \text{(Eq. 4.11)}$$

$$M_{mixture}(\theta) = \begin{cases} M_{unburned}, \theta < CA0 \\ M_{unburned} - \dfrac{HR(\theta)}{HR(CA100)} \dfrac{M_{unburned} - M_{burned}}{100}, CA0 \le \theta \le CA100 \\ M_{burned}, \theta > CA100 \end{cases} \quad \text{(Eq. 4.12)}$$

The temperature calculation in Eq. 4.7 also requires knowledge of the inducted mass, $m_{inducted}$, which includes the mass of both air and fuel entering the cylinder. This parameter is estimated using the mass of fuel injected, which is precisely measured, and the equivalence ratio as measured by the wideband-lambda sensors installed in each exhaust manifold. This calculation is shown in Eq. 4.13:

$$m_{inducted} = m_{fuel} + \left(\frac{AFR_{stoich} \cdot m_{fuel}}{\phi}\right) \quad \text{(Eq. 4.13)}$$

In analyzing the performance of different operating conditions, the power output and efficiency must also be calculated. The power output is calculated using the gross indicated mean effective pressure ($IMEP_g$). Gross IMEP is advantageous to use over net IMEP because it only considers the closed portion of the thermodynamic cycle (when the intake and exhaust valves are closed). Net IMEP is not relevant for most of the operating points run in the experiments because intake pressure boosting was provided by an external compressor, which did not provide the exhaust backpressure that would be seen with a turbocharger. As a result of the high intake pressure, and atmospheric exhaust pressure, the net IMEP would be inaccurate for production engine applications. $IMEP_g$ is calculated using Eq. 4.14:

$$IMEP_g = \frac{\sum_{\theta=-180°}^{+180°} P(\theta)\, dV(\theta)}{V_d} \quad \text{(Eq. 4.14)}$$

The numerator in Eq. 4.14 is the gross PdV work (over the compression and expansions stroke), while the denominator is the displaced volume. Normalizing the work output by the displaced volume is useful because it allows comparison of power outputs from engines of different size.

Thermal efficiency is calculated as the gross indicated efficiency, which also uses the PdV work over the closed portion of the thermodynamic cycle as the numerator. The thermal efficiency is calculated using Eq. 4.15:

$$\eta_{ind,g} = \frac{\sum_{\theta=-180^\circ}^{+180^\circ} P(\theta)\,dV(\theta)}{m_{fuel} LHV_{fuel}} \qquad \text{(Eq. 4.15)}$$

The denominator in Eq. 4.15 represents the amount of energy that is provided by the fuel, where LHV is the lower heating value of the fuel.

One final parameter of interest, which is calculated from the pressure data, is the ringing intensity [36]. The ringing intensity is a semi-empirically derived correlation which expresses the extent of ignition induced ringing in the combustion chamber. It is calculated as:

$$\text{Ringing Intensity} \approx \frac{1}{2\gamma} \frac{\left(\beta \frac{dP}{dt}_{\max}\right)^2}{P_{\max}} \sqrt{\gamma R T_{\max}} \qquad \text{(Eq. 4.16)}$$

where γ is the minimum of the specific heat ratio, β is a scaling factor that expresses the ratio of the measured amplitude of pressure oscillations over the maximum rate of pressure rise (set to 0.05 s^{-1} here), R is the gas constant for the mixture, and T_{max} is the maximum mass averaged in-cylinder temperature calculated from Eq. 4.7 [36]. According to the original paper by Eng [36], ringing intensities less than 2 MW/m^2 are considered acceptable, however later works by Dec, Saxena, and Bedoya used values of near 5 MW/m^2 [14,16,17,18,20,25,26,27].

5.2.2 Emissions-based computations

As will be discussed in Section 5.3 below, exhaust gases from a cylinder are sampled using a gas analyzer which measures unburned hydrocarbons, carbon monoxide (CO), carbon dioxide (CO_2), oxygen (O_2) and nitric oxides (NO_x). From these measurements the combustion efficiency and emissions indices can be calculated.

The combustion efficiency is an important parameter in determining the extent of fuel conversion for different operating conditions. It differs from the gross indicated efficiency calculated using Eq. 4.15 because it does not include thermodynamic and heat losses, but rather just focuses on the how much fuel energy is remaining in exhaust species that are not fully oxidized. Lower combustion efficiencies will cause lower indicated efficiencies, but it is possible to have lower indicated efficiency while still having high combustion efficiency (for example,

when significant negative work occurs from combustion before TDC). Combustion efficiency is calculated using Eq. 4.17:

$$\eta_{comb} = \frac{m_{fuel} LHV_{fuel} + \Delta H_{NO} n_{NO} - \Delta H_{CO} n_{CO} - LHV_{\text{iso-octane}} n_{\text{iso-octane}}}{m_{fuel} LHV_{fuel}} \quad \text{(Eq. 4.17)}$$

In Eq. 4.17, ΔH represents the enthalpy of formation of a given species, and n represents the number of moles of the given species. Eq. 4.17 is an energy analysis which considers how much unreleased energy is present in different exhaust emissions as a ratio of the total provided fuel energy. It is assumed that all NO_x exits the engine in the form of NO, and all unburned hydrocarbon are in the form of unburned iso-octane.

The exhaust gas analyzer reports exhaust species as mole fractions (either ppm or percent). Prior to entering the gas analyzer, the engine exhaust gases pass through a condenser which removes water. As a result, care must be taken in estimating the number of moles of a given species and corrections must be made to account for the water that was removed from the exhaust gases prior to entering the gas analyzer.

Reporting emissions in units of ppm or percent has limited usefulness because emissions regulations are typically specified in grams of pollutant per kWh of work output. For example, US2010 regulations for NO_x are specified as 0.27 g NO_x/kWh. The indicated specific NO_x emissions are calculated using Eq. 4.18:

$$ISNO_x = \frac{m_{NO_x}}{\sum_{\theta=-180°}^{+180°} P(\theta) dV(\theta)} \quad \text{(Eq. 4.18)}$$

The mass of NO_x emissions are estimated using ppm measurements from the exhaust gas analyzer, with corrections for water being removed from the gases prior to sampling. Eq. 4.19 shows the calculation for the mass of NO_x in exhaust gases and assumes that all NO_x exits the engine in the form of NO.

$$m_{NO_x} = M_{NO} \left(\frac{ppm_{NO_x}}{10^6} \right) \left(\frac{m_{inducted}}{M_{burned}} \right) \left(1 - x_{H_2O} \right) \quad \text{(Eq. 4.19)}$$

The mole fraction of water in Eq. 4.19 is estimated from the major exhaust species for a lean-burning chemical reaction as shown in Eq. 4.9.

5.3 Data acquisition and control system

A data acquisition and control system is attached to the engine to perform real-time analysis and control of the engine combustion. This system combines several sensors and actuators attached to a National Instruments hardware infrastructure with Labview as the control software.

As shown in Figure 5-2, thermocouples are connected at various locations on the engine. All thermocouples are type K, and a complete list of the thermocouple locations is presented in Table 5-2:

TC Name	TC Location
T_{amb}	Ambient air temperature – before heater
T_{heater}	Air temperature immediately following heater
$T_{1,in}$	Cylinder 1 intake – after fuel injector
$T_{2,in}$	Cylinder 2 intake – after fuel injector
$T_{3,in}$	Cylinder 3 intake – after fuel injector
$T_{4,in}$	Cylinder 4 intake – after fuel injector
$T_{1,Ex}$	Cylinder 1 exhaust
$T_{2,Ex}$	Cylinder 2 exhaust
$T_{3,Ex}$	Cylinder 3 exhaust
$T_{4,Ex}$	Cylinder 4 exhaust
$T_{cool,in}$	Coolant into engine
$T_{cool,out}$	Coolant out of engine
$T_{oil,in}$	Oil into engine
$T_{oil,out}$	Oil out of engine

Table 5-2 - Location of Thermocouples

Each engine cylinder is fitted with an in-cylinder pressure transducer and one spark-plug ion sensor. The pressure transducer is used to compute heat release rates, ringing intensity, and mass-averaged charge temperature (discussed further in Section 5.2). The spark-plug ion sensors are used in determining the time occurrence of combustion and in providing a second method to measure ringing.

There are five separate sampling points for exhaust gas analysis. One sampling port is installed on each cylinder's exhaust manifold for individual sampling of cylinder exhaust gases, and one sampling port is installed further downstream allowing simultaneous sampling of the overall engine emissions (from all four cylinders). The exhaust gases are drawn using a vacuum pump to a Horiba gas analyzer, which includes separate analyzers to determine concentrations of unburned hydrocarbons, oxygen, carbon monoxide, carbon dioxide and nitric oxides. The type of each analyzer is listed below in Table 5-3. It should be noted that the exhaust samples pass through a condenser which removes the water content in the exhaust samples (this is required to prevent damage to the exhaust gas analyzers).

Analyzed Gas	Type of Analyzer
Unburned hydrocarbons	Flame ionization detector
Oxygen	Magneto-pneumatic analyzer
Carbon monoxide	Infrared analyzer
Carbon dioxide	Infrared analyzer
Nitric oxides	Chemiluminescent analyzer

Table 5-3 - Types of exhaust gas analyzers utilized

Each cylinder is equipped with a throttle valve to control combustion timing (discussed further in Section 5.3.1). Fuel injection is performed using separate injectors in each intake manifold, and feedback control is performed using separate lambda sensors in each exhaust manifold (discussed further in Section 5.3.2). By combining the controllers for combustion timing, and

fuel injection a wide variety of engine operating set points can be maintained, including control of equivalence ratio, power output and combustion time.

5.3.1 Control of combustion timing with fast thermal management

The CA50 computed from in-cylinder pressure data serves as the feedback input parameter for the fast thermal management (FTM) system, which provides control of the combustion timing. By comparing the CA50 set point with the computed CA50 from the previous thermodynamic engine cycle, the system adjusts the intake charge temperature to either advance or delay the CA50. As shown in Figure 5-4, hotter intake temperatures result in combustion timing advance, while cooler temperatures result in a timing delay. As shown in Figure 5-2, the intake temperature is controlled by adjusting the relative amounts of mass flow of hot air and cold (room temperature) air. A throttle valve is installed on the cold air side, and a PID controller adjusts the position of this throttle to adjust the combustion timing.

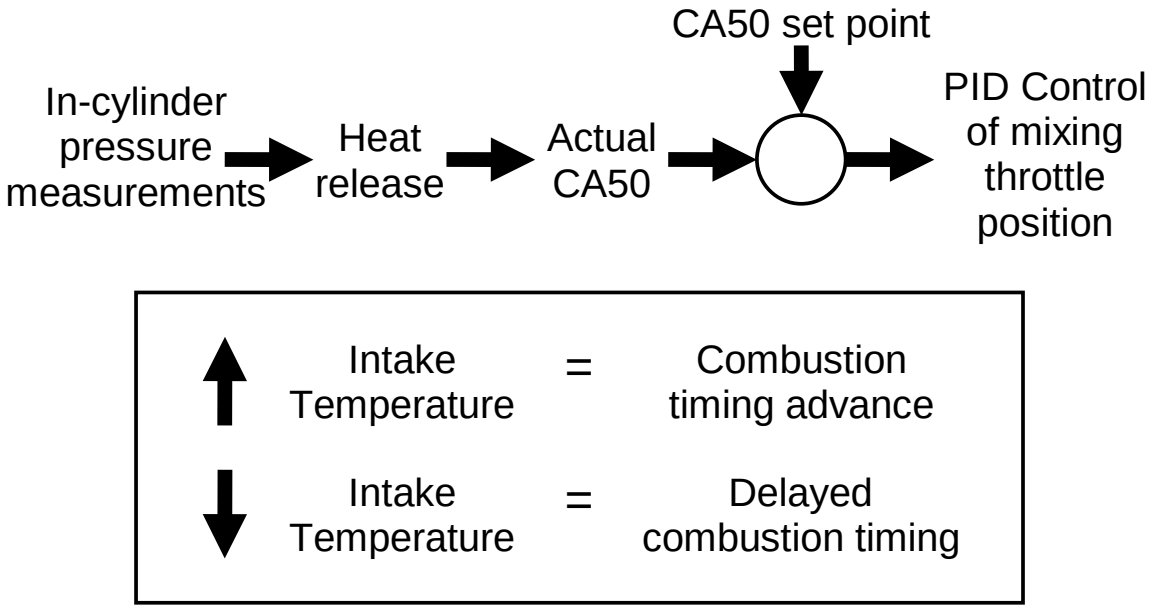

Figure 5-4 - Control methodology for fast thermal management system

5.3.2 Fuel injection control

As shown in Figure 5-2, fuel is injected in the intake manifolds following the mixing of hot and cold air. Each cylinder has its own fuel injector, allowing individual control of equivalence ratios. Each fuel injector is connected to a 12 V battery through a solid state relay allowing control of the amount of fuel injected by pulse width variation. The control side of the relays are connected to counter/timer outputs of the Labview data acquisition system to generate the pulse trains for fuel injector control. Figure 5-5 shows a schematic of the electrical connections for fuel injector control system.

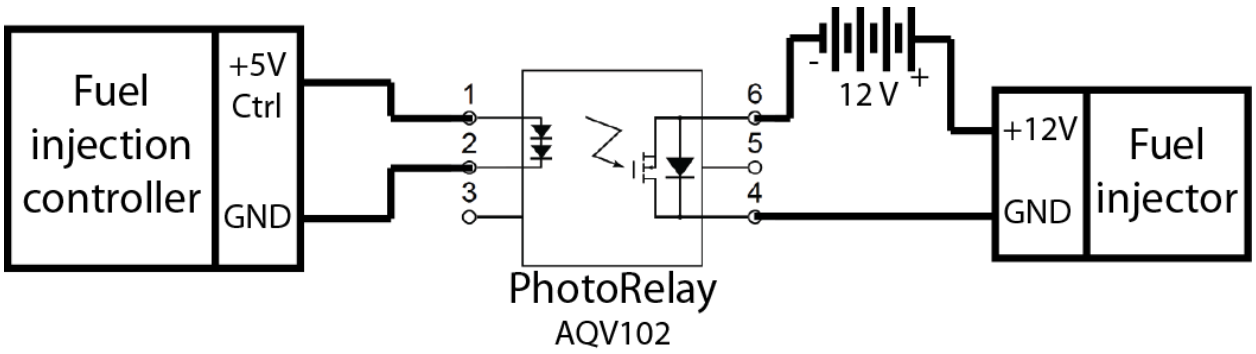

Figure 5-5 - Electrical connections for fuel injectors of each cylinder

The exhaust manifold of each cylinder has an Innovate Motorsports LC-1 wideband lamda sensor installed in the exhaust stream. These lambda sensors generate an analog voltage output that is proportional to the oxygen or unburned fuel fraction in the exhaust. By connecting the lambda sensors to the Labview data acquistion system, feedback control is performed on the fuel injector pulse width to ensure that specified equivalence ratio set points are maintained.

Using the pulsewidth of fuel injection and the intake pressure for a given operating point, the flowrate of fuel into the cylinder (and therefore also the mass of fuel injected per thermodynamic cycle) can be estimated using an equation of the form Eq. 4.20:

$$\dot{m}_{fuel} = \left(a \cdot P^{-b}\right) PW \qquad \text{(Eq. 4.20)}$$

In Eq. 4.20, the fuel flowrate is measured in g/min. P is the intake pressure (bar), and PW is the pulsewidth duration that the fuel injector is open (ms). a and b are tuning parameters that are determined from measurements of fuel flowrate over a range of intake pressures from naturally aspirated to 2.2 bar, and pulsewidths ranging from 2 to 20 ms.The fuel flowrates for these calibrations are performed by installing a scale underneath the fuel tank, and then measuring the change in mass for a given fuel injection condition for a predefined time period.

6 Power output in HCCI engines

6.1 Factors affecting power output

Power output in an HCCI engine is dependent on many other parameters for a given operating condition. Some of the factors affecting power output are expressed in Eq. 5.1:

$$\text{Power} = f(\phi, P_{in}, CA50, \omega, \dot{Q}_{out}, fuel, \%EGR) \qquad \text{(Eq. 5.1)}$$

In Eq. 5.1, power output is usually expressed as gross indicated mean effective pressure ($IMEP_g$), ϕ is the fuel-air equivalence ratio, P_{in} is the intake charge pressure, CA50 is the combustion timing as indicated by crank angle degree for 50% heat release, ω is the engine speed in revolutions per minute (RPM), $\dot{Q}_{out}$ is the rate of heat loss from the cylinder gasses to the walls, fuel is the type of fuel utilized, and %EGR is the fraction of exhaust gas recirculation that is included in the intake charge.

The combustion timing is controlled on the experimental engine using a fast thermal management system (illustrated in Figure 5-4), where the intake air temperature is used as a control mechanism in determining the combustion timing. Hotter intake temperatures cause earlier combustion timings because they result in faster rates of chemical reaction. The combustion timing is also affected by intake pressure, engine speed, heat transfer, fuel type, and EGR. As a result of the large number of factors affecting combustion timing (many of which are not directly controlled), feedback control through the thermal management system is required to maintain steady combustion timing.

The rate of heat loss from the engine can have significant effects on the overall power output. At conditions which result in high in-cylinder gas temperatures (such as at high equivalence ratios, or advanced combustion timings) higher rates of heat loss cause greater losses in overall efficiency and power.

Different fuels also affect power output, namely in their energy density and the modes of heat release for the given fuel. For HCCI combustion, which is primarily driven by chemical kinetics, an important fuel consideration is the extent to which a given fuel displays low temperature heat release (LTHR) characteristics. LTHR is where a fuel begins chemical reactions which lead to overall temperature rise at temperatures below 1000 K. In typical hydrocarbon fuels which exhibit LTHR, these low temperature reactions are usually extinguished at higher temperatures prior to reaching the hot ignition point. This behavior is referred to as a negative temperature coefficient, where heat release is lower at temperatures slightly higher than the low temperature heat release range. The fuel utilized in this study is commercial grade 91-octane gasoline as sold in California. This type of gasoline includes up to 10% Ethanol. Prior experimental and numerical studies have shown that gasoline exhibits little LTHR behavior over most operating conditions, however recent studies by Dec and Yang [14] have shown that gasoline shows an intermediate temperature heat release (ITHR) under conditions with elevated intake pressures. Further details and references regarding ITHR in Gasoline are given in section 3.4.

Exhaust gas recirculation is the addition of burned gases from previous cycles into the intake charge. These burned gases are non-reactive (except for leftover oxygen) and provide a means for achieving further charge dilution without changing the fuel-air equivalence ratio. In HCCI, the addition of EGR can be used for reducing excessive heat release rates.

Table 6-1 lists the range of equivalence ratios, intake pressures and combustion timings explored on all four cylinders in this study. The intake temperatures were set at appropriate levels for the desired combustion timings at the various equivalence ratios and boost pressures.

Parameter	**Range Tested**
Equivalence Ratio	0.20 – 0.50
Intake Pressure	1.0 – 2.0 bar Abs
Combustion timing	0 to ~20 deg ATDC

Table 6-1 - Range of parameters explored on the VW TDI HCCI Engine

6.2 The ringing limit

Ringing in HCCI engines is the occurrence of pressure waves that can cause an undesired audible noise in extreme cases. Even in inaudible cases, these pressure waves can damage an engine over time. Ringing occurs in conjunction with excessive pressure rise and heat release rates, and thus steps must be taken to avoid the harsh combustion regimes that cause these rapid pressure rise rates. Figure 6-1 shows an in-cylinder pressure trace for an operating condition which exhibits intense ringing. The pressure oscillations observed between -1 and 10 CAD are the physical manifestation of ringing.

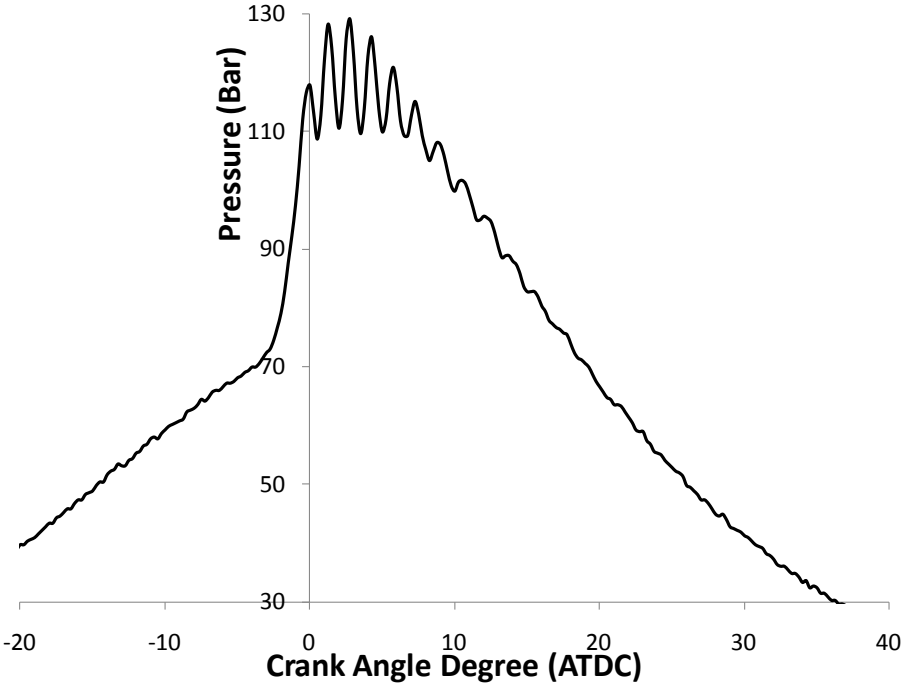

Figure 6-1 - In-cylinder pressure for a condition exhibiting intense ringing

The high frequency pressure oscillations depicted in Figure 6-1 are a manifestation of ringing, and these pressure oscillations are caused by pressure waves which propagate throughout the combustion chamber. Although HCCI is idealized as being a uniform autoignition event of the entire in-cylinder fuel-air mixture at once, in reality the ignition occurs sequentially over a short time at different spatial locations throughout the mixture. These sequential ignition events are caused by significant differences in localized temperatures which arise during the compression stroke. Laser diagnostic studies in optical-access HCCI engines [65,66] have quantified the spatial distribution of hotter and cooler zones in motoring and firing engines. These studies suggest that the temperature difference between the coldest and hottest zones in the core fluid at TDC can be as large as 100 K. These thermal gradients typically do not arise until the last 20 to 30 crank angle degrees before TDC [65].

Ringing coincides with higher load conditions; however, sequential ignition from thermal gradients will likely arise at all operating points (including lower loads). The pressure waves indicative of ringing, however, do not arise at lower load conditions (with lower fuel content). This may be caused by the pressure waves from sequential ignition being dampened enough to make the pressure waves undetectable with in-cylinder pressure sensing. At higher load conditions (with higher fuel content), however, enough acoustic energy is released from these sequential ignitions to cause detectable pressure waves. Furthermore, at higher load conditions, it is possible that there is constructive interference where the pressure wave from an early localized ignition causes ignition in different locations in a way that amplifies the early pressure waves. Finally, it is possible that the higher equivalence ratios at high load conditions influence the temperature sensitivity of fuel reactivity to further facilitate sequential ignitions which cause ringing.

Ringing differs from knocking in that knocking is caused by end-gas autoignition in a spark-ignited engine. In HCCI, autoignition is desired and the fuel-in-air mixture autoignites relatively uniformly. Both knocking and ringing cause pressure waves that can be measured using in-cylinder pressure transducers, however ringing typically has the majority of its acoustic wave energy in the 5 to 6 kHz frequency range, while knocking contains more energy in the 8 to 25 kHz range. The amplitude of pressure pulsations in HCCI can be an order of magnitude larger than knocking in spark-ignited engines, however cylinder linings can significantly dampen wave energies below 8 kHz [36]. This dampening effect can make it more difficult to detect ringing using externally mounted sensors.

A well accepted correlation to quantify ringing behavior using in-cylinder pressure measurements was derived by J.A. Eng (shown in Eq. 4.16). Numerous studies have demonstrated the ability of the ringing intensity correlation in Eq. 4.15 to quantify the extent of ringing over a wide range of engine operating conditions [14,20,36]. An acceptable limit for the maximum acceptable ringing intensity used in some studies is 5 MW/m^2 [14,20].

The primary method for avoiding ringing in an HCCI engine is to use highly dilute fuel-in-air mixtures. This can be accomplished with high fractions of EGR, or with lean equivalence ratios. The side effect of using diluted mixtures is that it causes lower power output, and thus other strategies must be used to control ringing while using richer fuel mixtures. One alternative strategy is to use highly delayed combustion timing since there is a higher rate of piston

expansion for a given engine speed at later crank angles after TDC. The faster piston expansion at later combustion timings counteracts the rapid heat release (and pressure rise) from autoignition, thereby causing lower ringing. A further strategy for reducing peak heat release rates (and therefore ringing intensities) is to use moderate amounts of temperature or mixture stratifications. Temperature stratifications cause spatial variations in the rates of chemical reaction to allow the hotter spatial zones to autoignite prior to the cooler zones [19]. Mixture stratifications can have a similar effect, however this strategy is only effective for fuels which exhibit ϕ-sensitivity (usually fuels with LTHR) [15]. Temperature stratification can be difficult to control in a production engine, however mixture stratifications can be easily achieved in an engine with direct injection by using multiple injection or late injection strategies.

6.3 The peak in-cylinder pressure limit

The peak in-cylinder pressure limit is a design consideration that is specific to a given engine. For the modified Volkswagen TDI engine used in this study, the peak pressure limit is 130 bar (absolute). The limit is determined by the high pressure capabilities of engine components such as the piston rings and head gasket which can be damaged by excessive pressures. Prolonged exposure to excessive pressure for these components can cause leaks to develop which will allow blowby and poor compression, and ultimately result in unburned fuel escaping from the engine. Figure 6-2 shows an in-cylinder pressure trace and the peak-pressure limits for the Volkswagen TDI engine used in this study.

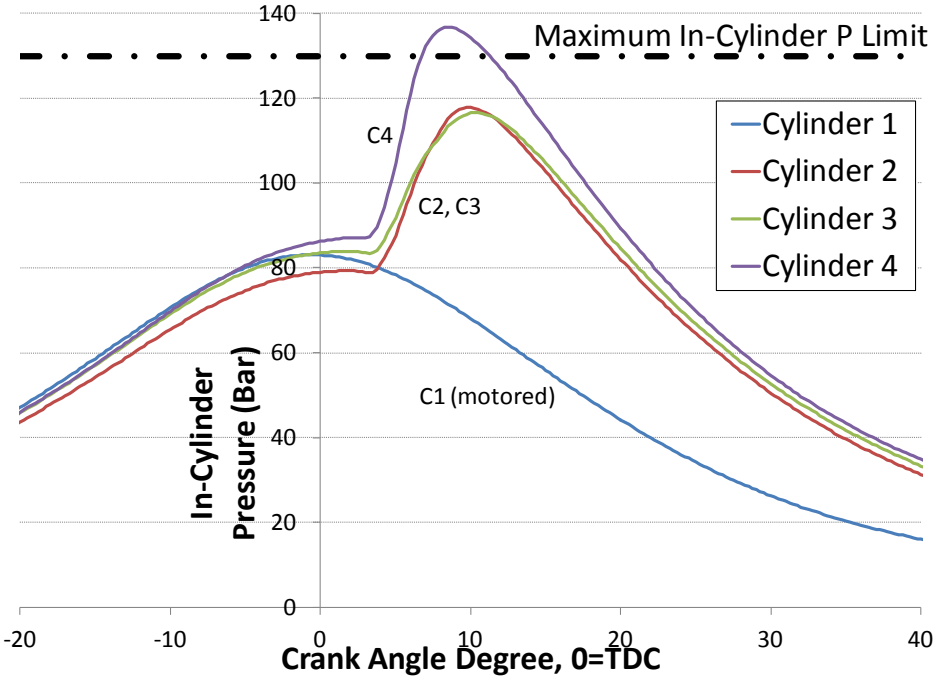

Figure 6-2 - Pressure trace showing VW engine in-cylinder peak pressure limits

Excessive in-cylinder pressures can be caused by a number of factors, including: 1) high intake pressures combined with high equivalence ratios which lead to high peak combustion pressures, 2) excessive ringing, which can cause the upper peak of the pressure pulsations (illustrated in Figure 6-1) to exceed the in-cylinder pressure limits, 3) early combustion where the heat release

and pressure rise from the combustion event occurs in a smaller volume, thereby producing high pressures, and 4) a misfiring cycle followed by a burning cycle which can cause more fuel to be present in a given cycle (although this is not a major problem in the VW TDI engine because of the 3 degree positive valve overlap). The peak in-cylinder pressure can be kept within safe limits through strategies that avoid these conditions. Aside from simply using lower equivalence ratios, and lower intake pressures, which will also cause lower power output, the use of more prolonged heat release and delayed combustion timing is an important technique in avoiding peak pressure limits. More prolonged heat release will cause the pressure rise from combustion to be more gradual, thus allowing piston expansion to play a more significant role in avoiding excessively high pressures. The use of delayed combustion timing allows the pressure rise to occur at a time when the cylinder volume is greater, and takes advantage of the faster rate of piston expansion that occurs with later combustion timings (illustrated in Figure 4-1 on page 21). The use of more gradual heat release and delayed combustion timing also help avoid ringing which prevents high pressure spikes from exceeding the peak-pressure limits.

6.4 The misfire limit

Misfire occurs when insufficient energy is provided to allow the fuel to reach its hot ignition point (see Chapter 3 for an explanation of hot ignition). As a result of the failure to ignite, in-cylinder pressures after top-dead-center remain low, resembling a motoring pressure trace. Little to no power is produced from a misfiring cycle, and a large amount of unburned fuel exits the engine through the exhaust manifold. Figure 6-3 illustrates the difference between a burning cycle and a misfiring cycle.

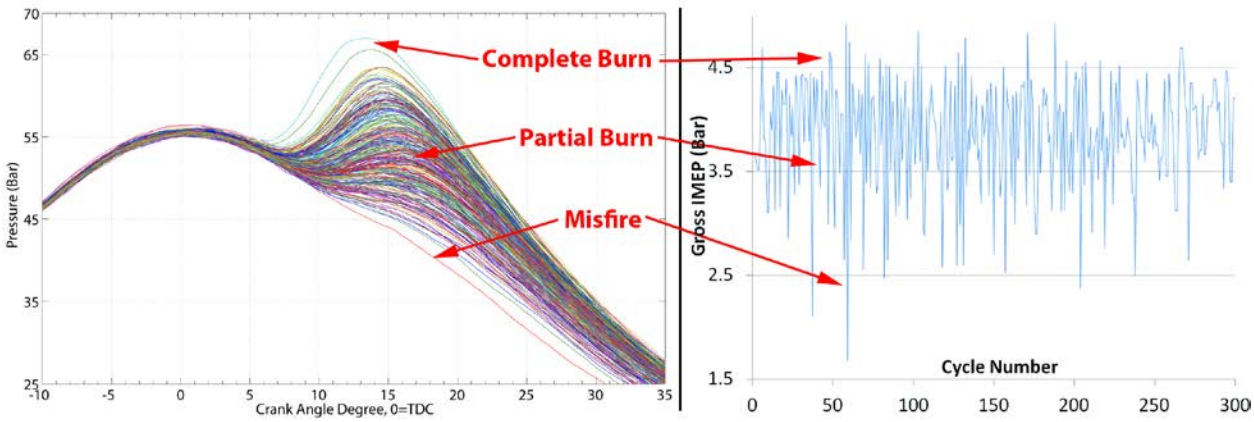

Figure 6-3 - In-cylinder pressure traces and gross IMEP for 300 consecutive cycles at an unstable operating point. Demonstrates burning cycles, partially burning cycles and misfiring cycles

As will be discussed in Chapter 7, the use of delayed combustion timing is very important for avoiding ringing and excessive efficiency losses from heat transfer. In some cases, it is desirable to delay the combustion timing right up until the point of misfire. In these cases a given cycle can misfire because piston expansion produces a quenching effect on the chemical reactions prior to the occurrence of hot ignition. As discussed in Section 3.4, the ITHR behavior of gasoline is critical for allowing delayed combustion timing since it counteracts the cooling effect

from piston expansion after TDC. This ITHR behavior increases with lower intake temperatures and with higher intake pressures up to a maximum at 1.8 bar (absolute) [14,16,20].

6.5 Low intake temperature limits

There are many techniques in HCCI for providing the energy required for achieving autoignition. Some methods include the use of higher intake temperatures, higher intake pressures, higher compression ratios, retaining hot EGR to heat the fuel-air mixture, or using fuels with greater reactivity. For the power output results presented in Chapter 7, high intake temperatures and high intake pressure are used in controlling the ignition timing, while all the other factors remain constant. As higher intake pressures were used, the requirement for higher intake temperatures was decreased in order to achieve combustion at a desired timing. If sufficiently high intake pressures are used for gasoline, another constraint is introduced because intake temperatures below ambient temperature would be required to avoid combustion before top-dead-center. Figure 6-4 illustrates how the intake temperature requirements decrease towards the low intake temperature limits when intake pressure is increased for gasoline-fueled experiments.

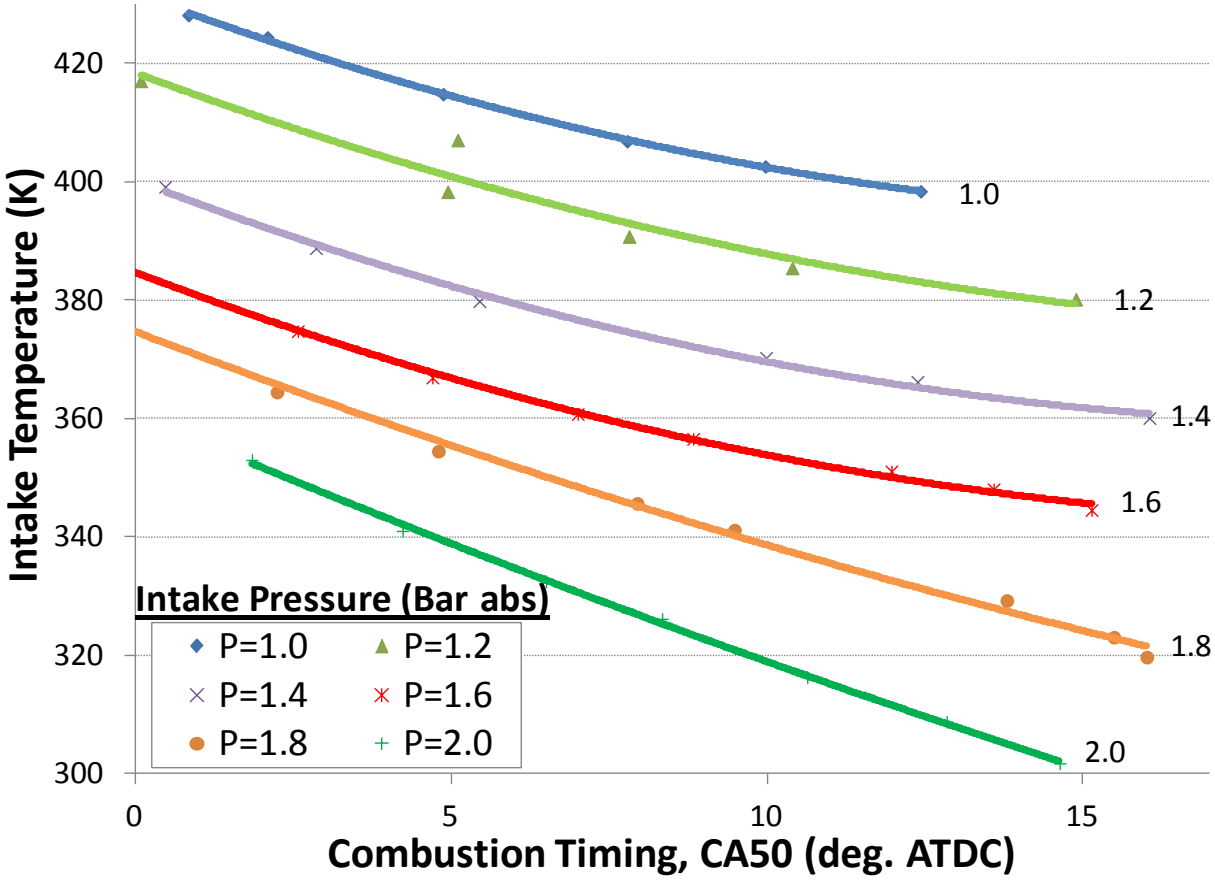

Figure 6-4 - Intake temperature requirements for maintaing constant combustion timing at different intake pressures
ϕ=0.45, 91-Octane Commercial Grade Gasoline, CR=17:1, 1800 RPM

Aside from simply avoiding the use of high intake pressures (which would subsequently constrain the maximum power output), one strategy for avoiding the low intake temperature limits is to use EGR to dilute the in-cylinder mixture. Studies by Dec et. al. [14], for example, use intake temperature as a control technique for combustion timing only up to the point where intake temperatures of 60°C are required. For conditions that would normally require lower intake temperatures, for example when using higher intake pressures, EGR is used to induce the required combustion timing delays.

6.6 Efficiency and emissions limits

In addition to considering the limits discussed in Sections 6.2 through 6.5, the overall efficiency and emissions at a given operating point should be considered as further limits. Operating points with poor overall efficiency or excessively high emissions should be avoided and an engine control system should be designed which considers these factors as part of its control strategy. In summary, the research discussed in chapter 6 shows:

1. Efficiency and power output are lower when the combustion timing is too early, or too late, and with increasing equivalence ratio the optimal efficiency and optimal power output occur with later combustion timings
2. Unburned hydrocarbon and carbon monoxide emissions are higher with conditions resulting in lower in-cylinder temperature, such as with excessively delayed combustion timing
3. Nitric oxide emissions are higher with conditions resulting in higher in-cylinder temperature, such as with excessively advanced combustion timing.

Detailed discussions regarding efficiency and emissions trends are discussed in Chapter 7.

7 Strategy for maximizing power output

In exploring detailed results for single-cylinder operation on cylinder 3 are first discussed, followed by multi-cylinder results. The trends presented in Figure 7-1 through Figure 7-16 for single-cylinder operation are identical to those seen in multi-cylinder operation. Single-cylinder mode is used because finer control of variables and more steady operation is possible on this research engine. The one key side-effect of operating in single-cylinder mode is that heat loss from the in-cylinder charge is enhanced because the engine block, oil and coolant are at lower temperatures, and heat sources from adjacent cylinders undergoing combustion processes are not present. This enhanced heat loss causes lower power output, lower efficiency, and slightly lower peak in-cylinder temperatures. Although the trends for power output, efficiency and in-cylinder temperature are identical between single-cylinder and multi-cylinder mode, the power output and efficiency results are also shown for multi-cylinder operation for thoroughness.

7.1 Effects of equivalence ratio and combustion timing (in single-cylinder mode)

For the experimental results presented in Figure 7-1 through Figure 7-8, the intake pressure was maintained constant at 1.8 bar absolute pressure, and different equivalence ratios and combustion timings were explored for their effects upon power output, ringing, emissions and efficiency.

Figure 7-1 shows the power output (as gross indicated IMEP) for different equivalence ratios and combustion timings. Gross IMEP is used instead of net IMEP because these experiments use an external compressor for providing the boost pressure, without adding exhaust backpressure. This results in net IMEP being artificially high, while gross IMEP allows separation of the effects of boost pressure. The results in Figure 7-1 show, as expected, that power output is higher with increased equivalence ratios. The test points for the lower equivalence ratios also show decreasing IMEP as the combustion timing is delayed further and this lower power output is caused by lower peak in-cylinder pressures and lower combustion efficiencies at delayed combustion timings (shown in Figure 7-4). Further delayed combustion timings (beyond roughly 15 degrees ATDC) were not explored because misfire was highly prevalent beyond the combustion timings presented. Additionally, the results show lower power output at highly advanced combustion timing (near TDC). This effect, which is more prevalent at higher equivalence ratios, is caused by several factors: 1) increased heat loss from higher peak temperatures (as seen in Figure 7-6), 2) increased heat loss from longer time for heat transfer, 3) increased heat loss because ringing increases the heat transfer coefficient, and 4) for highly advanced combustion timing, the early pressure rise from the autoignition process causes some negative work prior to the piston reaching TDC. An interesting behavior to note is that the highest power output for many equivalence ratios occurs at an intermediate combustion timing (not too early, or too late), however the intermediate timing demonstrating peak power output is increasingly delayed for higher equivalence ratios.

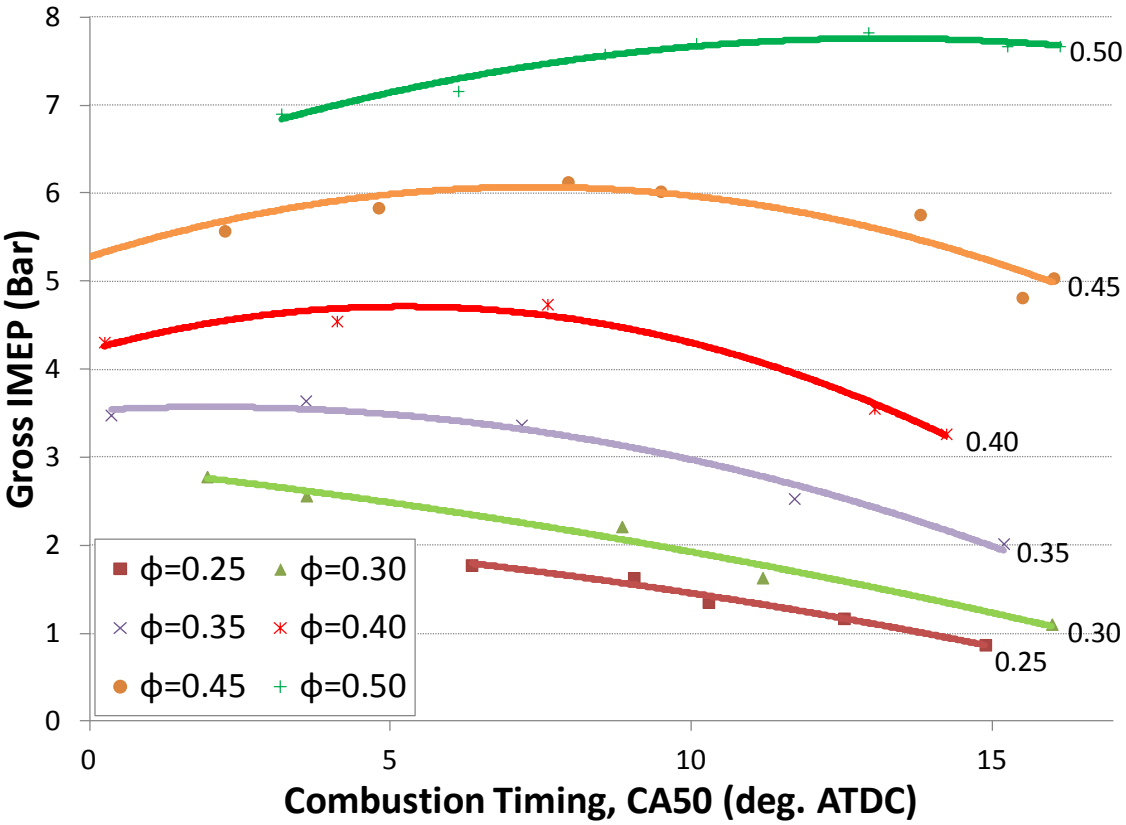

Figure 7-1 - Power output (Gross IMEP) for different equivalence ratios and combustion timings at P_{in}=1.8 bar and 1800 RPM in single-cylinder mode

Figure 7-1 shows that before the occurrence of misfire, power output generally increases with higher equivalence ratios and lowers slightly with highly advanced or highly delayed combustion timing. Figure 7-2 shows the corresponding ringing intensities for the test points in Figure 7-1. Ringing intensity is calculated using the correlation in Eq. 4.16 developed by Eng [36]. A well accepted ringing intensity limit is 5 MW/m^2 based on the onset of audible knocking and the appearance of pressure pulsations [14,36], and this value is indicated as the limit in Figure 7-2.

Figure 7-2 shows that ringing increases with higher equivalence ratios and advanced combustion timings. With a 1.8 bar intake pressure, equivalence ratios at and below 0.35 have acceptable levels of ringing for nearly all combustion timings tested. Beyond ϕ=0.35, ringing becomes unacceptable at advanced combustion timings. As equivalence ratios are increased the ringing limit is encountered at progressively later combustion timings. The results of Figure 7-2 show that highly delayed combustion timings for the highest equivalence ratio (0.50) allow acceptable operating conditions where power output is high while ringing is sufficiently low. The plot also suggests that slightly higher equivalence ratios with sufficiently delayed combustion timing (just prior to misfire) can allow even higher power output.

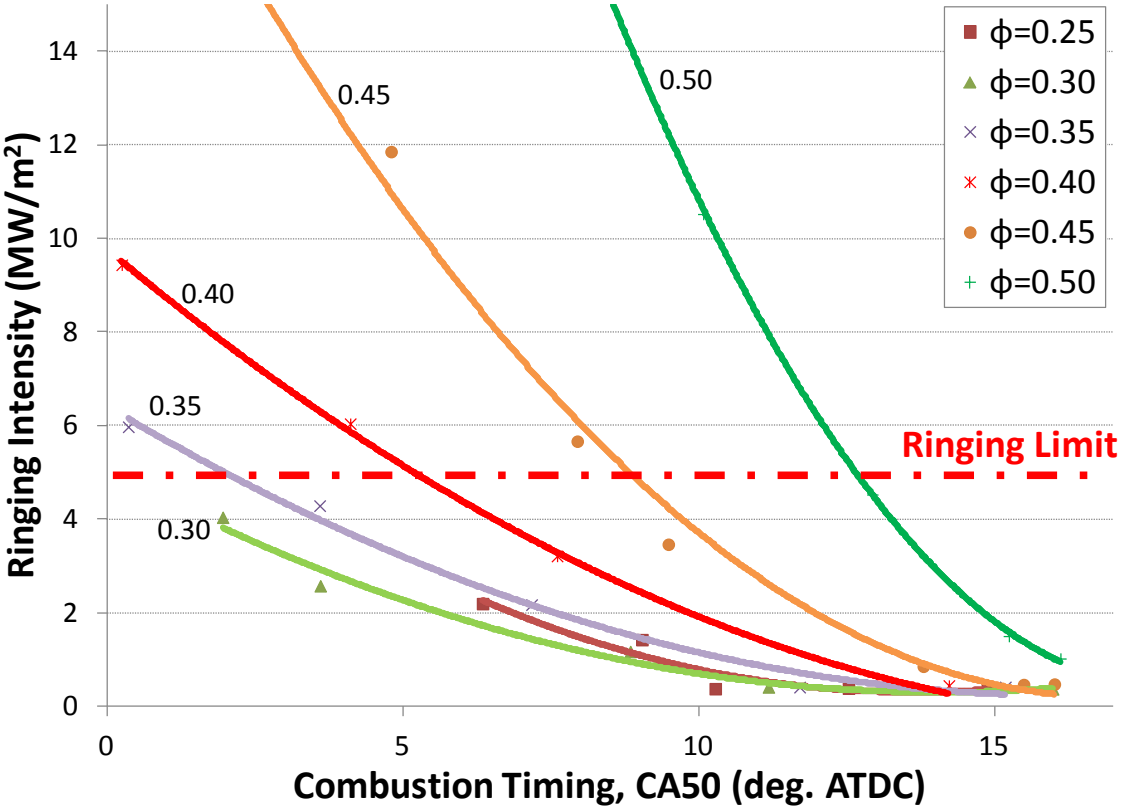

Figure 7-2 - Ringing intensity for different equivalence ratios and combustion timings at P_{in}=1.8 bar and 1800 RPM in single-cylinder mode

As observed in Figure 7-2, the ringing intensity increases with higher equivalence ratios and advanced combustion timings. These increases in ringing intensity can both be explained in terms of the peak pressure rise rate, which constitutes a squared term in Eq. 4.16. Ringing increases with higher equivalence ratios because more energy is released as increased amounts of fuel are provided. More importantly, the rate of this energy release (and thus the rate of pressure rise) in a relatively fast autoignition event is greater for higher equivalence ratios. Ringing increases with advanced combustion timing because the rate of piston expansion counteracting the pressure rise from autoignition is lower at advanced combustion timings.

Figure 7-3 shows the gross indicated efficiency for the different test points in Figure 7-1. It can be seen that beyond a local maxima for each equivalence ratio, the indicated efficiency decreases with delayed combustion timings. This reduction in indicated efficiency with late combustion timings is caused by a combination of reduced combustion efficiencies (shown in Figure 7-4) and lower peak in-cylinder pressures caused by delays in combustion timing. The reduced combustion efficiency at delayed combustion timings is caused by lower peak in-cylinder temperatures (shown in Figure 7-6) which causes incomplete oxidation and thus higher emission of unburned hydrocarbons and carbon monoxide (shown in Figure 7-7 and Figure 7-8). For higher equivalence ratios, it is also apparent that there are lower indicated efficiencies at advanced combustion timings; this is caused by increased heat loss and also negative work at advanced combustion timings. It is worth emphasizing that the highest power output points from Figure 7-1 show the highest indicated efficiency. Figure 7-3 also shows that indicated efficiency

increases for higher equivalence ratios, and this effect can be explained by the higher combustion efficiencies for higher equivalence ratios (shown in Figure 7-4). The higher combustion efficiencies with increased equivalence ratio are explained by referring to the hydrocarbon and CO emissions in Figure 7-7 and Figure 7-8 which show that the ppm levels of hydrocarbons and CO tend to decrease for higher equivalence ratios. This effect of higher combustion efficiency with increased equivalence ratio was also observed by Sjöberg et al. [38], and can be explained by the higher bulk gas temperatures caused by higher equivalence ratios allowing more complete oxidation, and thus higher combustion efficiency. It is worth re-stating that gross indicated efficiencies for a given cylinder operating in multi-cylinder mode were significantly higher (nearing 45% in some cases) than the single-cylinder efficiencies presented in Figure 7-3.

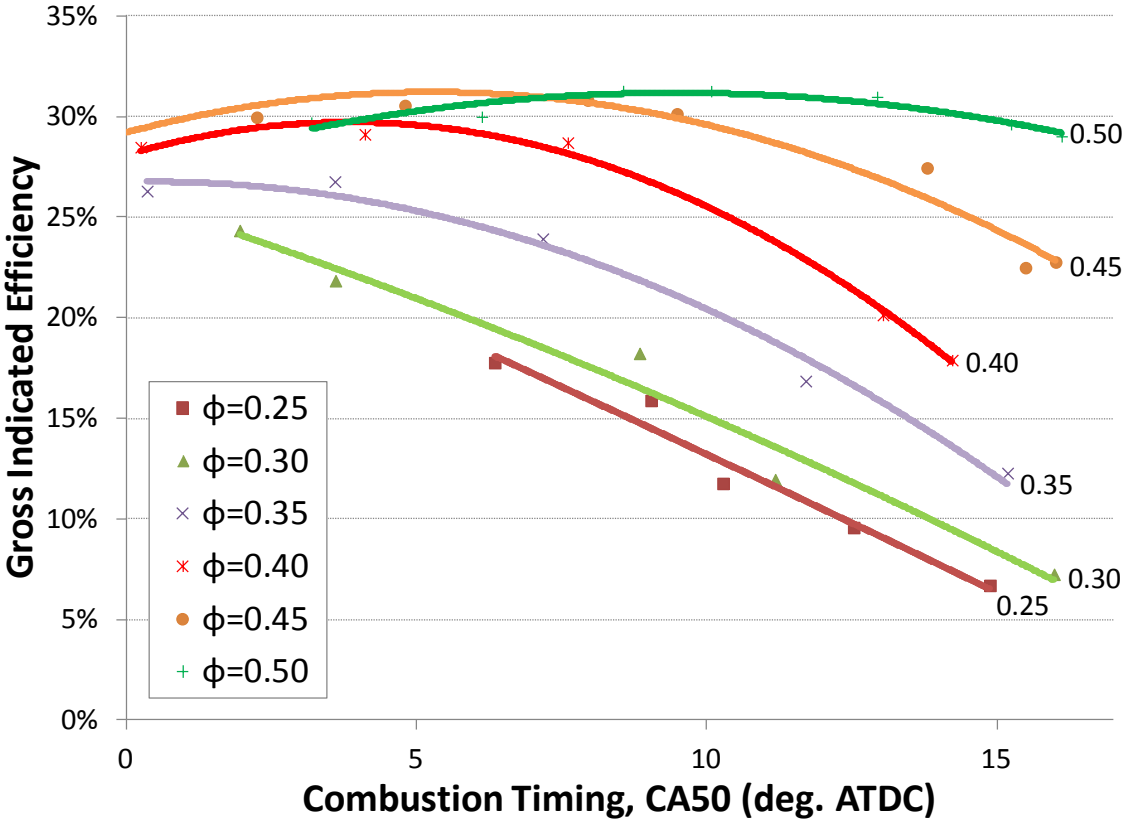

Figure 7-3 –Gross indicated efficiency for different equivalence ratios and combustion timings at P_{in}=1.8 bar and 1800 RPM in single-cylinder mode

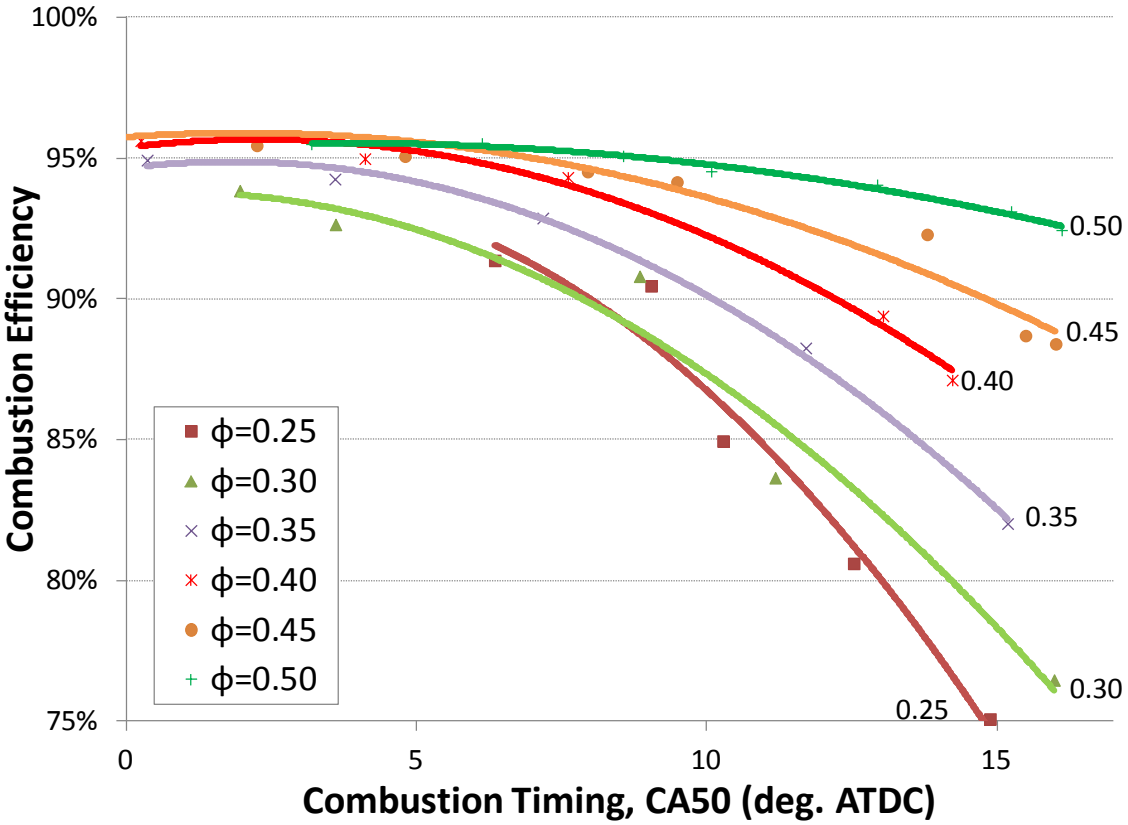

Figure 7-4 - Combustion efficiency for different equivalence ratios and combustion timing at Pin=1.8 bar and 1800 RPM in single-cylinder mode

Figure 7-5 shows the levels of NO_x emissions for the different test conditions from Figure 7-1. The results show that NO_x emissions generally increase with advanced combustion timings and higher equivalence ratios. The trends for NO_x emissions in Figure 7-5 can be partially explained in terms of peak temperatures which are plotted in Figure 7-6. It should be noted that the US 2010 NO_x emission regulations stipulate a maximum of 0.27 g/kWh, thus the NO_x emissions in these tests are between 10 and 140 times lower than the regulated amounts.

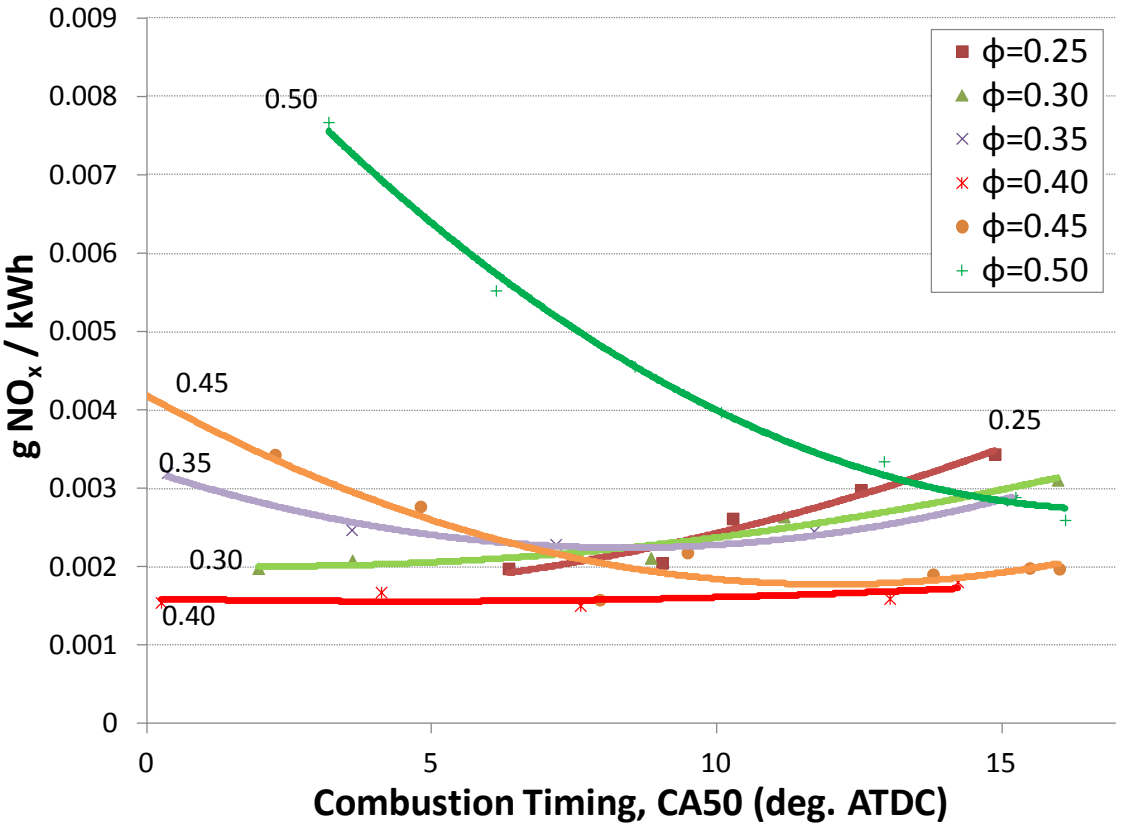

Figure 7-5 - NO_x emissions for different equivalence ratios and combustion timings at P_{in}=1.8 bar and 1800 RPM in single-cylinder mode

Figure 7-6 shows the mass averaged peak in-cylinder temperatures for the different conditions from Figure 7-1. The results show that peak temperature generally increases with higher equivalence ratio and advanced combustion timing. The peak temperature increases with higher equivalence ratio because more fuel energy is available for heating the in-cylinder charge. Peak temperature increases with advanced combustion timing because higher in-cylinder pressures are achieved at earlier combustion timings because of autoignition occurring within a smaller cylinder volume. The temperature trends for ϕ=0.45 and 0.50 can explain the higher NO_x emissions trends from Figure 7-5, where higher peak in-cylinder temperatures correspond with higher NO_x emissions. The lower equivalence ratios, however, defy the trends since there are test conditions with higher mass averaged peak temperatures, but the corresponding NO_x emissions are lower than the ϕ=0.45 and 0.50 conditions. This anomaly may be caused by minor charge stratification, which is enhanced for higher equivalence ratios. Although this hypothesis is difficult to verify in the current setup, it is supported by previous research relating a higher percent of fuel unmixedness to higher NO_x emissions [67]. Since the port fuel-injectors are positioned nearby the intake valves, it is possible that some charge stratification exists by the time TDC of the compression stroke is encountered, thereby causing locally higher temperatures than indicated by the mass averaged values plotted in Figure 7-6. It is worth restating that the mass averaged peak in-cylinder temperatures for a given cylinder were higher for multi-cylinder operation (up to 2200 K) and the NO_x emissions were slightly higher (roughly 1 ppm) as a result.

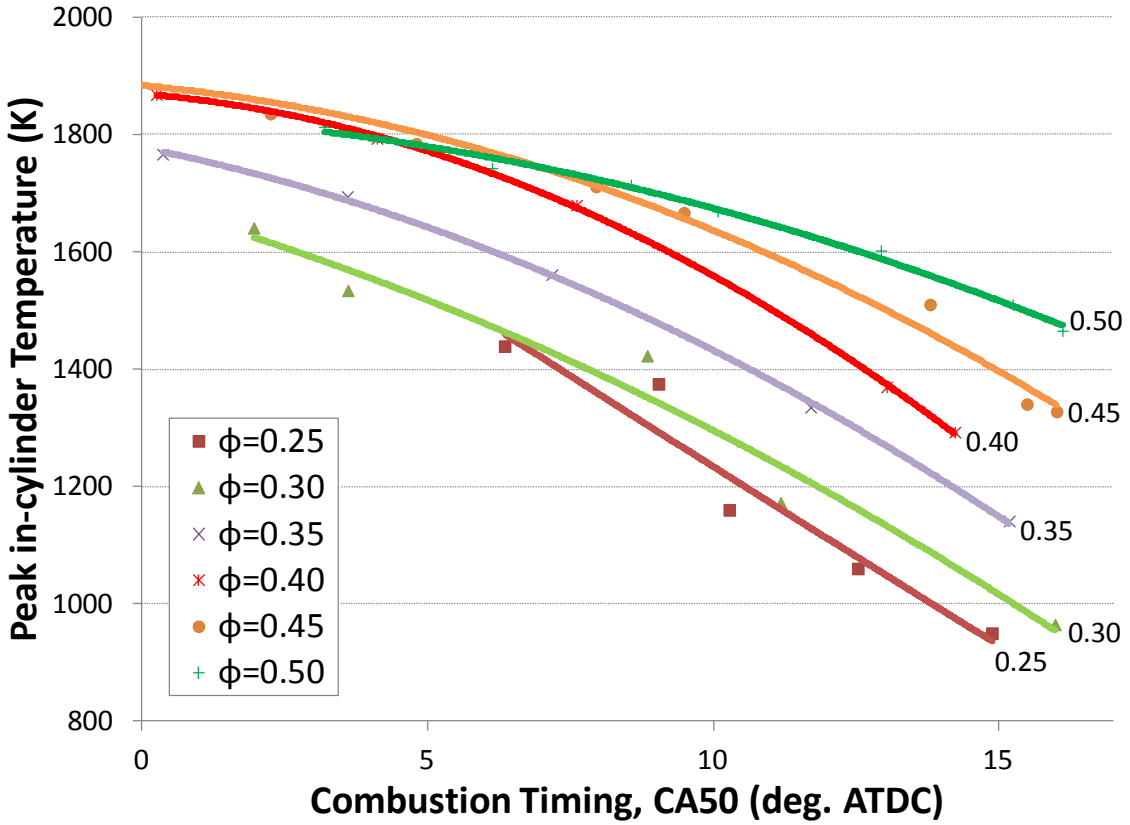

Figure 7-6 - Peak mass averaged in-cylinder temperature for different equivalence ratios and combustion timings at P_{in}=1.8 bar and 1800 RPM in single-cylinder mode

Figure 7-7 and Figure 7-8 show the unburned hydrocarbon and CO emissions for the test points from Figure 7-1. The trends from the two figures show that the hydrocarbon and carbon monoxide emissions increase with lower equivalence ratios and with delayed combustion timing. Unburned hydrocarbon emissions and CO emissions generally increase with delays in combustion timing because the temperatures achieved in the cylinder are too low for complete oxidation (CO oxidation requires roughly 1500 K [38,68]). As a result of the lower temperatures, the concentration of OH radicals, which are critical for the oxidation process, are insufficient for achieving complete combustion. This behavior can be emphasized by referring to Figure 7-6 which shows very low mass-averaged peak temperatures for delayed combustion timings (with some points showing mass averaged temperatures approaching the threshold for the hot ignition regime near 1000 K [33]). For lower equivalence ratios with delayed combustion timing, the peak temperatures are even lower resulting in CO emissions leveling off at very late combustion timings caused by further decreased oxidation of hydrocarbon molecules. The levels of unburned hydrocarbons and carbon monoxide emissions are relatively high, however the exhaust temperatures for similar test points in multi-cylinder mode is between 240 to 260°C. Further investigation is necessary to determine if these exhaust temperatures and high hydrocarbon and carbon monoxide emissions can create conditions that allow an oxidation catalyst to oxidize these harmful emissions if enough energy is provided to initially light off the catalyst.

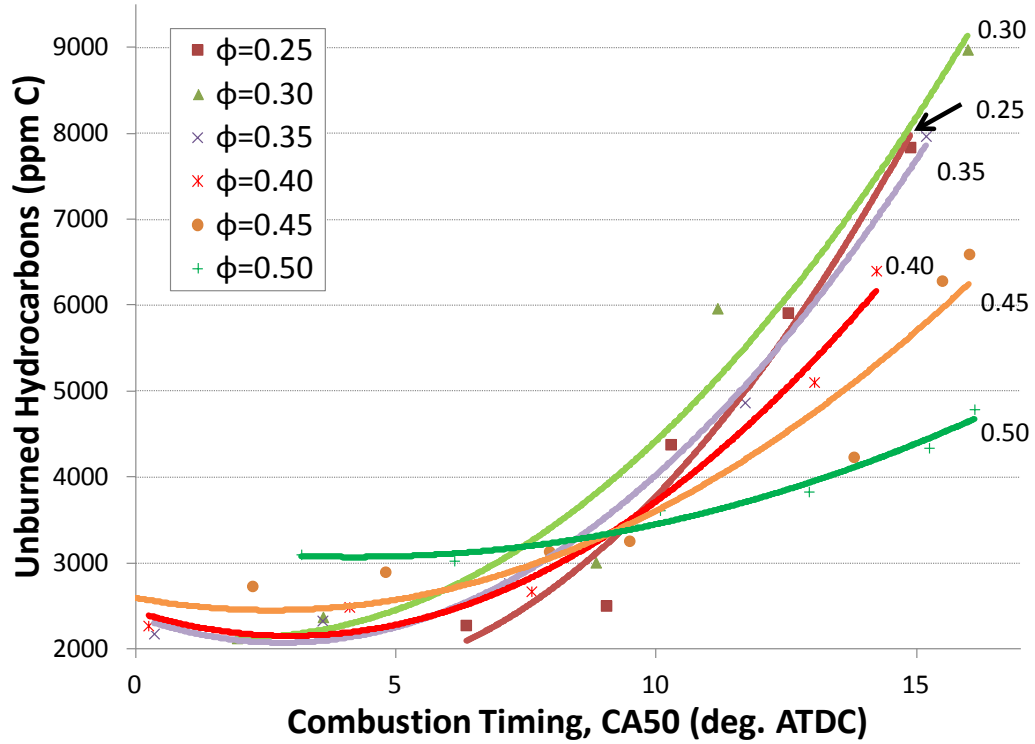

Figure 7-7 - Unburned hydrocarbons for different equivalence ratios and combustion timings at P_{in}=1.8 bar and 1800 RPM in single-cylinder mode

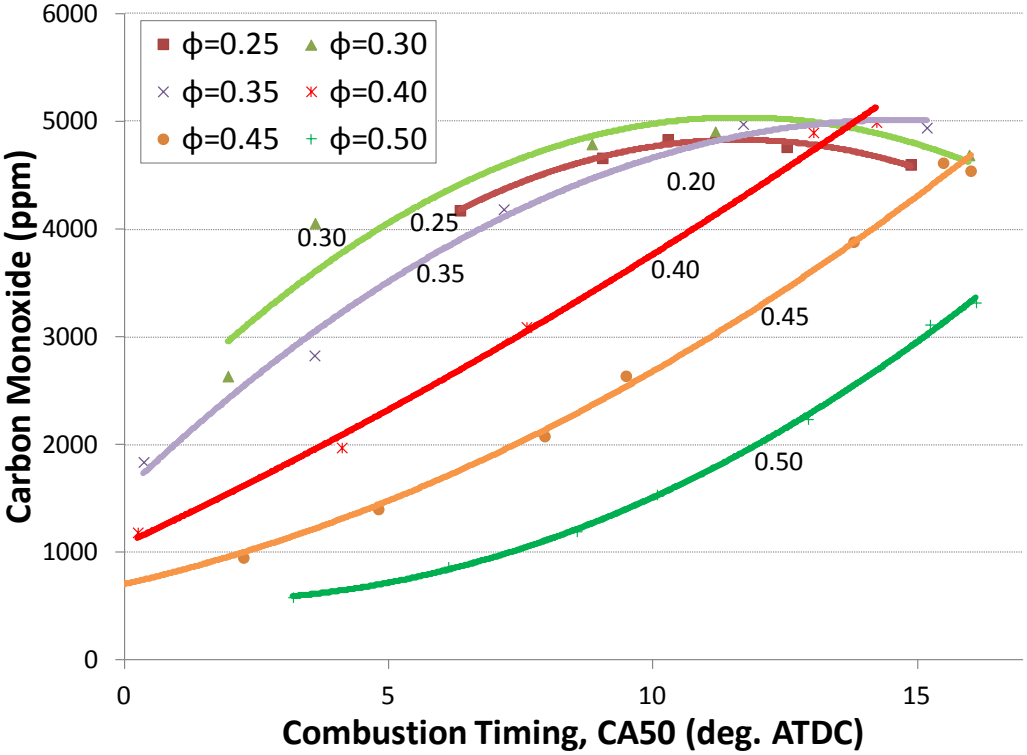

Figure 7-8 - Carbon monoxide for different equivalence ratios and combustion timings at P_{in}=1.8 bar and 1800 RPM in single-cylinder mode

The results summarized in Figure 7-1 through Figure 7-8 show that for a given intake pressure, high power output conditions can be achieved with high equivalence ratios, and ringing can be controlled with delayed combustion timing. The highest efficiency operating points occur at similar operating conditions as the high power output points. The combustion timing can only be delayed until the onset of misfire, and staying well within the misfire limit is advantageous in preventing efficiency losses from low combustion efficiency and thermodynamic losses.

7.2 Effects of intake pressure (in single-cylinder mode)

For constant intake pressure, Figure 7-1 through Figure 7-8 showed the effects of equivalence ratio and combustion timing upon power output and other parameters. In Figure 7-9 through Figure 7-16, the effects of changing intake pressure are explored while equivalence ratio is held constant at ϕ=0.45.

Figure 7-9 shows the power output for different intake pressures. As expected, power output increases with higher intake pressures since more fuel is provided for maintaining a constant equivalence ratio. At high intake pressures, the range of achievable combustion timings is constrained because of ringing and a loss of controllability caused by low intake temperatures (a point which will be addressed in a separate section below). This limited range of achievable combustion timings limits the maximum intake pressure that can be utilized, however other studies [14] have shown that EGR can help in avoiding ringing and thereby increases the operable range of intake pressures.

The power output results of Figure 7-1 and Figure 7-9 agree closely with the non-EGR results of Dec and Yang [14]. In their study, a maximum non-EGR power output of 8.8 bar gross IMEP at an intake pressure of 1.8 bar was identified, while the results of the present study (summarized in Table 7-1) reveal a maximum power output of 9.02 bar gross IMEP at an intake pressure of 1.6 bar. The relative agreement between the Dec and Yang result compared with the present result gives further confidence in the maximum non-EGR power output achievable in an HCCI engine, particularly because different experimental conditions were used in the two studies. In the Dec and Yang study, a larger cylinder volume (0.98 L/cylinder) was used at a slower engine speed of 1200 RPM with a compression ratio of 14:1. The present study uses a cylinder volume of 0.475 L/cylinder with an engine speed of 1800 RPM with a compression ratio of 17:1.

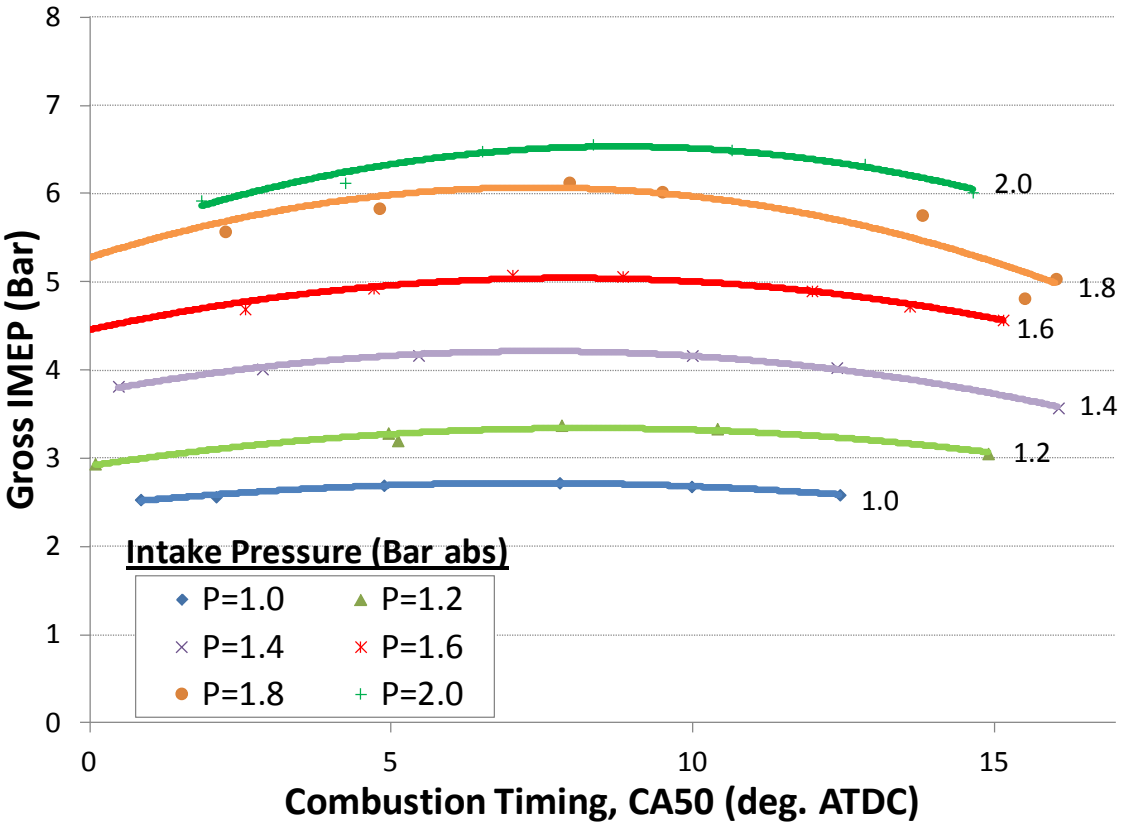

Figure 7-9 - Power output for different intake pressures and combustion timings at ϕ=0.45 and 1800 RPM in single-cylinder mode

As discussed above, the range of achievable combustion timings at high boost pressure is restricted by ringing limits and loss of controllability caused by low intake temperature requirements. Figure 7-10 shows the ringing intensity for different intake pressures. As in Figure 7-2, ringing decreases with delays in combustion timing. Figure 7-10 also shows that for constant equivalence ratios, ringing intensity increases with higher intake pressures. The results show that for a given equivalence ratio, higher intake pressures cause the requirement of later combustion timings to achieve sufficiently low levels of ringing. Thus, as intake pressure is increased, the acceptable operating regions of combustion timing become more narrowly bounded by ringing limits, low temperature controllability limits (not shown in the figure) and misfire limits. Alternatively, operating with higher boost pressures and acceptable levels of ringing can be achieved with lower equivalence ratios, however this will cause limited gains in power output with higher boost pressures, a result which was confirmed in the Dec and Yang study [14].

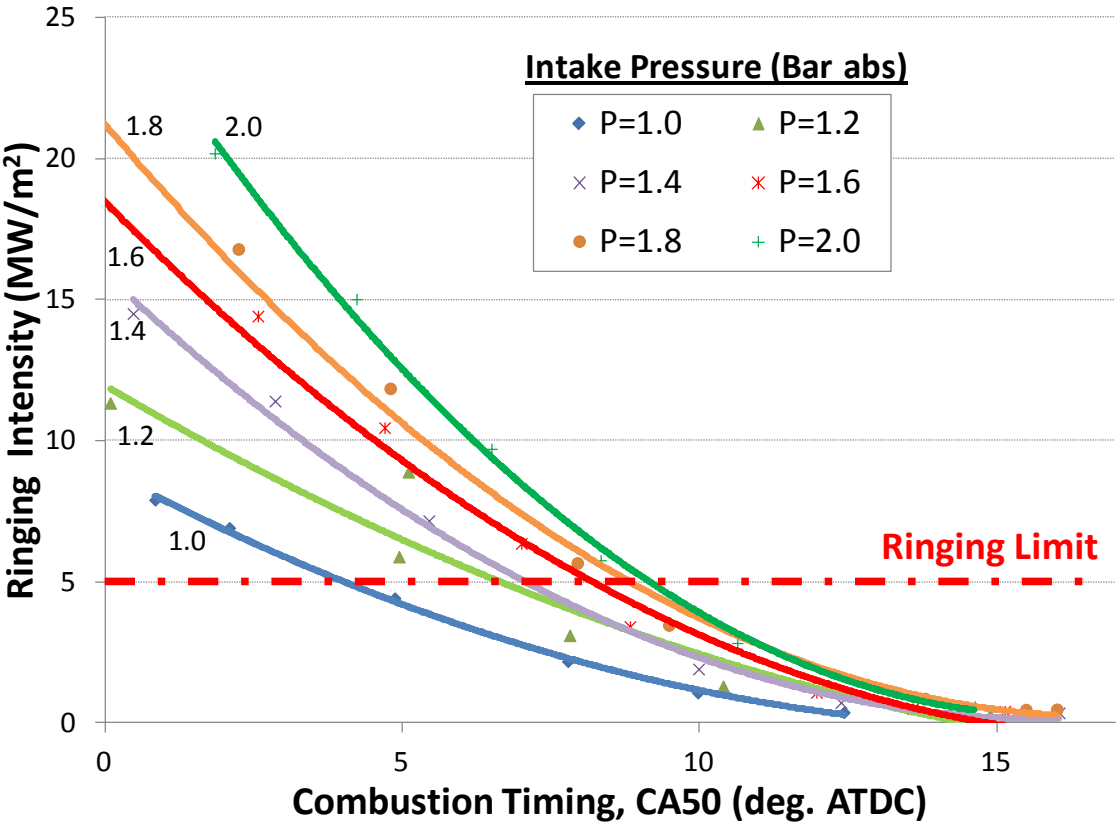

Figure 7-10 - Ringing intensity for different intake pressures and combustion timings at ϕ=0.45 and 1800 RPM in single-cylinder mode

Figure 7-11 shows the effects of intake pressure on the gross indicated efficiency. The results show that indicated efficiency generally increases with higher intake pressures, however the highest intake pressure (2.0 bar) displays a lower indicated efficiency than the 1.8 bar data. The discussions accompanying Figure 7-3 showed that indicated efficiency decreases with delayed combustion timings, however this effect is less apparent for higher equivalence ratios. Since the results of Figure 7-11 are for ϕ=0.45, the decreases in indicated efficiency with delayed combustion timing are not as apparent as with lower equivalence ratios. The effect of lower indicated efficiencies at highly advanced combustion timing (caused by more heat loss and negative work on the piston) shown in Figure 7-3 is also apparent in Figure 7-11. Figure 7-12 shows the combustion efficiency for each intake pressure. The combustion efficiency results complement the indicated efficiency, showing that with higher intake pressure there is generally higher combustion efficiency. It is again worth mentioning that the gross indicated efficiencies for a given cylinder operating in multi-cylinder mode were significantly higher than the efficiencies presented in Figure 7-11.

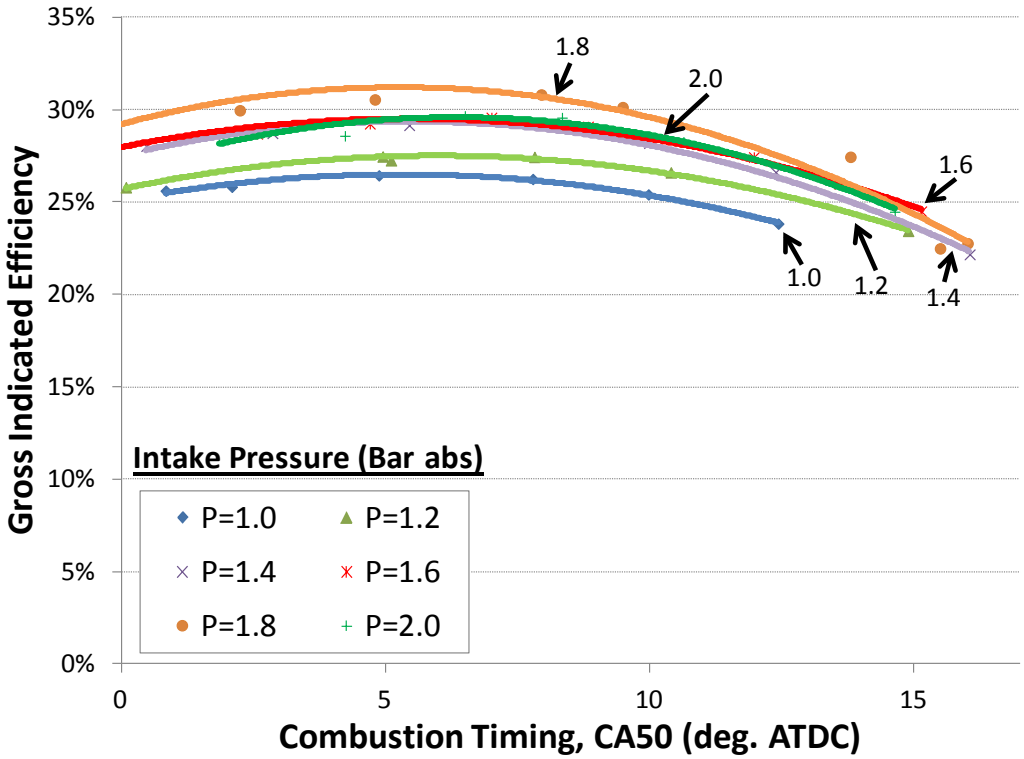

Figure 7-11 – Gross indicated efficiency for different intake pressures and combustion timings at ϕ=0.45 and 1800 RPM in single-cylinder mode

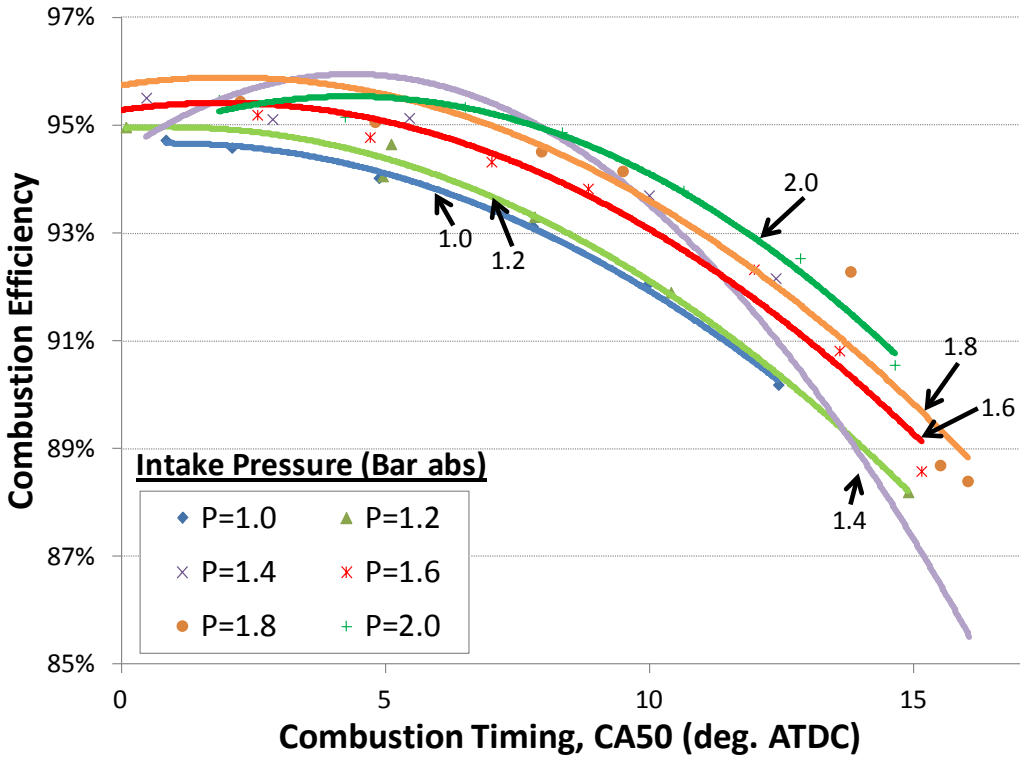

Figure 7-12 - Combustion efficiency for different intake pressures and combustion timings at ϕ=0.45 and 1800 RPM in single-cylinder mode

Figure 7-13 shows the trends in NO_x emissions with different intake pressures and combustion timings, and Figure 7-14 shows the mass averaged peak in-cylinder temperature for the different conditions. The NO_x emissions indicate that generally higher intake pressures cause lower NO_x emissions, and this trend is supported by the generally lower peak in-cylinder temperatures at the higher intake pressure. The one notable exception in the peak in-cylinder temperature data is the lower temperatures seen in the 1.0 bar cases, which also have a higher NO_x emission. It is worth mentioning that the increased NO_x emissions seen in the 1.0 bar test cases are negligibly greater (less than 1 ppm) than data for other intake pressures. All test points in Figure 7-13 have NO_x levels that are between 40 and 180 times lower than the US 2010 NO_x emissions regulations.

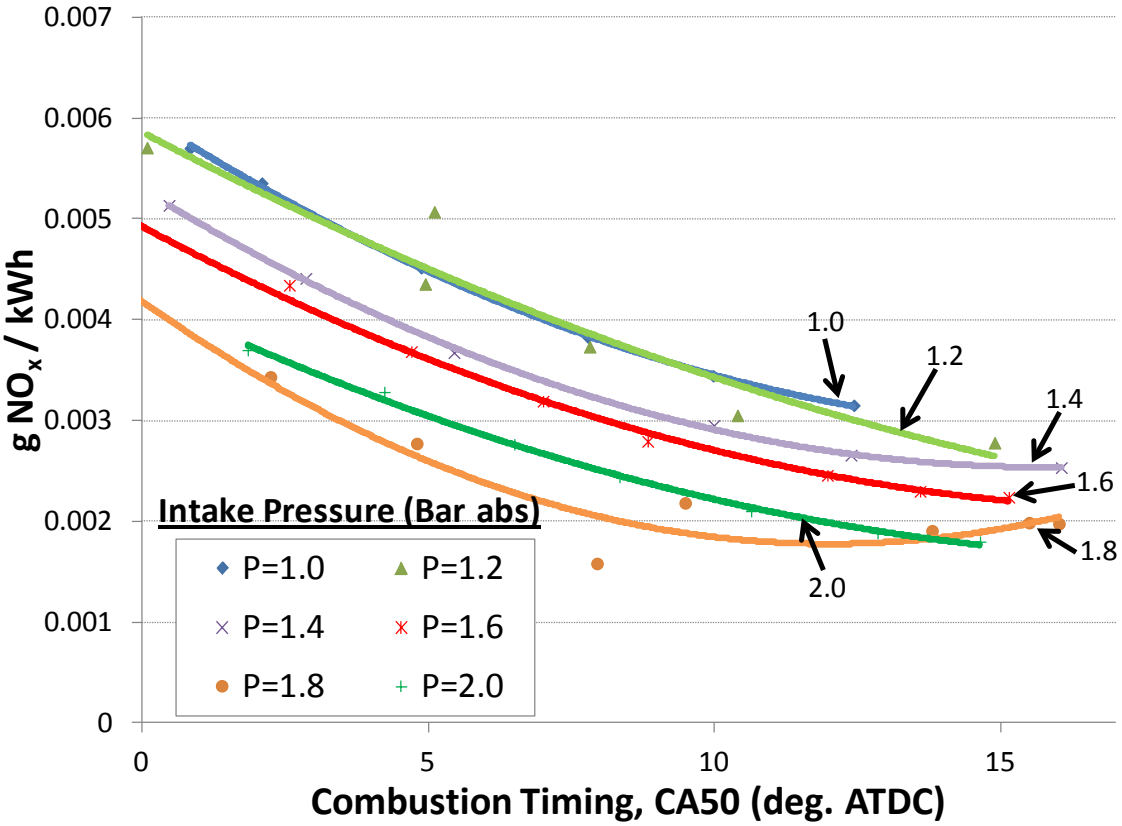

Figure 7-13 - NO_x emissions for different intake pressures and combustion timings at ϕ=0.45 and 1800 RPM in single-cylinder mode

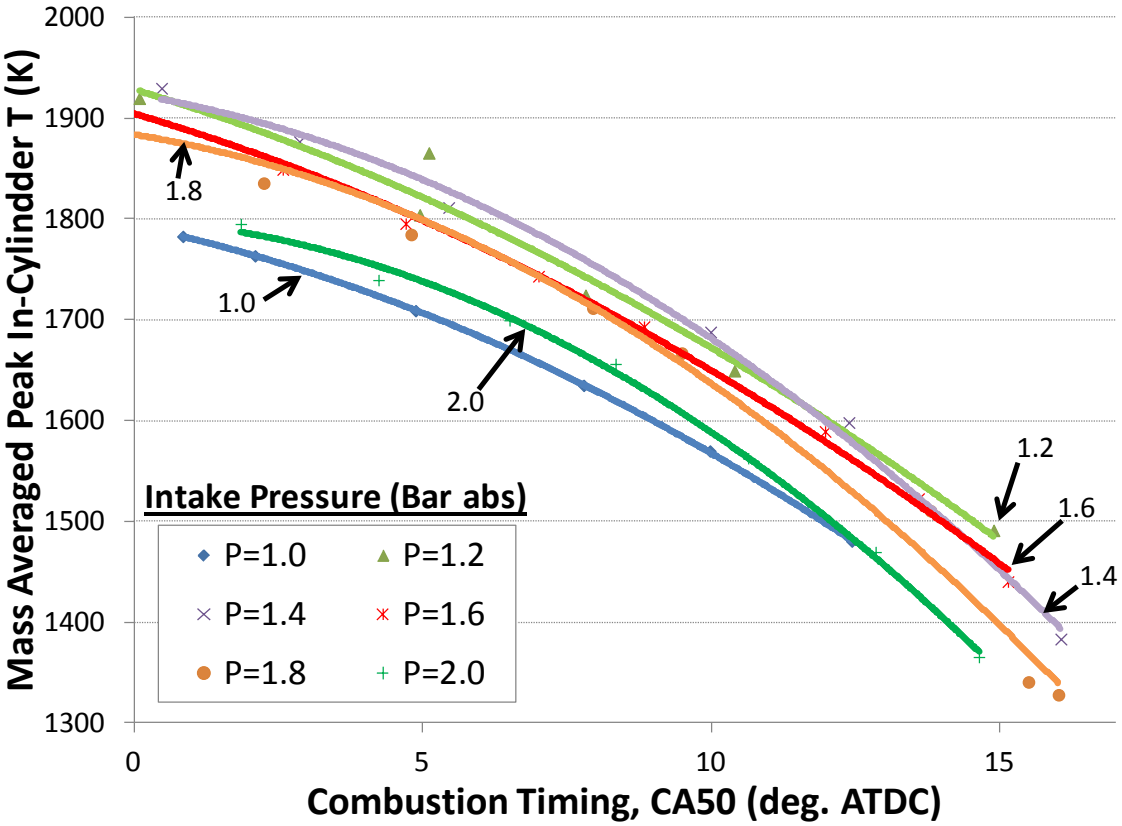

Figure 7-14 - Mass averaged peak in-cylinder temperature for different intake pressures and combustion timings at ϕ=0.45 and 1800 RPM in single-cylinder mode

Figure 7-15 shows the trends for unburned hydrocarbon emissions for different intake pressures and combustion timings, and Figure 7-16 shows the CO emissions for the same test conditions. As seen in Figure 7-7 and Figure 7-8, unburned hydrocarbon and carbon monoxide emissions increase with delays in combustion timing. As seen in Figure 7-15, unburned hydrocarbon emissions generally decrease with higher intake pressures. Figure 7-16 shows higher levels of CO emissions with higher intake pressures. The higher CO emissions with increased boost pressure may be caused by the presence of more CO near the cold-boundary layers of the cylinder which cannot locally achieve the 1500 K required for complete oxidation [38,68].

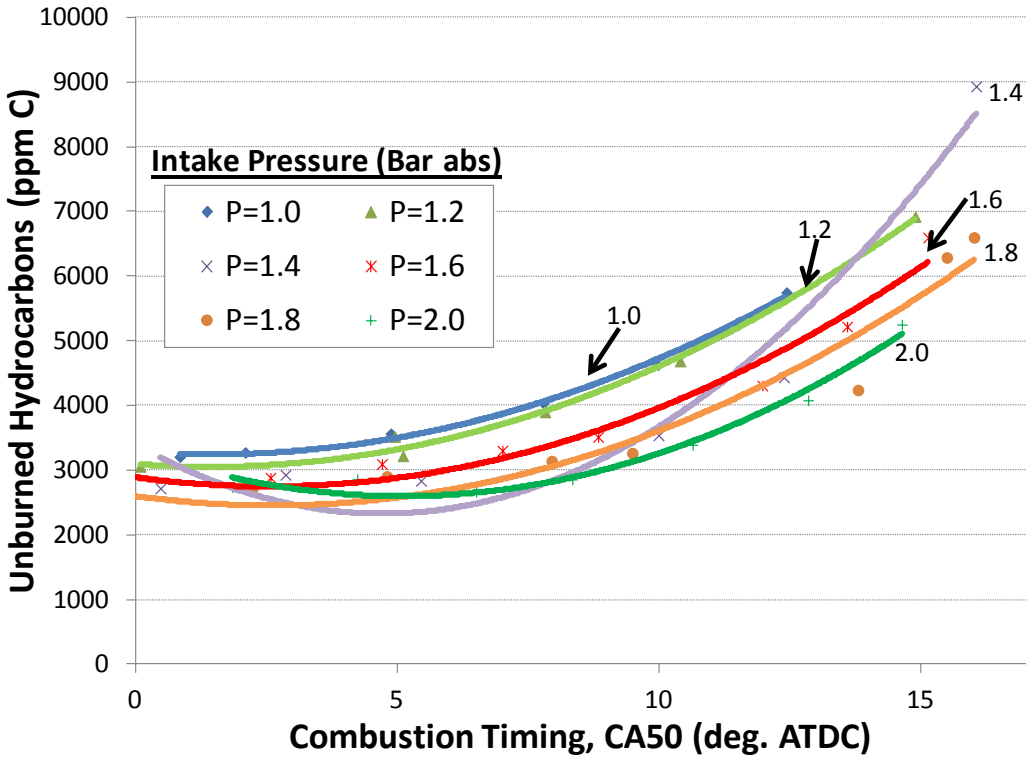

Figure 7-15 - Unburned hydrocarbon emissions for different intake pressures and combustion timings at ϕ=0.45 and 1800 RPM in single-cylinder mode

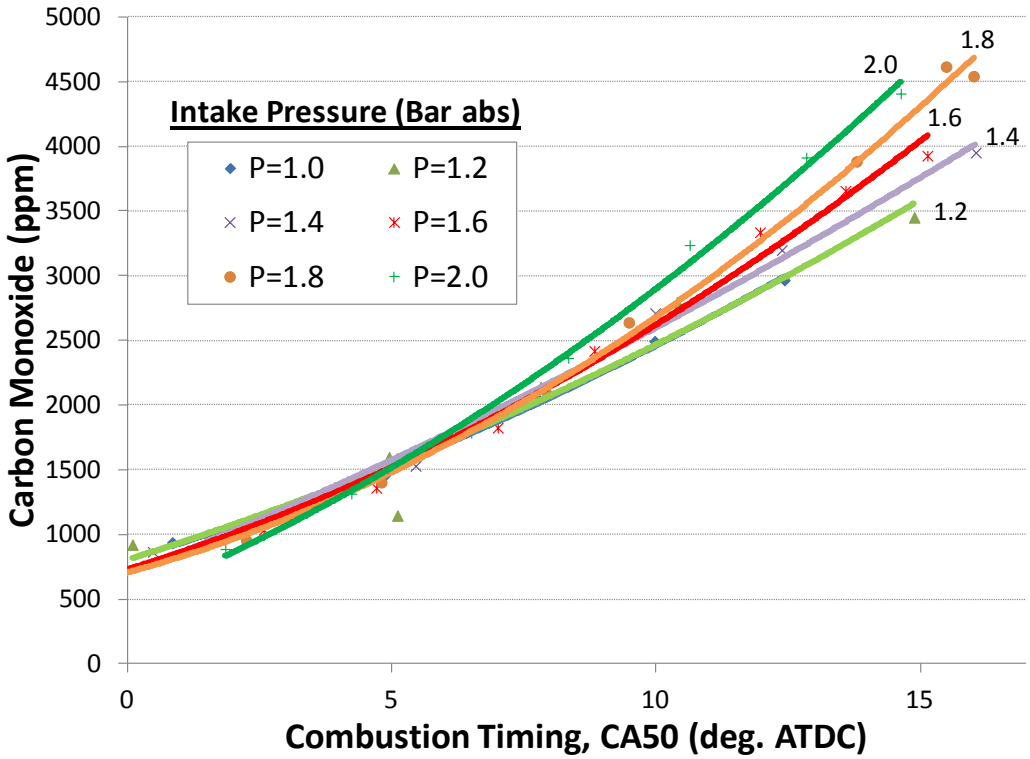

Figure 7-16 - Carbon monoxide emissions for different intake temperatures and combustion timings at ϕ=0.45 and 1800 RPM in single-cylinder mode

Figure 7-9 through Figure 7-16 showed the effects of different intake pressure on power output, ringing, efficiency and emissions while holding equivalence ratio constant for single-cylinder operation. The results show that higher intake pressures allow higher power output (up to a point which is limited by ringing and controllability), while also increasing ringing, efficiency and CO emissions, and decreasing NO_x, peak in-cylinder temperature and unburned hydrocarbons.

7.3 Multi-cylinder operation for high power output

7.3.1 Power and efficiency trends in multi-cylinder mode

All data presented up to this point has been conducted in a single-cylinder operating mode, allowing finer tuning of each control variable, and a greater ability for maintaining steady state conditions. The following sections discuss multi-cylinder data. Comparing the single-cylinder data from Figure 7-1 through Figure 7-16 with corresponding multi-cylinder data shows very similar trends and similar absolute values for data points, with two notable exceptions: 1) For a given operating point (equivalence ratio, boost pressure and combustion timing), the power output was higher in multi-cylinder mode, and 2) for the same given operating points, the gross indicated efficiency was higher in multi-cylinder mode. These notable differences are caused by enhanced heat loss which occurs in single-cylinder mode because of a colder engine block. For reference, Figure 7-17 and Figure 7-18 show the power output and gross indicated efficiency for cylinder 3 while all cylinders are firing.

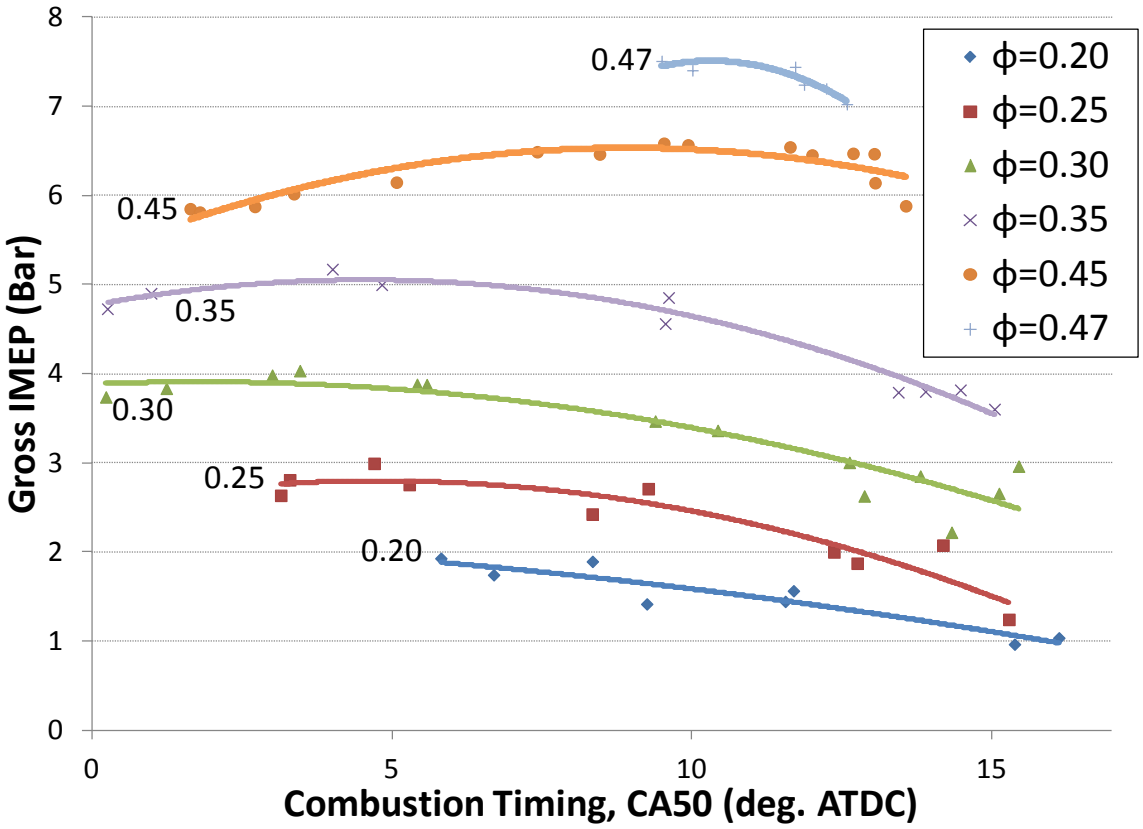

Figure 7-17 - Power output (Gross IMEP) for different equivalence ratios and combustion timings at P_{in}=1.8 bar and 1800 RPM in multi-cylinder mode

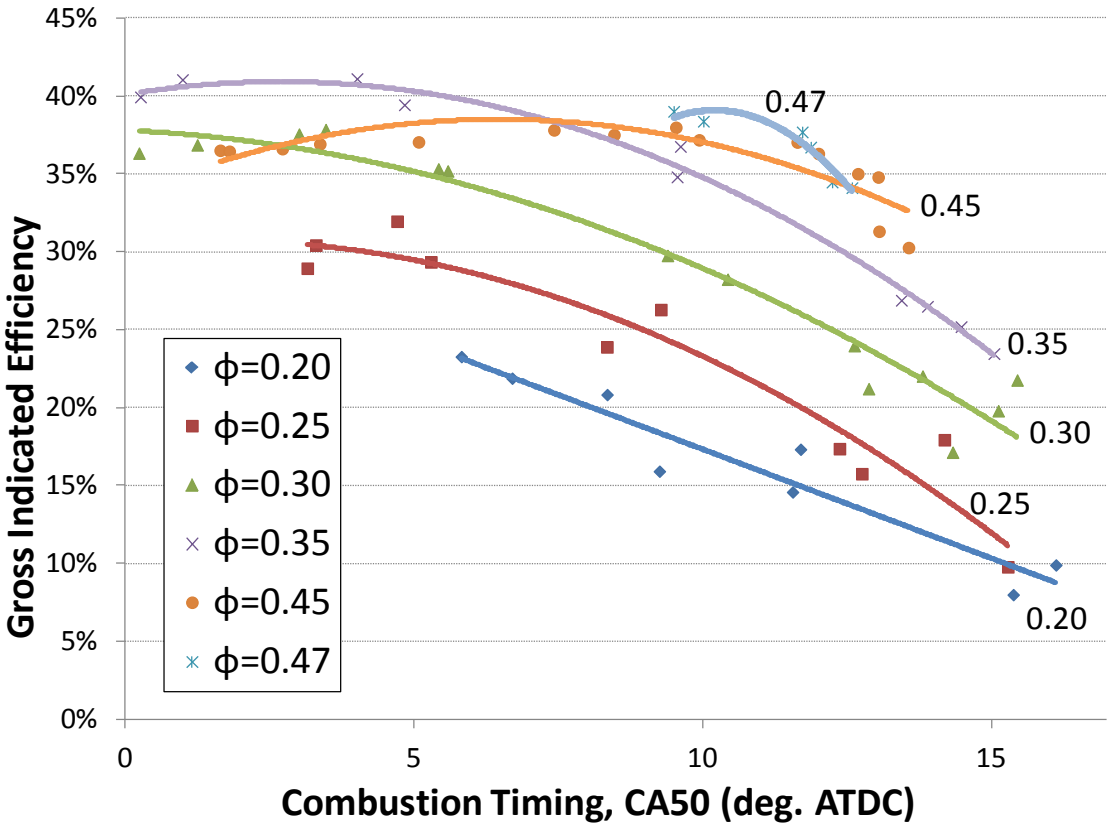

Figure 7-18 - Indicated efficiency for different equivalence ratios and combustion timings at Pin=1.8 bar and 1800 RPM in multi-cylinder mode

7.3.2 Thermal management for multi-cylinder control

As a result of variations between cylinders, an important obstacle in multi-cylinder engines is the requirement for control of individual cylinders. The differences between cylinders include variations in the intake flow between cylinders, differences in heat transfer between cylinders, variations in fuel injection and variations in the geometric tolerances. In thermal control of HCCI engines, these differences between cylinders cause the requirement for different intake temperatures for maintaining the same combustion timing across all cylinders. For a fixed equivalence ratio (ϕ=0.45) and intake pressure (P_{in}=1.8 bar), Figure 7-19 shows the differences in intake and exhaust temperatures across the four cylinders for different combustion timings. The results show that for this test condition, differences in the required intake temperature across different cylinders can be as high as 15°C.

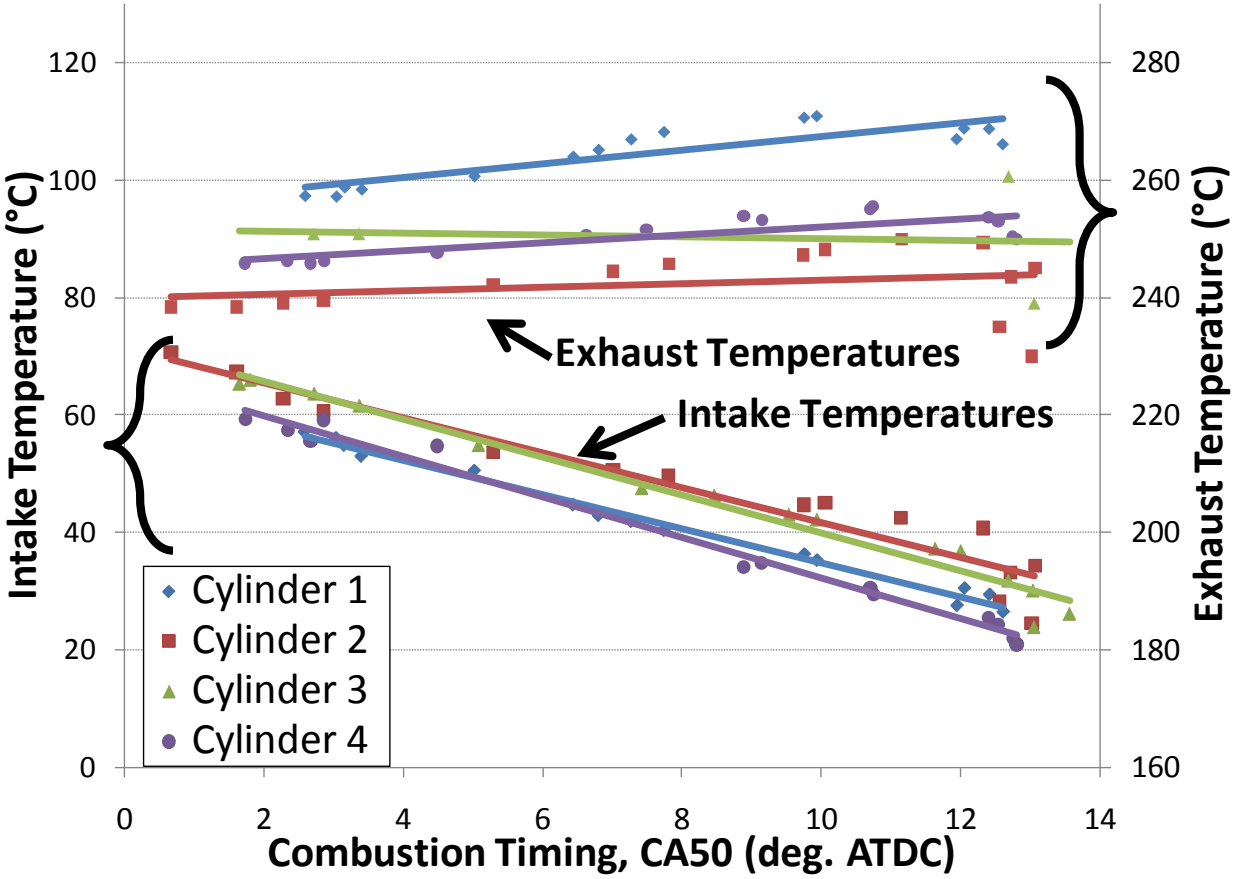

Figure 7-19 - Intake and exhaust temperatures for different combustion timings for each cylinder, with P_{in}=1.8 bar, ϕ=0.45 and 1800 RPM

The intake temperature results from Figure 7-19 show that advanced combustion timings require intake temperatures well above ambient conditions. At the conditions plotted (ϕ=0.45 and P_{in}=1.8 bar), these advanced combustion timings result in unacceptably high ringing intensities, however at lower power output conditions higher intake temperatures may also be required in achieving a desired operating condition. Figure 7-19 shows that exhaust temperatures are much higher than the required intake temperatures (this is also true for many other high power output test points). The excess heat from exhaust gases can be used for heating the intake charge in conditions where elevated intake temperatures are required. Fast thermal management, in these cases, can be carried out by varying the flow rate of the intake charge through an air-to-air heat exchanger with the exhaust gases enabling the desired intake air temperatures. When lower intake temperatures are required, more air will bypass the heat exchanger.

7.3.3 Cylinder-to-cylinder cross-talk

An additional challenge with multi-cylinder thermal control of HCCI combustion is the effect which individual cylinder control has upon its neighboring cylinders. With fast thermal control, rapid changes in intake temperature are achieved by altering flow paths for intake air (for example, varying the amount of air which flows through a heat exchanger). Sudden changes in the flow dynamics for one cylinder can also affect the flow dynamics of intake air into

neighboring cylinders, thereby inadvertently changing the intake temperature and combustion timing in neighboring cylinders. Figure 7-20 demonstrates these coupled effects between cylinders by showing the changes in intake temperatures that are induced upon cylinders 2, 3, and 4 when the thermal control throttle for only cylinder 1 is changed.

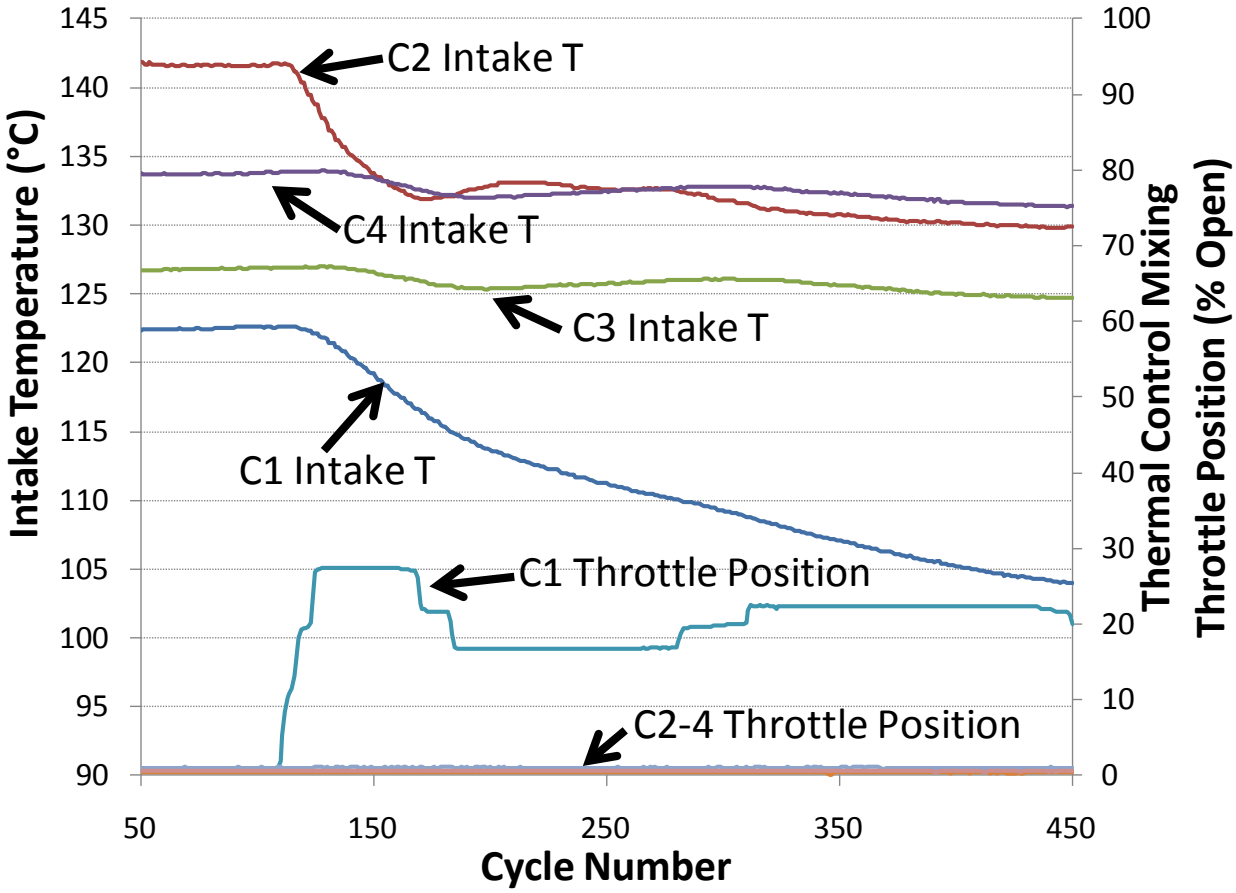

Figure 7-20 - Variations in intake temperature induced on neighboring cylinders because of coupled flow dynamics

Figure 7-20 shows the effects of changing the thermal control mixing throttle position for cylinder 1 from fully closed to 20% open. Under the configuration utilized on this engine, when the mixing throttles are opened further, the intake temperature is lowered thereby enabling later combustion timings. Opening the mixing throttle for cylinder 1 from 0 to 20% open resulted in a decrease of 18°C in the cylinder 1 intake temperature. The intake temperature into other cylinders was also affected, with a rapid decrease of 9°C for cylinder 2, and a gradual decrease of approximately 2°C for cylinders 3 and 4. These coupled flow dynamics can result in longer settling times for reaching desired combustion timing set points and poor disturbance rejections (in fact there will be disturbance propagations between cylinders). The disturbance propagation behavior that can result from coupled flow dynamics is particularly problematic at high power output conditions, where stable combustion is achieved near the limits of misfire, ringing, maximum in-cylinder pressure limits and loss of controllability. Disturbance propagation under these conditions can cause misfiring, ringing, or excessive peak cylinder pressures which accelerate engine wear in neighboring cylinders. The effects of disturbance propagation can be

minimized using well-designed intake manifolds which limit coupling of flow dynamics and well tuned control algorithms that account for coupling of flow dynamics between neighboring cylinders.

7.4 Effects of exhaust backpressure

All of the results presented thus far have utilized boosted intake pressures while exhaust pressures were maintained at atmospheric levels. In a production engine, boost pressures would likely be achieved using a turbocharger which also induces backpressure in the exhaust. Higher exhaust backpressures can affect the intake temperature requirement for different combustion timings, the combustion performance and emissions through higher fractions of burned residuals remaining in the cylinder from previous cycles.

In the following section, the effects of increasing exhaust backpressure are investigated. Experimental tests are conducted with an intake pressure of 1.8 bar, with a fixed amount of fuel injection and at two different combustion timings. Exhaust backpressures are increased in 50 kPa increments until the maximum backpressure that would be induced by a turbocharger. The maximum backpressure from a turbocharger under given engine conditions was calculated using compressor and turbine work analysis presented by Heywood [69] as shown in Eq. 5.2:

$$P_{\text{exh}} = P_{\text{amb}}\left[1-\frac{\dot{m}_i \cdot c_{p,i} \cdot T_i}{\eta_c \cdot \dot{m}_e \cdot c_{p,e} \cdot \eta_T \cdot T_{\text{exh}}}\left\{\left(\frac{P_{in}}{P_{\text{amb}}}\right)^{\frac{\gamma-1}{\gamma}}-1\right\}\right]^{\frac{-\gamma_e}{\gamma_e-1}} \qquad \text{(Eq 5.2)}$$

In Eq. 5.2, P_{exh} is the calculated exhaust backpressure caused by the turbocharger, P_{amb} is the ambient pressure, m_i is the mass flow rate of the intake charge entering the turbocharger compressor, m_e is the mass flow rate of burned gases passing through the turbocharger turbine, $c_{p,i}$ and $c_{p,e}$ are the specific heats of the intake and exhaust mixtures respectively, T_i and T_{exh} are the intake and exhaust temperatures respectively, γ and γ_e are the specific heat ratios of the intake and exhaust charges respectively, η_C is the isentropic efficiency of the compressor (assumed 0.60) and η_T is the isentropic efficiency of the turbine (assumed 0.65). Using Eq. 5.2, the maximum backpressure induced by a turbocharger at the conditions tested is near 2.5 bar (absolute).

Figure 7-21 shows a plot of the intake temperature and combustion timings that were achieved using an intake pressure of 1.8 bar, and with constant fuel injection. The results show that combustion timings were near 10 degrees ATDC for the different exhaust backpressures, however the intake temperature required in maintaining these combustion timings decreased as higher exhaust backpressures were used. This behavior is caused by increased amounts of hot residuals which cause higher bottom dead center temperatures, and thus requiring cooler intake temperatures for fixed combustion timing. As is consistent with Figure 7-19, the intake temperature for a given combustion timing is different for each cylinder, however, the magnitude of these intake temperature differences seem insensitive to the exhaust backpressure.

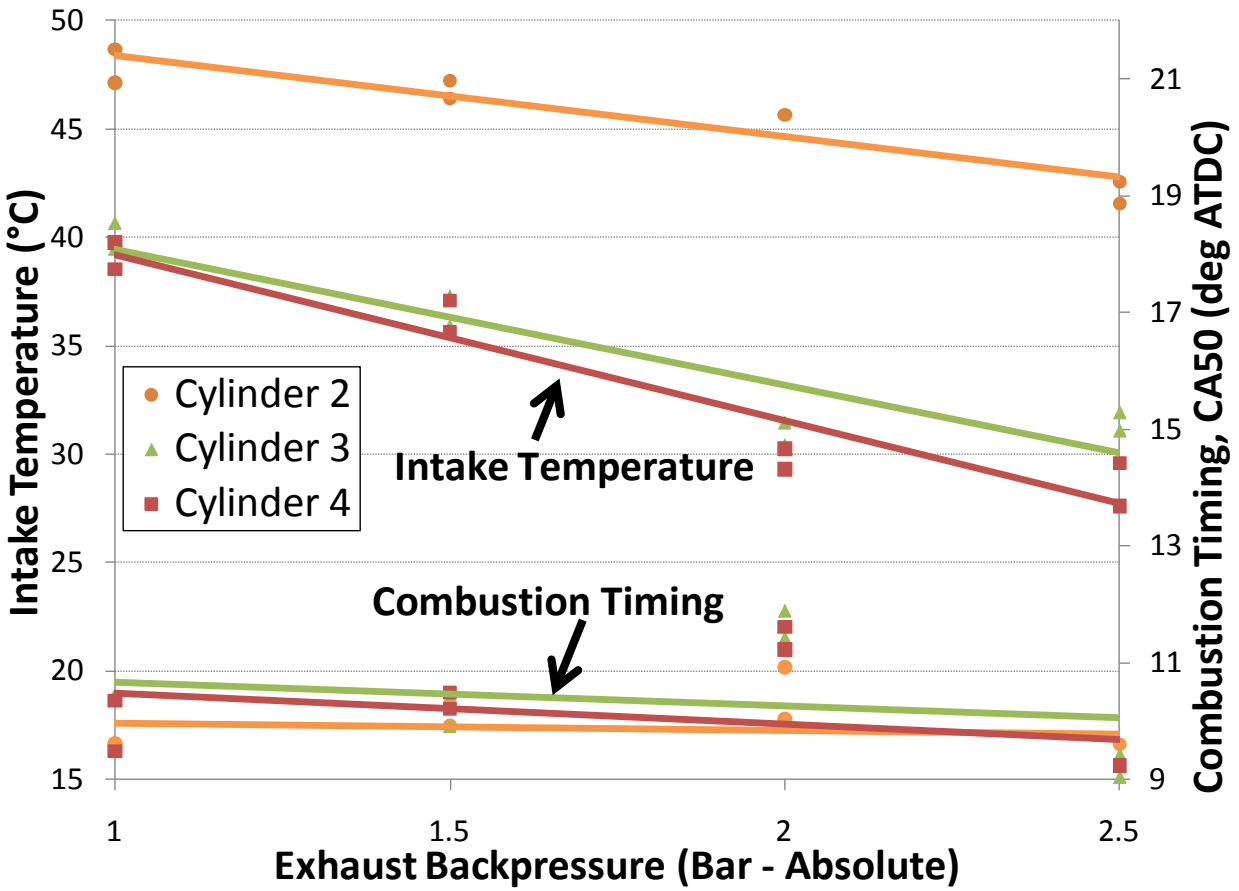

Figure 7-21 - Changes in intake temperature required for maintaining fixed combustion timing with increasing exhaust backpressure with fixed fuel injection, P_{in}=1.8 bar and 1800 RPM

Figure 7-22 and Figure 7-23 show the power output and ringing intensity for different exhaust backpressures at two different combustion timings when fixed intake pressure and fuel injection are maintained. The results show that increased exhaust backpressure does not affect the gross power output or the ringing behavior. Since the power output and fuel injection remain constant, the indicated efficiency also remains insensitive to changes in exhaust backpressure.

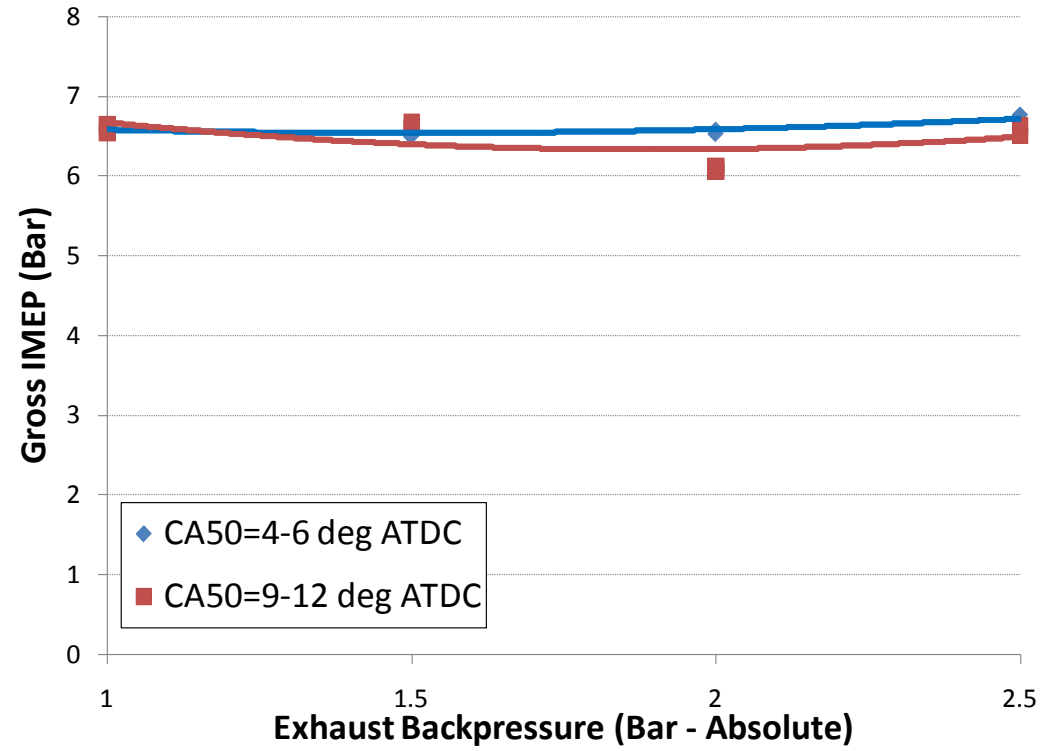

Figure 7-22 - Power output vs. exhaust backpressure for different combustion timings, at P_{in}=1.8 bar, 1800 RPM and with fixed fuel injection

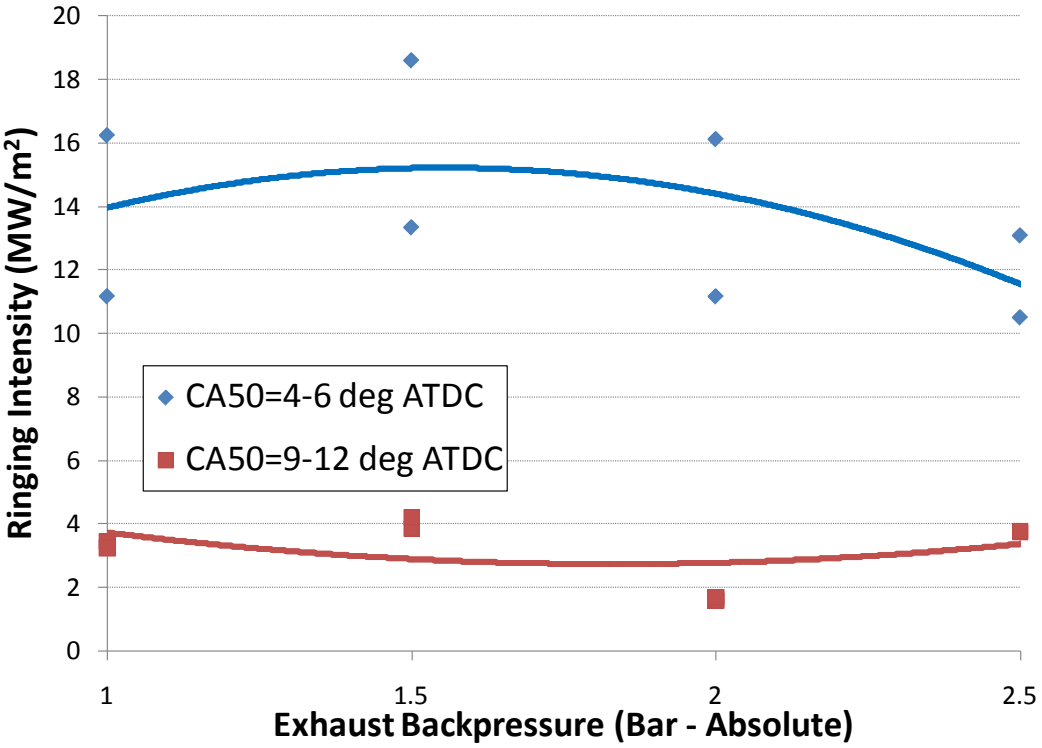

Figure 7-23 - Ringing intensity vs. exhaust backpressure for different combustion timings, at P_{in}=1.8 bar, 1800 RPM and with fixed fuel injection

Figure 7-24, Figure 7-25 and Figure 7-26 show the emissions for increasing amounts of exhaust backpressure. Figure 7-24 shows slightly decreasing NO_x emissions for advanced combustion timings with increasing exhaust backpressures, possibly caused by the dilution effect of additional residuals. Figure 7-25 shows that unburned hydrocarbon emissions for delayed combustion timings are reduced with increasing exhaust backpressures. Finally, Figure 7-26 shows that carbon monoxide emissions are insensitive to the exhaust backpressure.

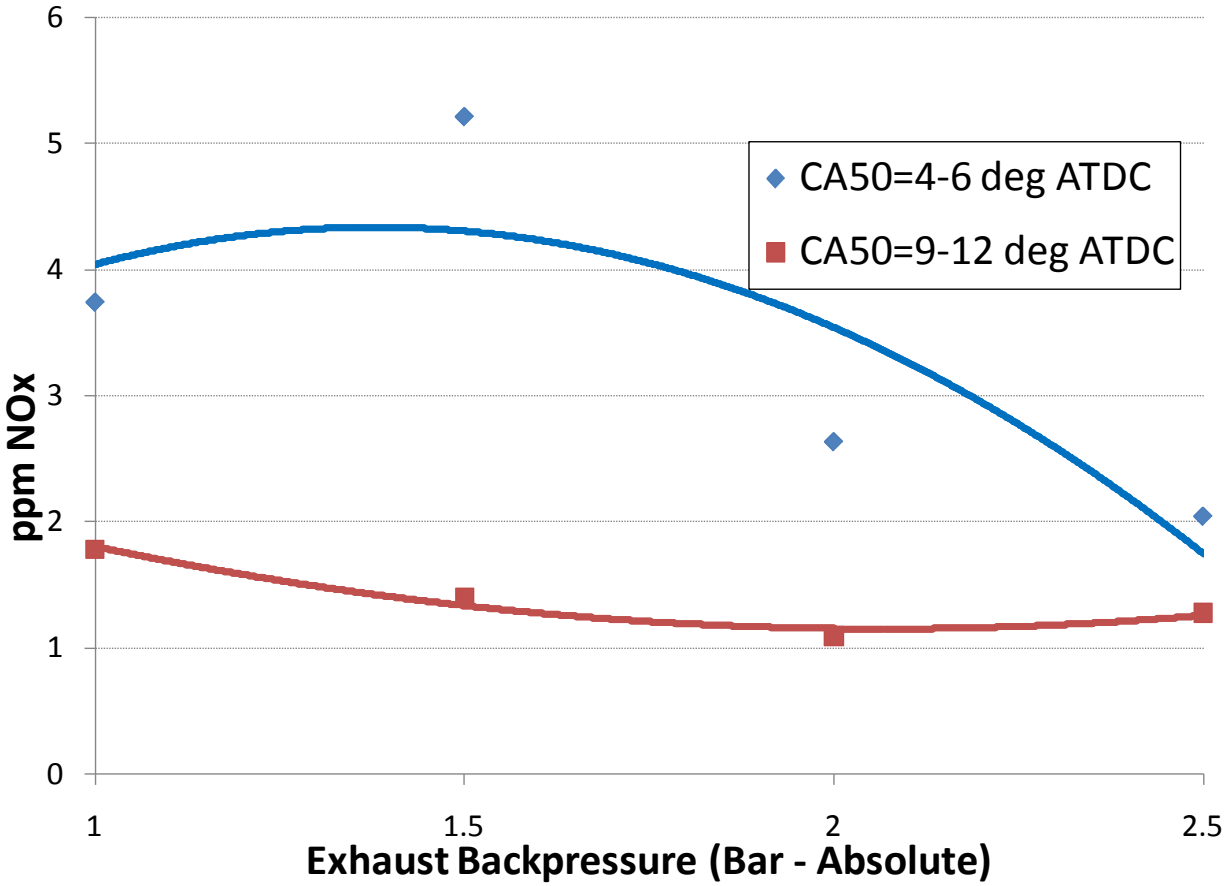

Figure 7-24 - NO_x emissions vs. exhaust backpressure for different combustion timings, at P_{in}=1.8 bar, 1800 RPM and with fixed fuel injection

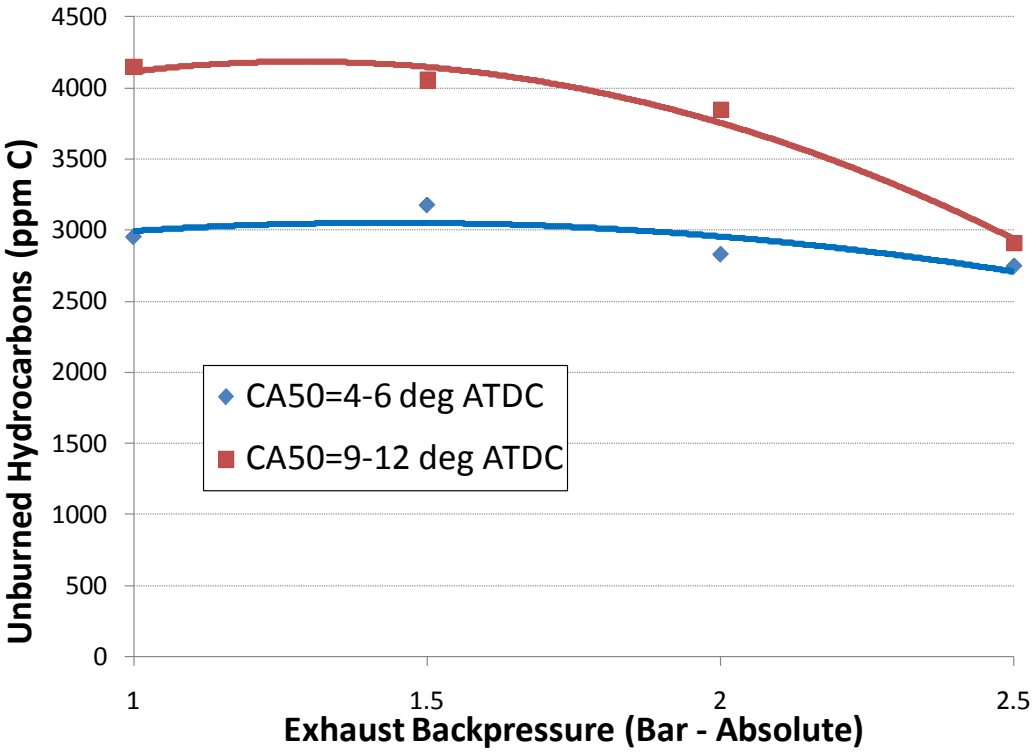

Figure 7-25 - Unburned hydrocarbon emissions vs. exhaust backpressure for different combustion timings, at P_{in}=1.8 bar, 1800 RPM and with fixed fuel injection

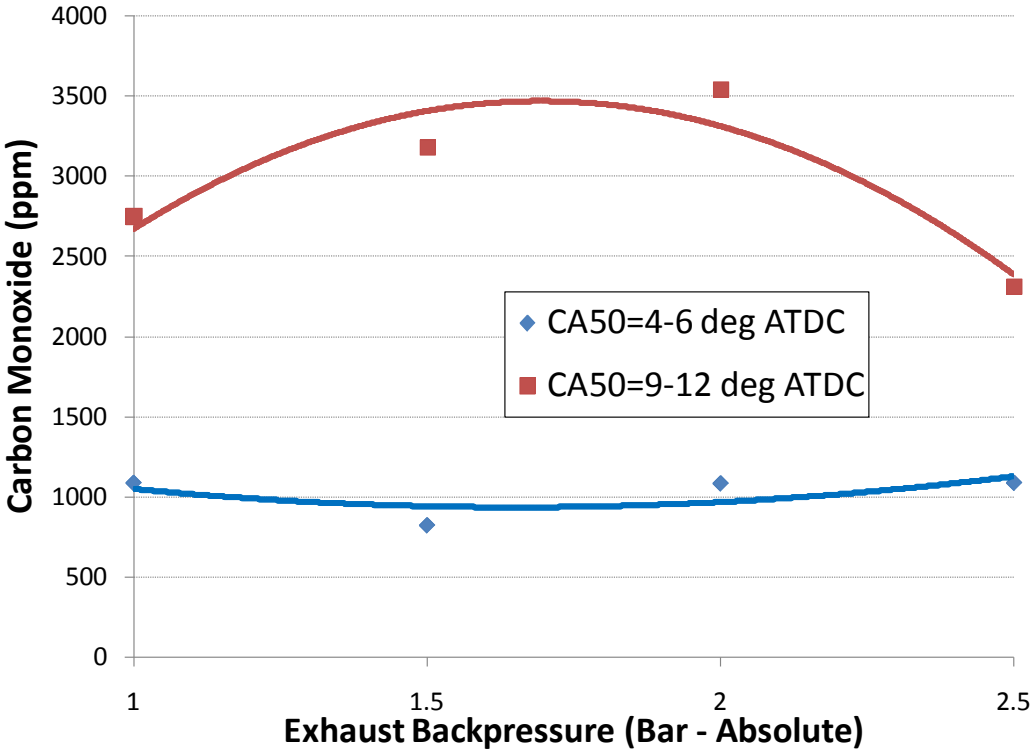

Figure 7-26 - Carbon monoxide emissions vs. exhaust backpressure for different combustion timings, at P_{in}=1.8 bar, 1800 RPM and with fixed fuel injection

Figure 7-21 through Figure 7-26 showed the effects of increasing exhaust backpressures for simulating the effects of a turbocharger. The results showed that with increasing exhaust backpressures, lower intake temperatures are required in maintaining fixed combustion timing. No effects were observed on power output, ringing or carbon monoxide emissions with increasing exhaust backpressures, however NO_x and unburned hydrocarbons showed slight decreases with increased exhaust backpressure.

7.5 Engine conditions at maximum power operating point

In the sections 7.1 and 7.2, it was found that power output can be increased with higher equivalence ratios and higher intake pressures, while delayed combustion timings are used in enabling acceptable levels of ringing. Using this strategy, the highest power output test point was identified at an intake pressure of 1.6 bar. It is possible that slightly higher power output can be achieved at higher boost pressures since the high equivalence ratio ringing limits were not explored as thoroughly for these higher pressures. The details for the present high power test point are given in Table 7-1.

Figure 7-27 shows a 300-cycle average of in-cylinder pressure and heat release rate for cylinder 3.

Table 7-1 - Detailed list of parameters for the maximum power output condition

Parameter	Cylinder 3 Value
Intake pressure (bar)	1.6
Equivalence Ratio	0.56
CA50 (deg ATDC)	15.77
Engine Speed (RPM)	1800
Compression Ratio	17:1
Intake T (°C)	45.8
Exhaust T (°C)	290
Gross IMEP (bar)	9.02
Ringing intensity (MW/m^2)	5.66
COV of Gross IMEP	5%
T.Hc emissions (ppm C)	4561
% O_2 in exhaust	14.06
CO emissions (ppm)	1188
% CO_2 in exhaust	4.86
NO_x (g NO_x / kg fuel)	0.23

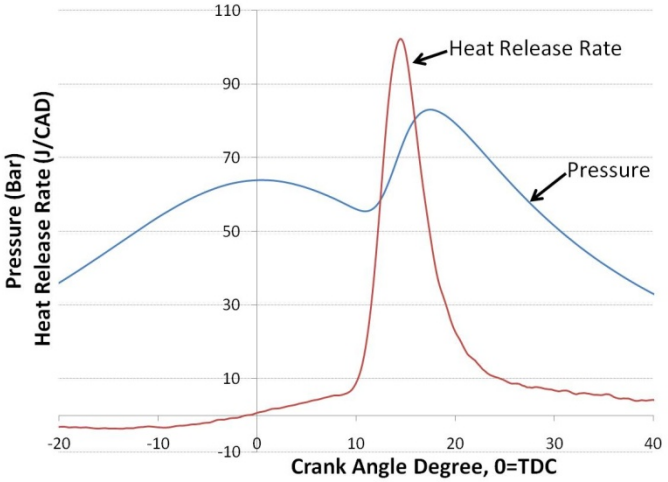

Figure 7-27 - 300-cycle average of in-cylinder pressure and heat release rate for single-cylinder mode at a high power output condition

8 Detecting combustion characteristics with ion sensors

In HCCI engines, sparkplug ion sensors can provide a signal for feedback control of combustion timing. Traditionally, in HCCI research engines, sensing of combustion timing is accomplished using piezoelectric pressure transducers, however these sensors are to date too expensive for use in production engines [70]. Sparkplug ion sensors are far more cost effective, particularly for engines that transition between spark-ignited and HCCI cycles during their operation because a sparkplug is already installed in each cylinder. The challenge is that in HCCI cycles, very lean mixtures are used and the ion signal from very lean combustion can be difficult to distinguish from background noise [71,72,73].

8.1 Introduction to ion sensing in engines

8.1.1 Ionization theory

Ionization currents that are sensed in engines are predominantly produced through two reaction pathways: chemi-ionization and thermal-ionization. The important reactions driving chemi-ionization are [70,74,75,76]:

$$CH + O \rightarrow CHO^+ + e^- \quad \text{(Eq. 6.1)}$$
$$CHO^+ + H_2O \rightarrow H_3O^+ + CO \quad \text{(Eq. 6.2)}$$
$$H_3O^+ + e^- \rightarrow H_2O + H \quad \text{(Eq. 6.3)}$$

A key reaction driving thermal-ionization is [76,77]:

$$NO \rightarrow NO^+ + e^- \quad \text{(Eq. 6.4)}$$

In spark-ignited engines, ion sensors typically detect two peaks in the ion signal. The first peak is caused by chemi-ionization as the flame passes over the sensor, and the second peak is from thermal-ionization caused by high temperatures in the burned gases [71,74].

In HCCI engines, a single peak in ion current from only chemi-ionization is typically observed. Equivalence ratios and temperatures are generally too low in HCCI engines for thermal-ionization to have a significant impact on the ion signal [71,74,76]. The major species responsible for the ion signal observed in HCCI combustion is the H_3O^+ ion [70,71,74,75,76,78,79].

Although sparkplug ion sensors have been demonstrated as an inexpensive and accurate way to measure combustion parameters in an HCCI engine, these sensors only capture localized measurements within the vicinity of the sensor's electrode gap [71,74,79]. A study in an optical access engine has shown that the ions responsible for chemi-luminescence must be in contact with the sensing electrodes for ion current to start flowing through a measurement circuit. This requirement of close proximity of ion species to the sensing electrodes is the cause of timing offsets between pressure-based and ion-based measurements of combustion timing because the autoignition reactions that produce ionized species typically do not start near the sensing electrodes [71].

8.1.2 Uses of ion sensors in engines

8.1.2.1 Ion sensors in SI engines

Numerous studies have shown the ability for ion sensors to detect and quantify knocking in spark-ignited engines [77,80,81]. Ion sensors for knock detection can potentially be more effective than traditional knock sensors because they are not affected by poor noise transmission through the engine block, and interference from other noise sources at higher engine speeds.

8.1.2.2 Ion sensors in HCCI engines

HCCI engines require accurate sensors to determine the time-occurrence of combustion. Pressure sensors are typically used in laboratory applications; however these sensors and their associated charge amplification and signal processing electronics may be prohibitively expensive for production applications. Ion sensors are a less expensive alternative to pressure sensors for sensing of combustion timing as part of a feedback control system.

Many prior studies have demonstrated the effectiveness of using ion sensors in detecting combustion timing [70,71,74,75,78,82,83,84]. The signal from ion sensors, however, is affected by many combustion parameters.

Dilution effects on ion signal in HCCI:

Ion sensors are very sensitive to the equivalence ratio, and the ion signal can be undistinguishable from noise at low equivalence ratios [71,72,75,78,85,86]. Higher equivalence ratios in combination with charge dilution from EGR can allow greatly enhanced ion signals [77,87]. EGR causes substantial increases in the concentration of available CH molecules which are a precursor of H_3O^+ [87].

Temperature effects on ion signal in HCCI:

Ion sensors are also very sensitive to the in-cylinder temperature. Higher ion signals are observed with higher in-cylinder temperatures [70,72,75,85,87]. Previous research has shown that temperature does not influence ion reaction rates significantly, but rather concentrations of reactants that promote ion formation are higher with higher temperatures [87]. Several other engine parameters affect the ion signals because of this temperature effect.

Intake pressure effects on ion signal in HCCI:

Higher intake pressures cause lower ion signals. This is because higher pressures can enhance radical recombination rates, and cause a lower intake temperature requirement for maintaining a fixed combustion timing [70,75].

Fuel effects on ion signal in HCCI:

Fuels having a higher octane number typically show higher ion current, and allow distinguishable ion signals at lower loads [85]. These higher octane fuels exhibit a higher ion current because they require higher intake temperatures to achieve a desired combustion timing [70,75,85]. Higher octane fuels also have combustion timing as indicated by CA50 and ION50 agreeing more closely [85]. Fuels with low temperature heat release, such as n-heptane or Diesel, only show detectable ion signals at higher equivalence ratios as the low temperature reactions typically do not lead to detectable ion currents [85]

Geometry and location effects on ion signal in HCCI:

Ion sensors with larger electrode areas allow higher ion current signals. For sparkplug ion sensors, this is often achieved by removing the side electrodes to allow more access to the center electrode [71,74]. The location of the sensing electrodes within the combustion chamber is also important as ion sensors only produce localized measurements [79,85]. Offsets in timing between CA50 and ION50 can be caused because combustion rarely starts in the volume near the ion sensors, however smaller offsets between CA50 and ION50 are observed with larger sensing electrodes because they measure over a larger volume [74].

Bias voltage effects on ion signal in HCCI:

Larger bias voltages across the sensing electrodes give better ion signals [74,75]. Beyond 250 V, however, the increase in ion signal with higher voltages starts to decline [74].

Other factors with effects on ion signal in HCCI:

After prolonged use, deposits can accumulate on sensing electrodes causing deteriorated ion signals. Self-cleaning mechanisms can be employed in an engine control strategy by burning off deposits through short periods of high temperature operation [78].

Previous studies have shown that pressure oscillations can be estimated from ion signals [71]. When HCCI becomes excessively violent, ion sensors have been shown to display ringing in the ionization signals [78]. Few other studies aside from Strand, et al, and Huang et al. have discussed the prospect for ion sensors to detect ringing in HCCI engines. At least in the author's knowledge, no prior research has shown the ability for ion sensors to quantify ringing behavior in HCCI engines, therefore this topic is explored in Section 8.3.

8.2 Extending the lower equivalence ratio limits for ion sensors

Although ion sensors present a cost effective way of detecting combustion characteristics for feedback control of HCCI engines, these sensors are ineffective at lower equivalence ratios. At low equivalence ratios there is an insufficient concentration of ionized species and electrons causing the ion signal to be indistinguishable from background noise. The use of fuel additives to enhance the ion signal is one approach to dealing with this problem. The primary objective of the

research presented in this section is identification of the minimum concentration of an acetate additive that will produce discernable ion signals in a combustion engine under equivalence ratios as lean as 0.20 while operating with HCCI combustion. A secondary objective is characterization of the side effects of using fuels containing KOAc additives. In this research, different concentrations of KOAc additive are explored in Ethanol fuel.

8.2.1 Autoignition of ethanol with KOAc additives in HCCI engines

Previous research has shown that ethanol behaves as a true single-stage ignition fuel in HCCI conditions, thus it displays little low temperature heat release behavior [20]. In analyzing the results of this study, the heat release behavior is examined to ensure that introduction of additives do not change the expected heat release profiles for ethanol.

High temperature ignition, which serves as the primary source of heat release for ethanol, is driven by the chain branching reaction $H + O_2 \rightarrow O + OH$ [33]. Additionally, reactions between OH radicals and fuel molecules play an important role and detailed chemical pathways are explained in the Westbrook reference [33].

Potassium compounds such as KOAc are known fire suppressants and are used in class F and class K fire extinguishers. These extinguishers use both chemical and smothering effects to suppress fires. Since our experiments use only small amounts of KOAc, the chemical effects of KOAC are most important, and several pathways through which the KOAc may inhibit autoignition are listed below:

1. The K atoms combine with OH to inhibit chain propagation reactions involving OH radicals, such as $OH + H_2 \rightarrow H_2O + H$. Possible reaction paths are [88]:

   $K + OH + M \rightarrow KOH + M$
   $K + O_2 + M \rightarrow KO_2 + M$ with $KO_2 + OH \rightarrow KOH + O_2$

2. The K atom dissociated from KOAc participates in reactions that consume H radicals, thereby competing with chain branching reactions such as $H + O_2 \rightarrow OH + O$. The main possible reaction path is:

   $H + H + K \rightarrow H_2 + K$ (similar to flame inhibition reactions in [89])

8.2.2 Gas phase ionization of potassium

A possible pathway for introducing additional electrons for ion sensing is through the gas phase ionization of potassium atoms, through a chemical reaction of $K \leftrightarrow K^+ + e^-$. The equilibrium concentrations of electrons or K^+ ions can be determined using Eq. 6.5:

$$K_P = \frac{N_{e^-}^2}{N_K}\left(\frac{P}{N_{\text{total}}}\right) = \exp\left(-\frac{\theta_K}{T}\right) \qquad \text{(Eq. 6.5)}$$

In Eq. 6.5, K_P is the equilibrium constant for a given state, N_i is the number density and θ_K = 50,379 K is the first ionization energy of potassium [90]. This expression suggests that for a given initial concentration of potassium atoms the number of ions and electrons that are available will decrease as the temperature decreases. Using the first ionization energy (50,379 K) for potassium atom, it is determined that at tempe;ratures around 2,000 K, each 20 K decrease in peak temperature will cause a 15% decrease in the number of available electrons for the ion sensor, and this effect is even more pronounced for lower temperatures.

8.2.3 Increasing HCCI ion signals using KOAc additives

The major results related to the improvement of ion signal-to-noise ratio are shown in Figure 8-1. Two major results can be seen from Figure 8-1, the first is that even for very low equivalence ratios, such as 0.20, KOAc concentrations as low as 180 mg/L (~107 ppm) in Ethanol produce distinguishable ion signals. For this study, an ion signal-to-noise ratio above 4.0 is classified as being distinguishable from noise.

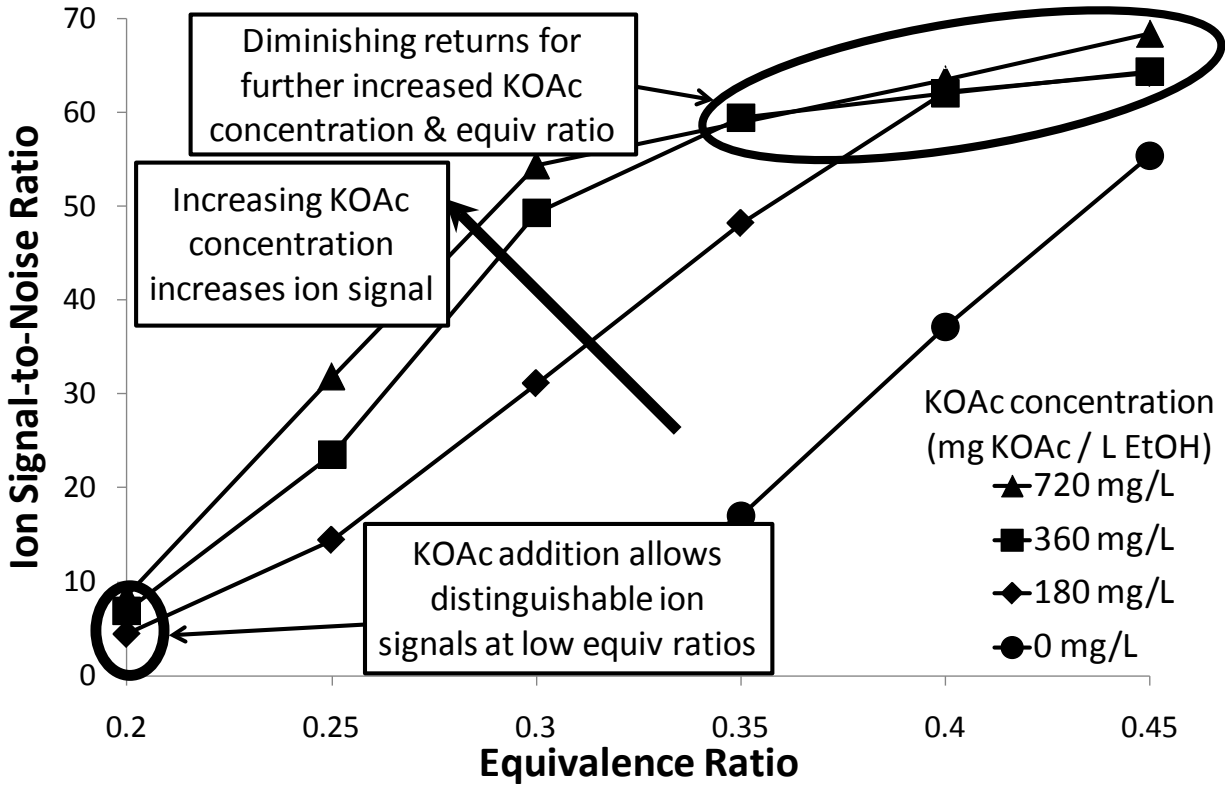

Figure 8-1 - Tests indicating that small amounts of KOAc in EtOH produce distinguishable ion signals at low equivalence ratios, and diminishing returns for higher KOAc concentrations.

For an equivalence ratio of 0.25, Figure 8-2 shows the tremendous increase in ion signal that can be achieved by adding small amounts of KOAc to Ethanol. Clearly, without the addition of KOAc, the ion signals are too weak for detecting the start of combustion. Adding a small amount of KOAc leads to a tremendous increase in the ion signal.

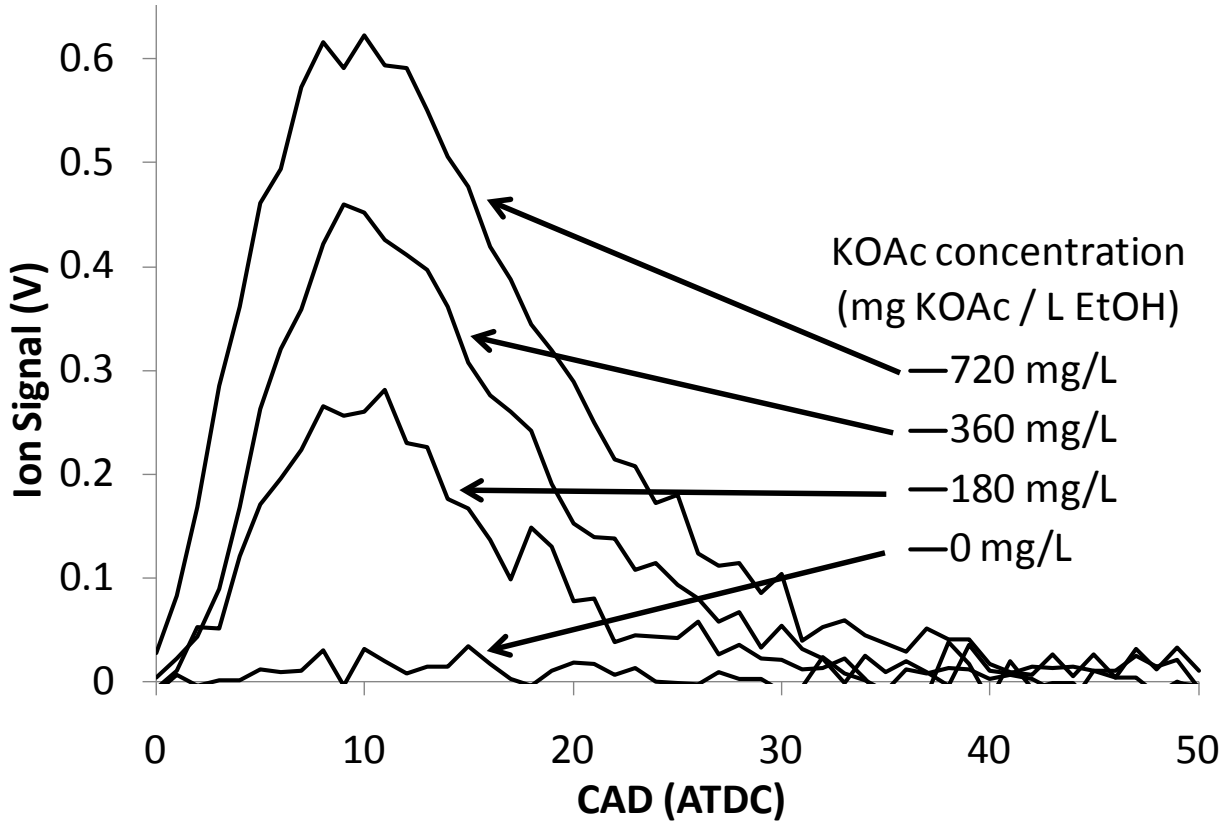

Figure 8-2 - At equivalence ratio of 0.25, below the saturation point, ion signal increases when KOAc concentration increases. (50 cycle average)

The second major result that can be seen in Figure 8-1 is that there is an upper limit beyond which increased concentrations of KOAc or increased equivalence ratios do not produce further gains in the ion signal-to-noise ratio. From Figure 8-2 it can be seen that the enhancement effect of KOAc upon ion signals is not linearly proportional to the amount of KOAc added. The ion signal benefit between 0 to 180 mg/L of KOAc is greater than the benefit from 180 to 360 mg/L. These diminishing returns can be explained in terms of peak in-cylinder temperatures which have a major impact upon the ionization of K atoms, and Figure 8-3 shows that the peak mass-averaged in-cylinder temperature decreases as KOAc concentrations are increased.

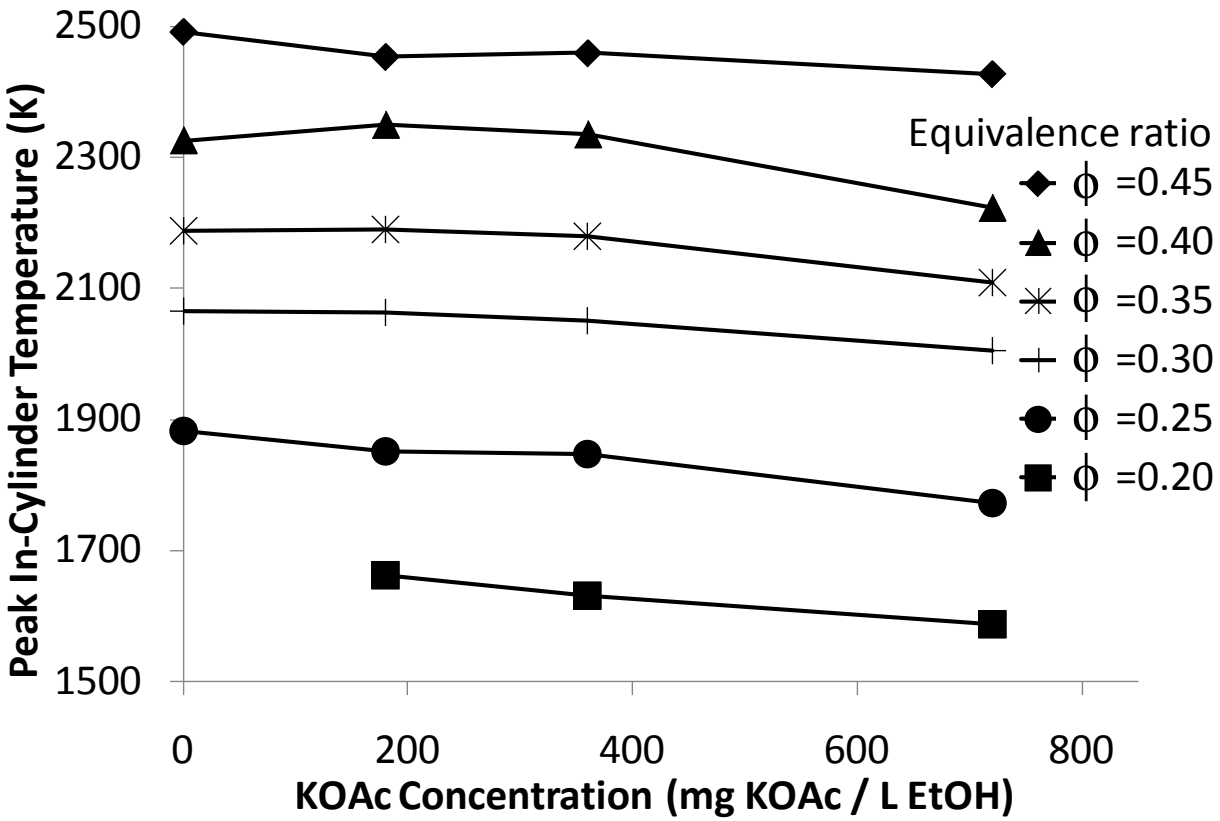

Figure 8-3 – Dispite increases in intake temperature, the mass averaged peak cylinder temperature decreases as KOAc concentration increases

As shown in Figure 8-3, the peak mass-averaged temperature decreases 60 to 100 K between KOAc concentrations of 0 and 720 mg/L in Ethanol. As described using the gas phase ionization of potassium ions a decrease of 60 K in peak temperature causes a 32% reduction in the number of potassium ions and electrons. Thus, the addition of K atoms through KOAc in EtOH creates more electrons for ion sensing only up to the point where the effects of decreased peak cylinder temperatures cause a reduction in the extent of potassium ionization.

The reduction in peak cylinder temperature is likely caused by combustion timing delay as KOAc concentrations were increased. Figure 8-4 shows the delay in crank angle degree for 50% heat release (CA50) as KOAc concentrations are increased:

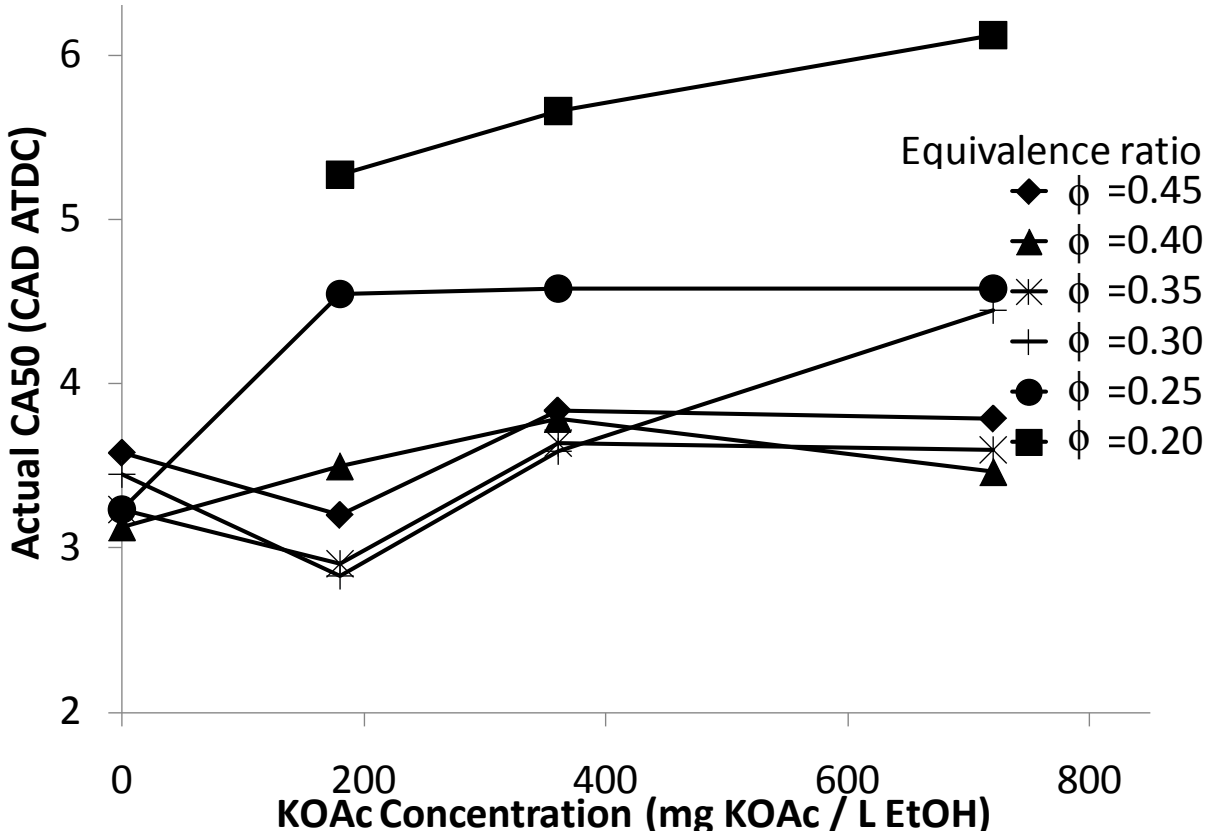

Figure 8-4 - Actual CA50 for each test point generally increases with KOAc addition dispite higher intake temperatures

8.2.4 Side effects on HCCI heat release rates from KOAc addition

The decreased peak in-cylinder temperature and delayed CA50 with increasing KOAc concentrations observed above point towards an interesting side effect of KOAc addition on Ethanol HCCI combustion. Heat release analysis on the pressure data shows that addition of KOAc causes lower heat release rates. Figure 8-5 shows that the peak heat release rate generally decreases with increasing KOAc concentration.

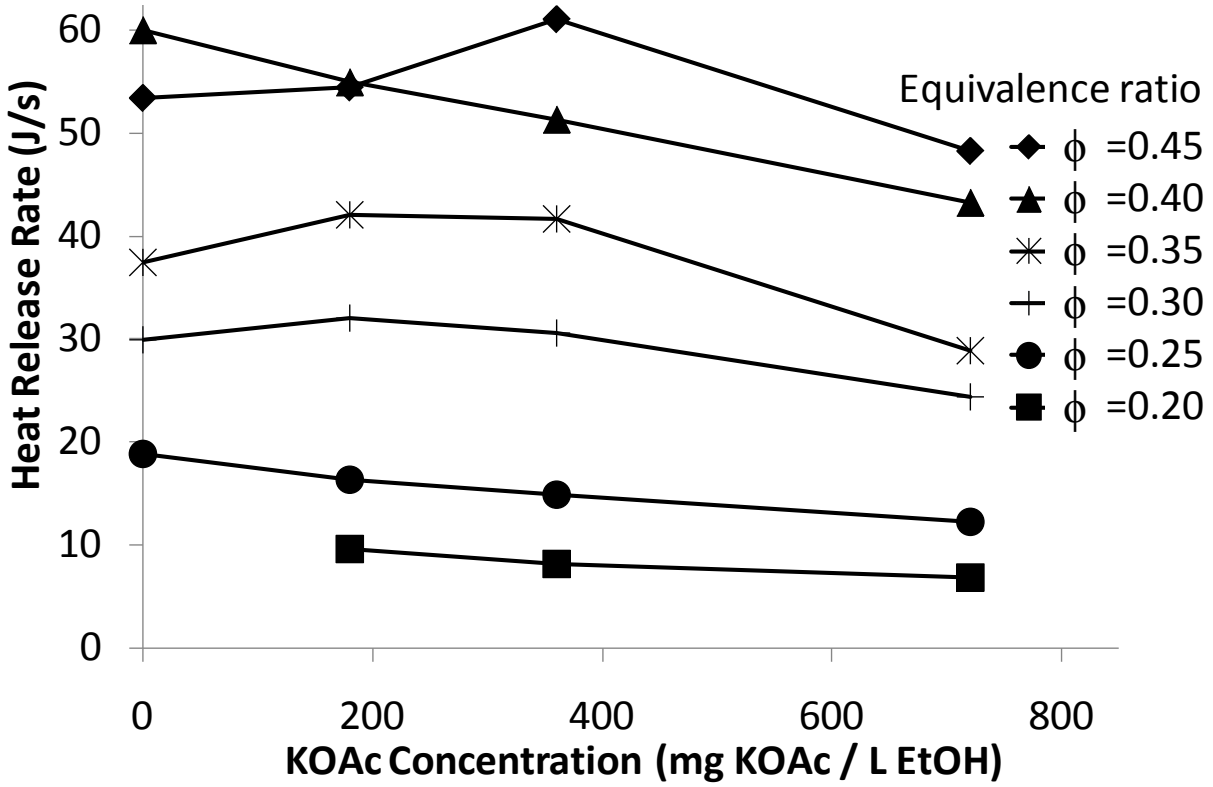

Figure 8-5 – Maximum Heat Release Rate for various KOAc-in-EtOH fuels shows a decreasing trend with KOAc addition

Figure 8-5 shows a trend of decreasing heat release rates with increased KOAc concentration, particularly for low equivalence ratios. Some of the higher equivalence ratio points seem to defy this trend, however these higher heat release cases may be explained by overcompensation of increases in intake temperature in attempts to maintain fixed CA50. Further insight into the heat release rates can be gained from Figure 8-6, which compares the heat release rates at equivalence ratio 0.25 for a variety of KOAc concentrations. Note that as presented in Figure 8-4, the CA50 for these runs are kept nearly constant at 4.5 degrees after top-dead-center, except for the first run with no additive.

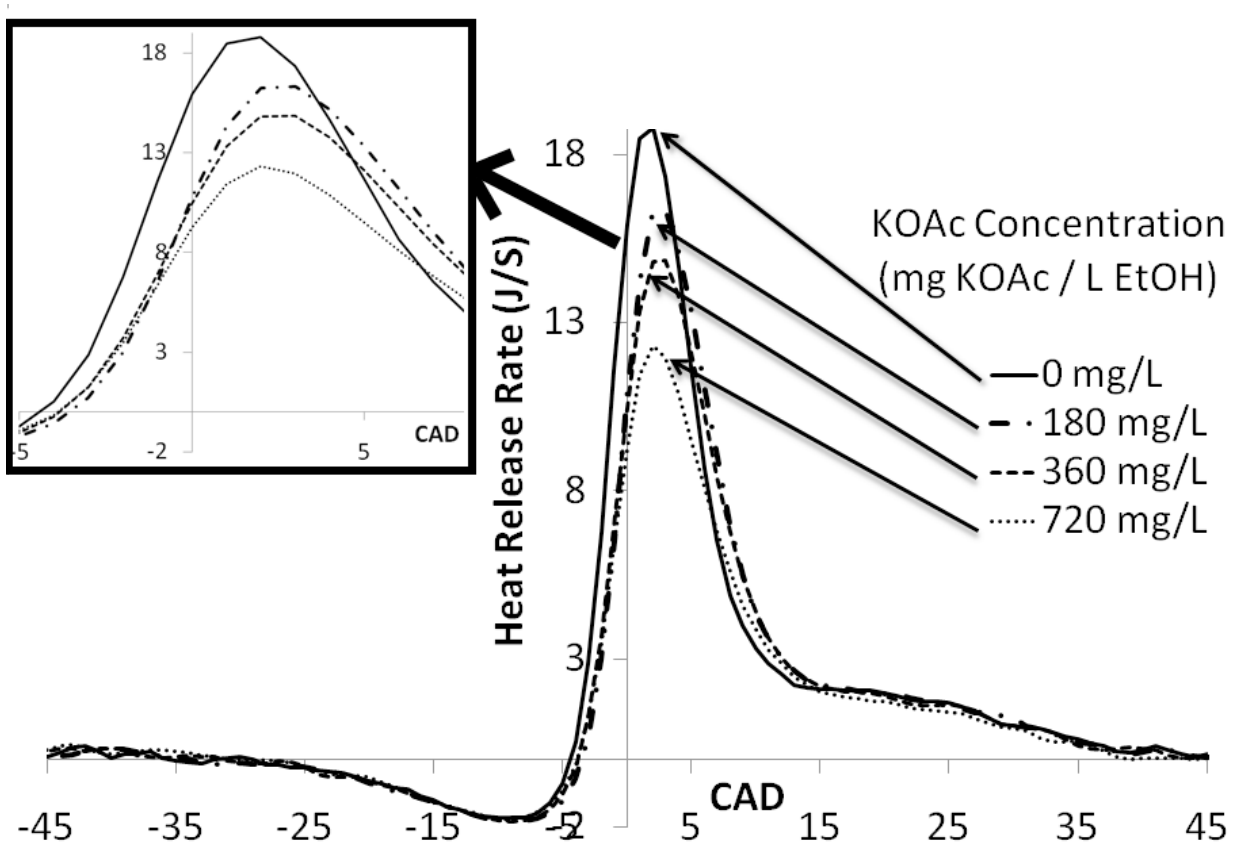

Figure 8-6 - Heat release rates for various KOAc-in-EtOH concentrations shows no change in LTHR, but different peak HRRs

There are two important features worth noting in Figure 8-6. First, addition of small amounts of KOAc in Ethanol does not alter the main Ethanol heat release pathways. In particular, the enhancement of ions by the K atoms is insufficient to induce low temperature heat release (LTHR). Second, the peak heat release rate decreases as KOAc concentrations are increased. This trend can be seen more directly from the zoomed in view presented on the left side of Figure 8-6, where the lower traces correspond to increased KOAc concentrations. It is interesting to note that analysis of cumulative heat release revealed little change to the combustion duration defined by the time period between CA5 to CA90.

Intake temperatures were gradually increased with higher KOAc concentrations to compensate for the lower heat release rate caused by KOAc addition. Although some points in Figure 8-5 defied the trend of lower maximum heat release rates with increased KOAc concentrations, the intake temperatures shown in Figure 8-7 remove any doubts of this trend. Figure 8-7 shows that higher intake temperatures are required to cancel the effects of lower heat release rates caused by KOAc addition. This allowed the CA50 to be bounded between 3 to 6 degrees aTDC, rather than allowing excessive CA50 delays as KOAc concentration was increased. The increases in intake temperature to maintain relatively constant CA50 are shown in Figure 8-7.

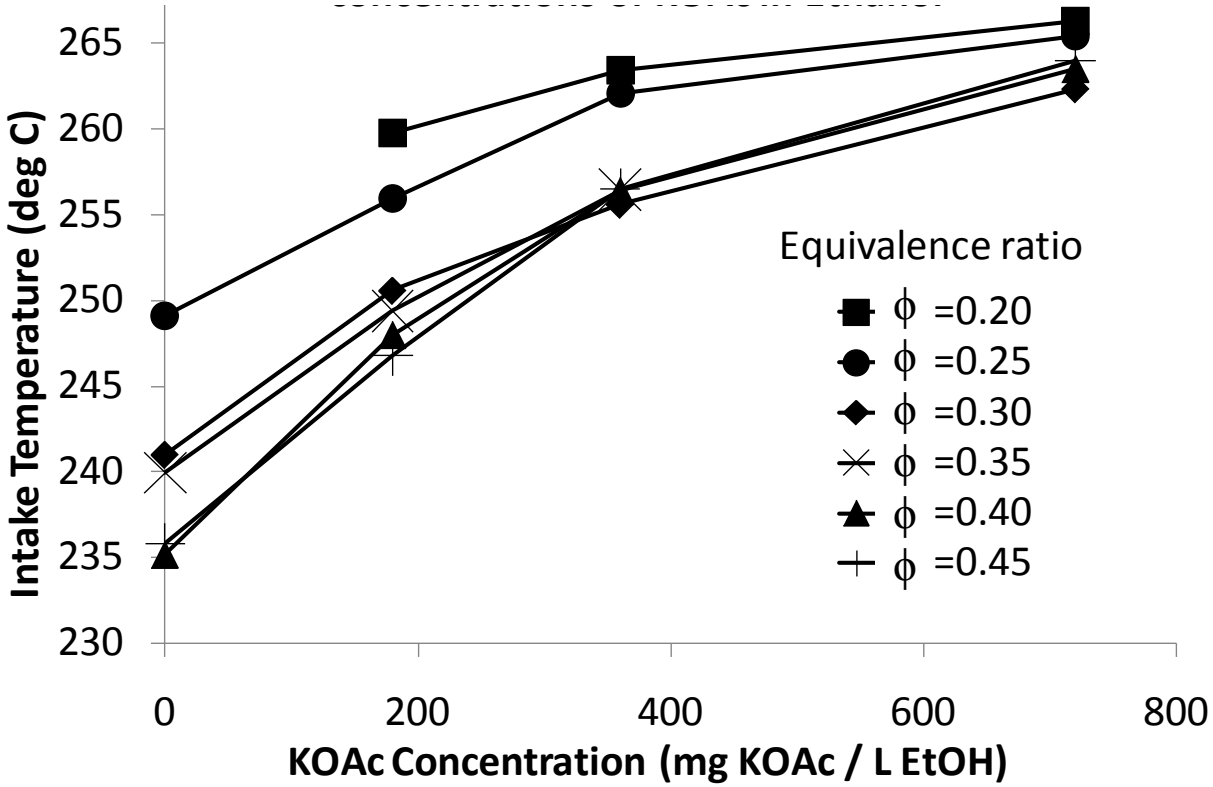

Figure 8-7 - To maintain relatively constant CA50, required intake temperature increases to offset the HRR reductions caused by increased KOAc concentration

The side effect of decreased heat release rates with higher KOAc concentrations causes a reduction in the in-cylinder pressures. Figure 8-8 shows in-cylinder pressure traces for a number of test points at equivalence ratio 0.25 with various concentrations of KOAc. The in-cylinder pressures are seen to decrease with increasing KOAc concentrations. These reduced in-cylinder pressures are caused by lower heat release rates which delay the pressure rise from combustion farther into the expansion stroke.

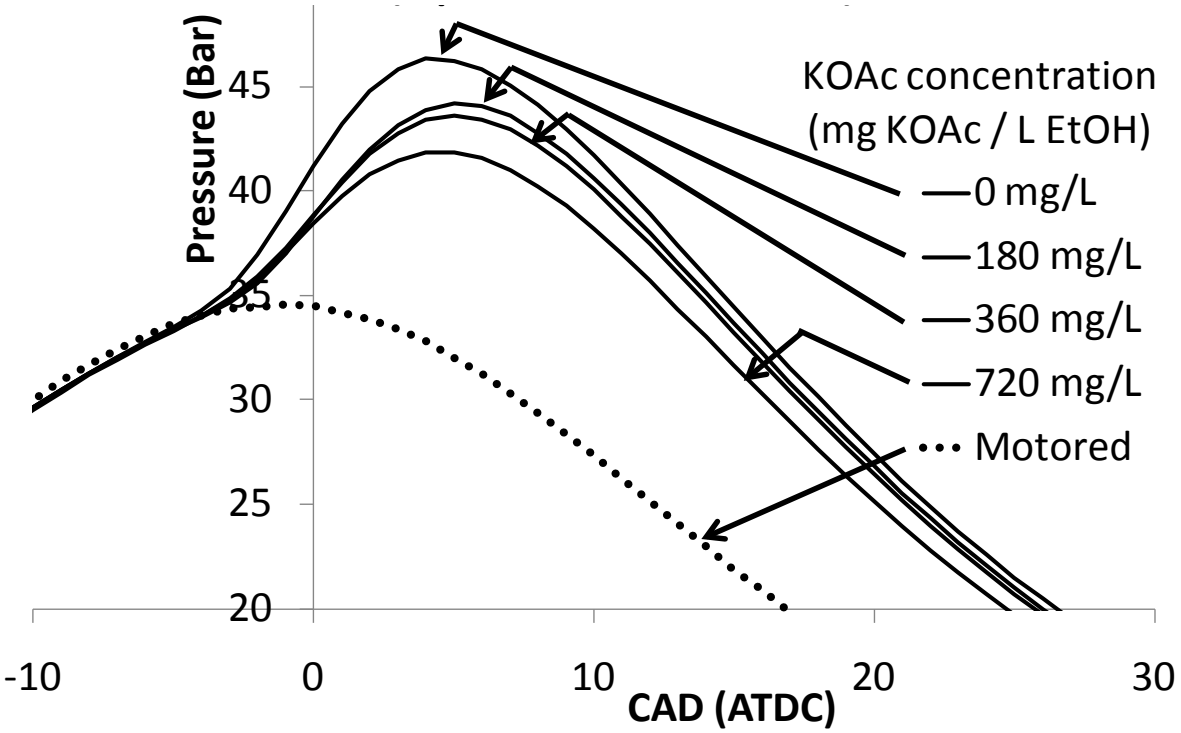

Figure 8-8 - At equivalence ratio of 0.25, peak pressure decreases as KOAc concentration increases. (50 cycle average)

The lower in-cylinder pressures with higher KOAc concentrations (seen in Figure 8-8) cause lower overall power output. Figure 8-9 shows that the indicated mean effective pressure (IMEP) decreases with increased concentrations of KOAc. The loss in power output ranges from 2 to 10% when 180 mg/L of KOAc is added to the fuel.

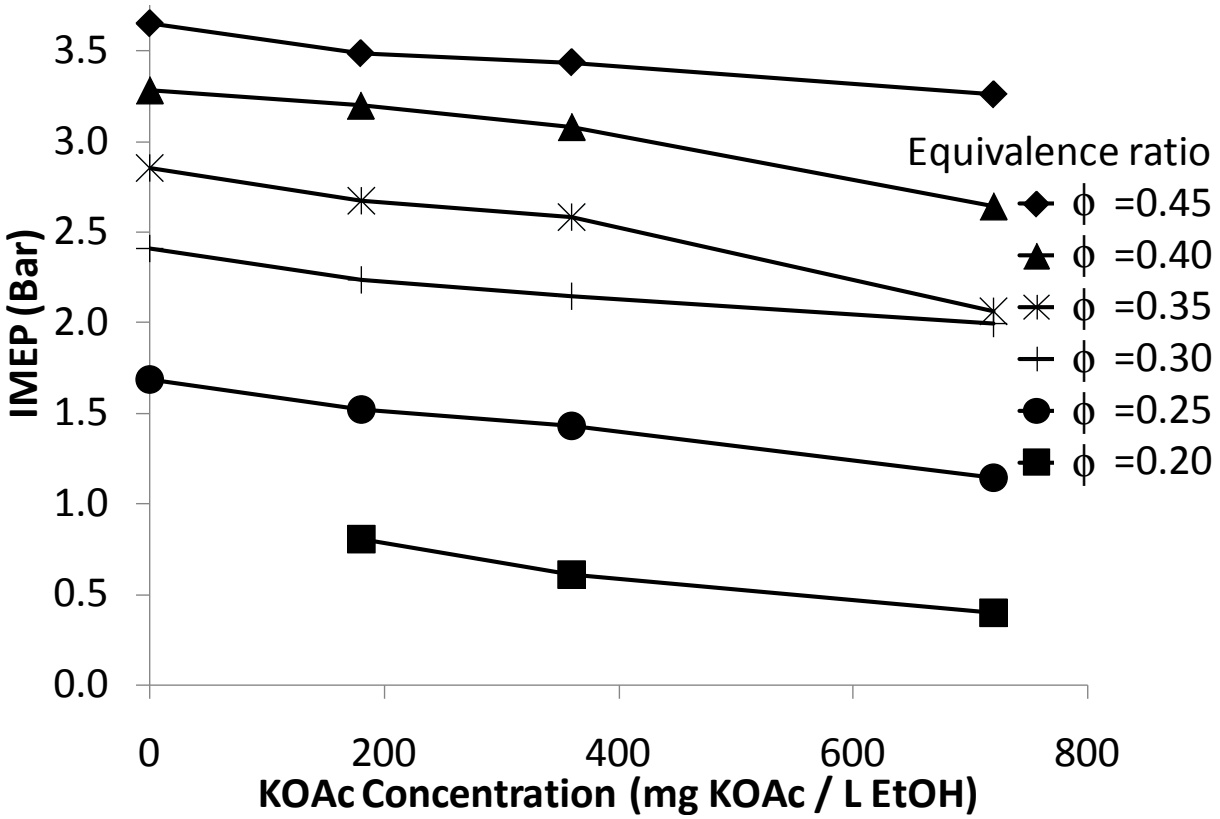

Figure 8-9 - Power output for various KOAc-in-EtOH fuels shows power output decreases with increasing KOAc content, due to lower peak pressures caused by reduced HRR

By combining the ion signal and heat release results observed from Figure 8-1 through Figure 8-9 it is apparent that adding small amounts of KOAc to Ethanol causes an enhancement of the ion signal. This enhancement is sufficiently great such that distinguishable ion signals can be observed at equivalence ratios as low as 0.20, thereby enabling control of HCCI engines using ion sensors. The side effect of adding KOAc to the fuel, however, is that it causes reduced heat release rates which can ultimately effect the power output and overall efficiency. The reduced heat release rates can be overcome by using higher intake temperatures, or the reduced heat release rates can be minimized by using even smaller concentrations of KOAc additive.

8.3 Detecting HCCI ringing using ion sensors

Engine damage can be caused by prolonged operation of an HCCI engine under conditions of excessive ringing. The maximum power (and often the maximum efficiency) operating points in thermally controlled HCCI engines typically occur near the boundaries of intense ringing [17]. To operate at the highest power and efficiency points while avoiding excessive ringing, it is important for an engine controller to consider ringing intensity as an input parameter. Ringing intensity, however requires acquisition of in-cylinder pressure measurements requiring expensive in-cylinder pressure transducers, charge amplifiers and signal conditioning electronics. The purpose of the research in this section is to demonstrate that ringing can be characterized with information from a less expensive sparkplug ion sensor. A correlation for quantifying ringing using ion sensors is introduced and verified over a range of engine operating conditions.

8.3.1 Quantifying ringing intensity using ion current signals

The results of this research suggest that ringing intensity can be quantified from an ion current signal using Eq. 6.6:

$$\text{Ion RI} \approx \frac{\alpha \cdot \left(\frac{P_{in}}{P_{atm}} \cdot \frac{d\text{Ion}}{dt}_{\max} \right)^2}{\sqrt{Ion_{\max}}} \qquad \text{(Eq. 6.6)}$$

In Eq. 6.6, "Ion RI" is the ringing intensity (MW/m^2) as quantified by the ion current signal, P_{in} is the intake charge pressure (bar), P_{atm} is atmospheric pressure (~1 bar), $dIon/dt_{max}$ is the peak ion signal rise rate (μA/s), and Ion_{max} is the maximum of the ion current signal (μA). α is a scale factor determined from experimental data to convert from units of ion current into the accepted units of ringing intensity.

Values for the scaling factor α are shown for two equivalence ratios in Table 8-1:

Table 8-1 - Scaling factors for ion ringing correlation

	Φ=0.50	**Φ=0.45**
α [$MW \cdot s/\mu A^{1.5} \cdot m^2$]	4.81058×10^{-6}	3.05551×10^{-5}

The scaling factors presented in Table 8-1 are determined from engine data at a naturally aspirated operating condition. For each equivalence ratio, the engine is operated at several combustion timings (shown in Figure 8-10), and the scaling factor is determined as the ratio of the average of ringing intensities at various combustion timings over the average of ion signal characteristics for the same combustion timings, as shown in Eq. 6.7. The same scaling factor for a given equivalence ratio can be used at higher intake pressures.

$$\alpha = \frac{\langle RI \rangle}{\left\langle \left(\frac{d\text{Ion}}{dt}_{\max} \right)^2 \Big/ \sqrt{\text{Ion}_{\max}} \right\rangle} \qquad \text{(Eq. 6.7)}$$

8.3.2 Verification of ion ringing intensity correlation with engine data

Figure 8-10 and Figure 8-11 show a comparison of the pressure-based (Eq. 4.16) and ion-based (Eq. 6.6) ringing intensity across a wide range of engine conditions.

Figure 8-10 shows two equivalence ratios at naturally aspirated conditions. For a wide range of combustion timings (CA50), the ion-based ringing intensity closely agrees with the pressure-based ringing intensity. The maximum error between pressure- and ion-based ringing intensities in Figure 8-10 is 0.82 MW/m^2. The values of α presented in Table 8-1 were used for the ion data presented in Figure 8-10.

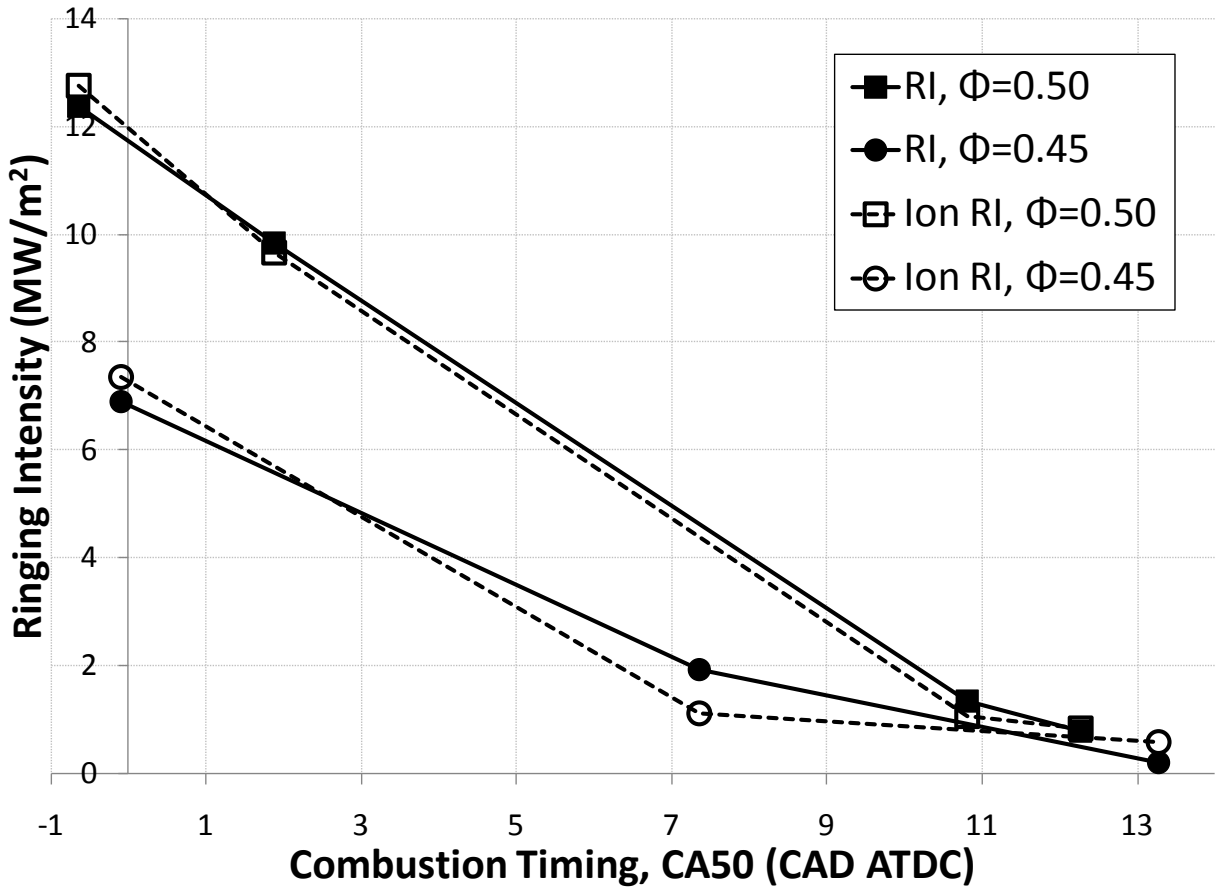

Figure 8-10 - Pressure and ion based ringing intensity show close agreement for naturally aspirated experimental data at two equivalence ratios

Figure 8-11 shows the test conditions at elevated intake pressures for various equivalence ratios and combustion timings. Twelve different operating conditions are plotted and the vast majority have an absolute error less than 2 MW/m^2 between the pressure- and ion-based ringing intensities. Three data points, however, have a larger absolute error near 6 MW/m^2.

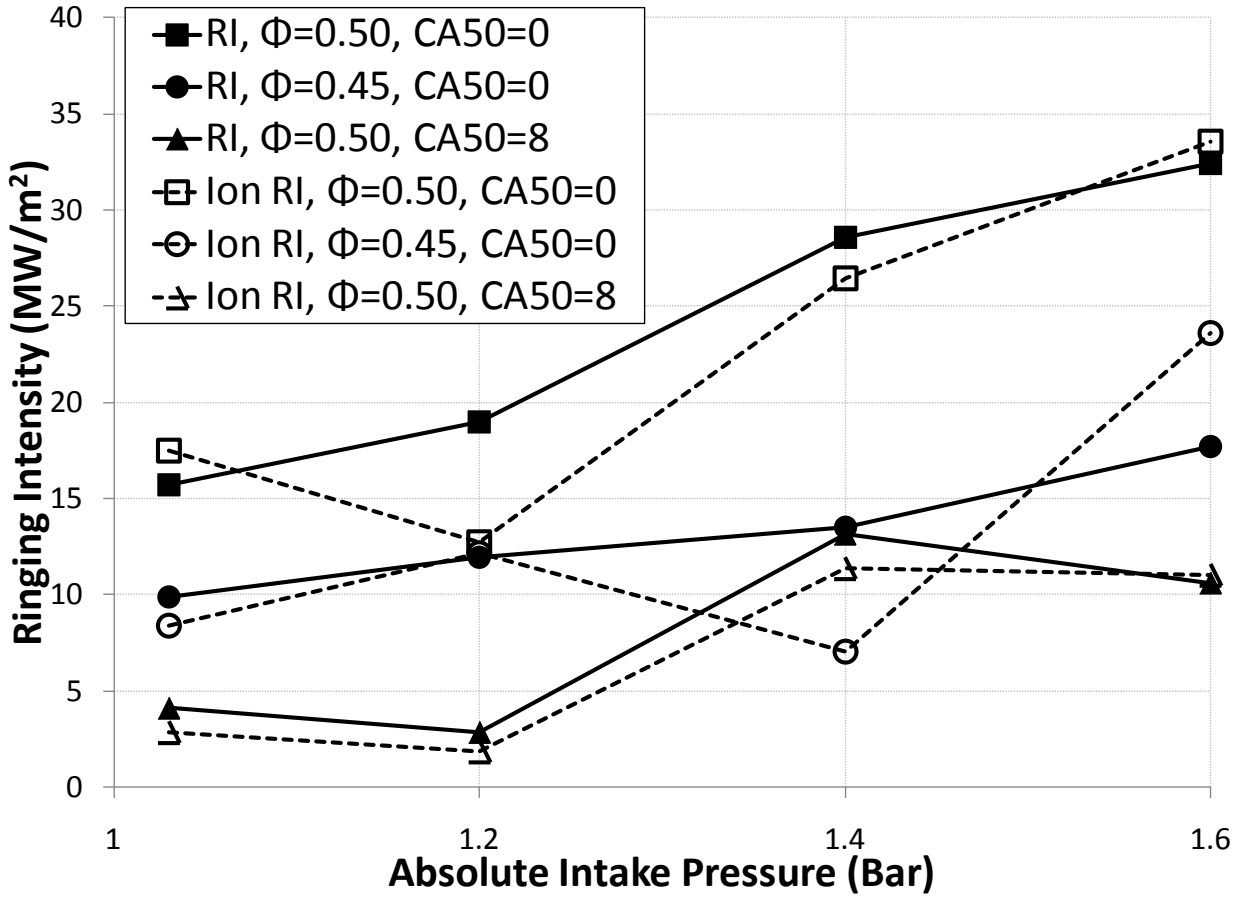

Figure 8-11 - Pressure and ion based ringing intensity show close agreement for a majority of test points spanning several intake pressure conditions

The results of Figure 8-10 and Figure 8-11 suggest that the ion ringing intensity correlation of Eq. 6.6 is relatively effective at estimating the ringing intensity. Uniformly, the ion ringing intensity correlation was able to distinguish between test conditions that were either above or below the accepted 5 MW/m^2 ringing limit. Ringing intensity for all test points below the ringing limit was quantified fairly accurately.

8.3.3 Theoretical justification for ion ringing intensity correlation

The ion ringing intensity correlation presented in Eq. 6.6 was the most effective at estimating ringing as compared with numerous other combinations of ringing characteristics that were explored as part of this study. The ion ringing intensity correlation was developed on the basis that ion current signals are more distinguishable under conditions of intense ringing.

The most important aspect of the pressure-based ringing intensity correlation (Eq. 4.16) is the peak pressure rise rate, thus an accurate predictor of this parameter is required in the ion signal. Experimental data presented in Figure 8-12 shows that the peak ion rise rate is an excellent indicator of this parameter. A linear fit of each data set in Figure 8-12 is drawn and R^2 values are shown to compare the linear fit with the actual data. The near-unity R^2 values and slopes of the

linear fit suggest that the ion rise rate is an excellent predictor of the pressure rise rate. The ion rise rate shown on the y-axis of Figure 8-12 was rescaled to match the pressure rise rate units in a similar fashion as was used in Eq. 6.7 by scaling by the ratio of the average pressure rise rate and ion rise rate.

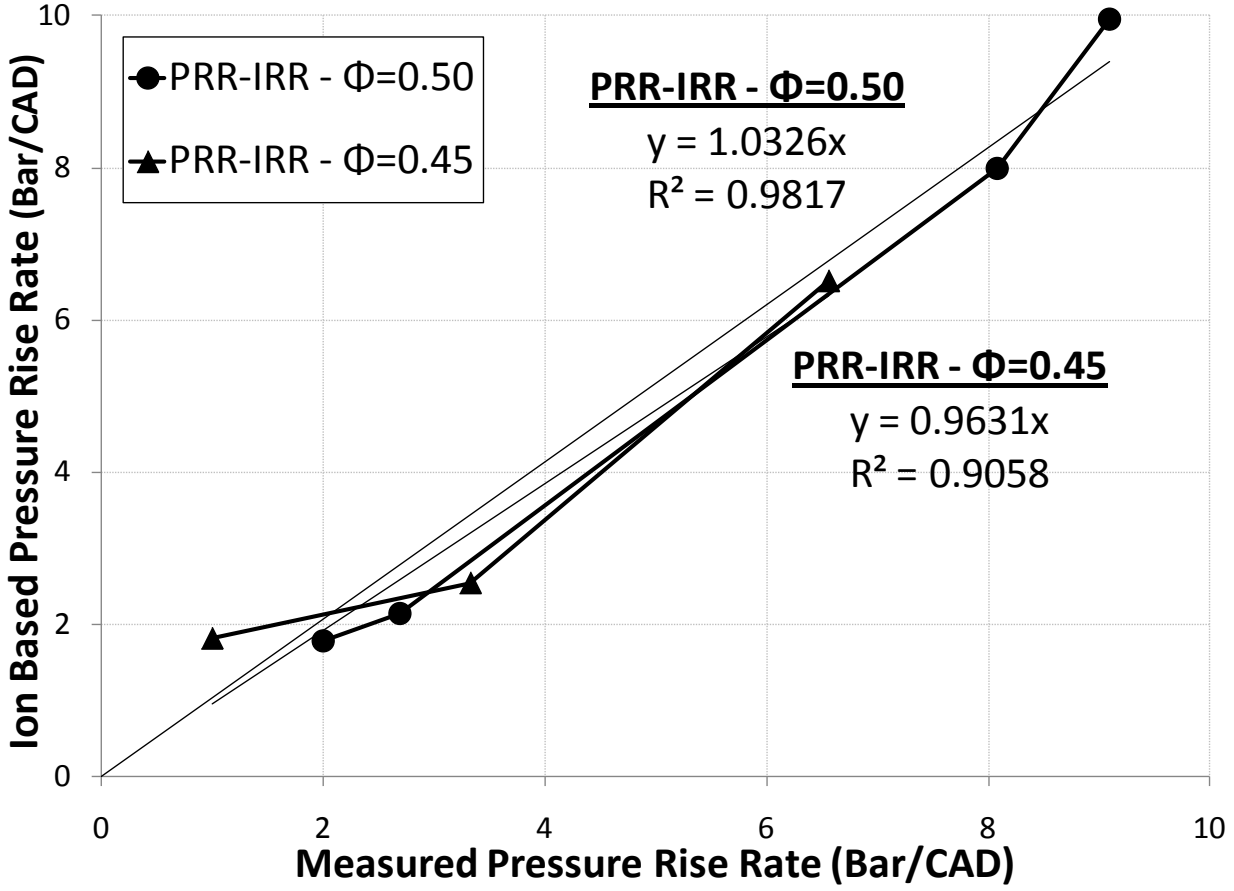

Figure 8-12 - Comparison of peak pressure-rise-rate with the rescaled ion-rise-rate shows a nearly 1-to-1 correlation between the two parameters

In order to quantify the ringing intensity effectively, an ion-based estimate of peak in-cylinder pressure and peak in-cylinder temperature are also required (as in Eq. 4.16). These two parameters are more difficult to estimate, however prior studies have shown that the ion-current signal is greater under conditions with higher in-cylinder temperature [70,72,75,85,87]. From ideal gas law, it is known that pressure and temperature rise proportionally to one another. As a result, the maximum ion current is used as an indicator of both the peak pressure and peak temperature in the denominator of Eq. 6.6. The $Ion_{max}^{-½}$ term is used because the maximum current captures both the peak pressure (a P^{-1} term in Eq. 4.16) and peak temperature (a $T^{+½}$ term in Eq. 4.16).

8.3.4 Cycle-to-cycle ringing predictions from ion ringing intensity correlation

As demonstrated for 300-cycle averages in Figure 8-10 and Figure 8-11, the ion ringing intensity correlation predicts the ringing intensity over a wide range of operating conditions that capture

various degrees of ringing. In Figure 8-13 and Figure 8-14, the ringing intensity and ion ringing intensity are compared on a cycle-by-cycle basis. Figure 8-13 corresponds to a test point where the ion ringing intensity agrees very closely with the pressure-based ringing intensity, while Figure 8-14 corresponds to a test point where the ion ringing intensity underpredicts the pressure-based ringing intensity. In both Figure 8-13 and Figure 8-14 it is apparent that the ion ringing intensity spans a wider range than the pressure ringing intensity. As a result, for effective feedback control it may be required to take several-cycle averages of ion ringing intensity to remove the greater noise in ringing intensity estimates.

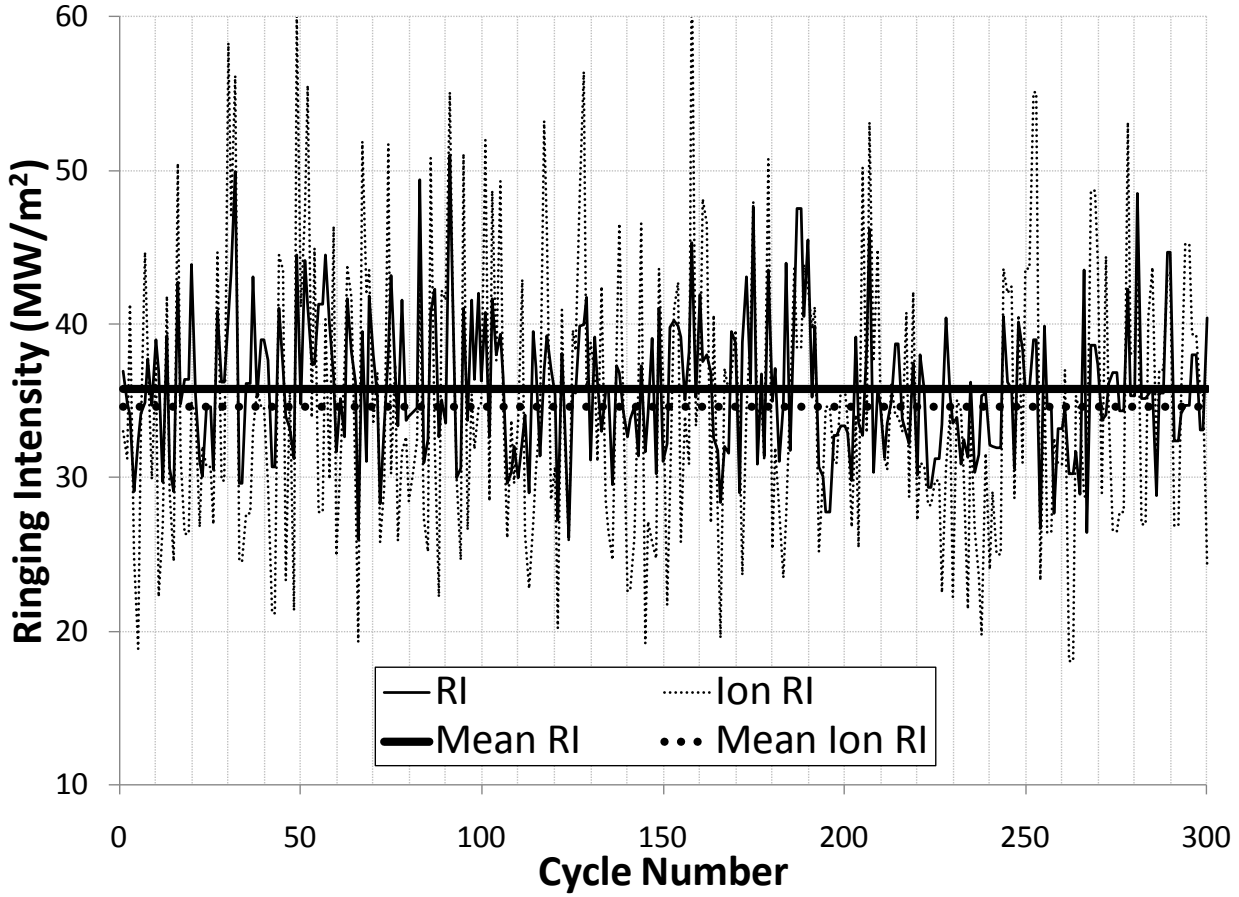

Figure 8-13 - Cycle-to-cycle comparison for ϕ=0.50, P_{in}=1.6 bar, CA50=0 test point shows ion ringing intensity spans a wider range, but has a very similar mean value to pressure ringing intensity

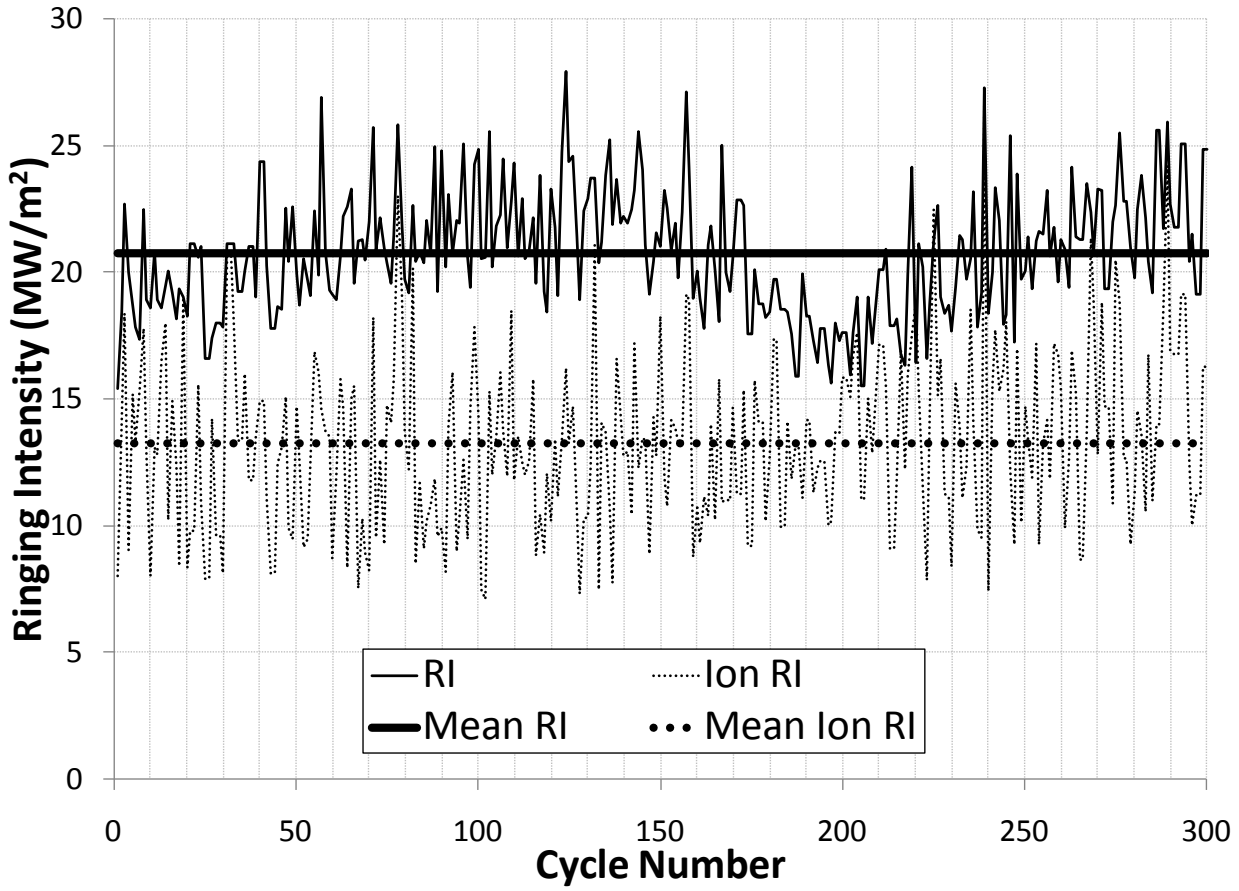

Figure 8-14 - Cycle-to-cycle comparison for ϕ=0.50, P_{in}=1.2 bar, CA50=0 test point shows ion ringing spans a wider range, and has a lower mean value than pressure ringing intensity

The larger fluctuations of ion ringing intensity in Figure 8-13 and Figure 8-14 are caused by fluctuations in the ion rise rate. Small differences in the ion rise rate can have a large effect upon the ion ringing intensity because of the squared term in Eq. 6.6. These fluctuations may be caused by cycle-to-cycle differences in localized mixture fraction near the ion sensor, which can be minimized with more intense turbulence. The effects of these fluctuations upon a control system can be virtually eliminated by taking several-cycle averages of the ion ringing intensity.

8.3.5 Effects of sensor and measurement circuit parameters on ion ringing correlation

Figure 8-15 shows the effect of varying the resistance of the measurement circuit (depicted in Figure 8-16) upon ion rise rate while ringing intensity is maintained constant. As lower resistances are used, the ion rise rate increases. A similar trend is seen in the maximum ion current. The effect of changing the resistance can be corrected for by multiplying the result of the ion ringing intensity by an additional term $(R_{new}/R_{base})^2$, where R_{new} is the new resistance installed in the measurement circuit and R_{base} is the original resistance at which the scaling factor α was quantified (1.029 MΩ in this study).

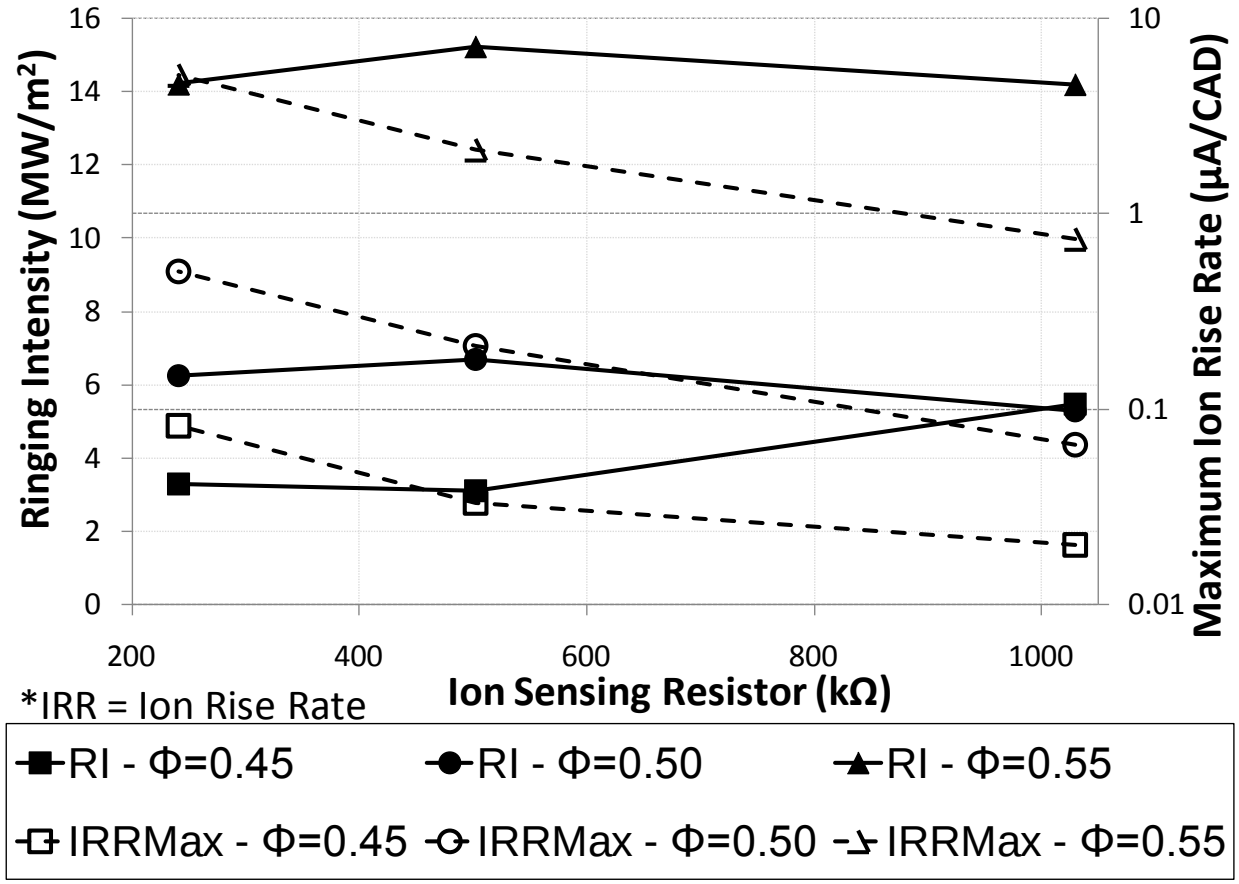

Figure 8-15 - Effect of measurement circuit resistor on ion-rise-rate

Figure 8-17 shows the effect of changing the bias voltage across the ion sensor upon the ion rise rate. The ringing intensity is maintained relatively fixed while the bias voltage is changed. Higher ion rise rates are observed with higher bias voltages, and similar trends are seen in the maximum ion current. As a result, ion ringing intensity increases as the bias voltage increases. At very low bias voltages, the ion signal becomes less distinguishable from noise, making it difficult to determine the ion ringing intensity.

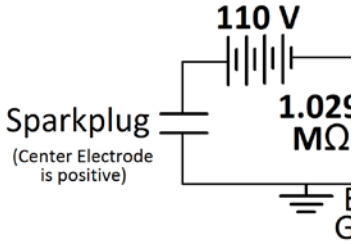

Figure 8-16 - Measurement circuit for ion sensing

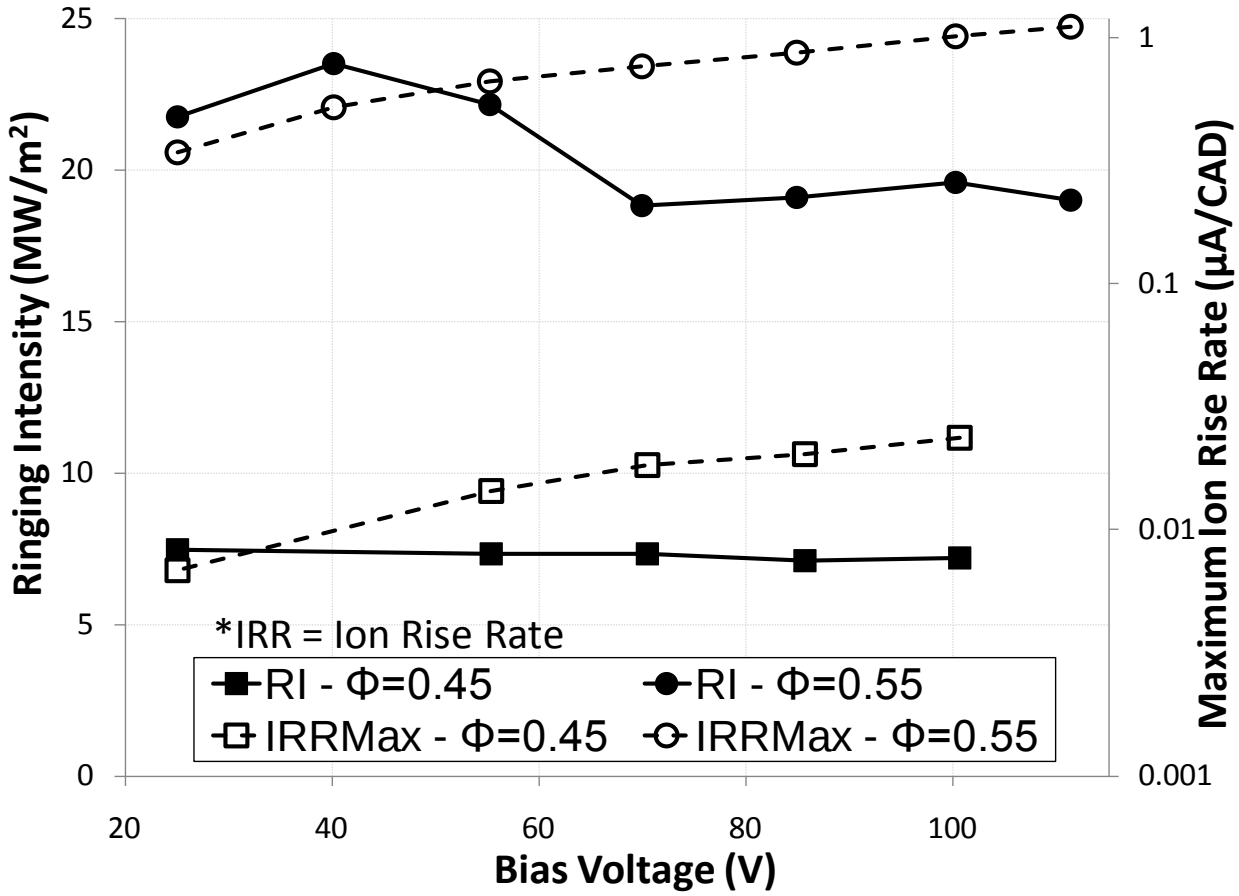

Figure 8-17 - Effect of bias voltage on ion-rise-rate

Extensive prior research [70,71,74,75,78,82,83,84] has shown the ability for ion sensors in an HCCI engine to measure combustion timing for use in feedback control. The research presented in this chapter reveals methods to extend the useful operating range of ion sensors into lower power output conditions (specifically low ϕ), and also a method to quantify the ringing intensity for feedback control at high power settings. Combining these results with prior studies makes control of HCCI engines with ion sensors more realizable for production applications.

9 Summary of results and conclusions

HCCI engines have the potential to enable automotive and stationary power generation with high efficiency and cleaner emissions without the need for expensive after treatment systems. HCCI is efficient allowing lower CO_2 emissions, like Diesel engines, and has low particulate matter emissions, like spark-ignited engines. The low in-cylinder temperatures allow for low nitric oxide emissions, and the use of oxidation catalysts with HCCI engines can allow low unburned hydrocarbon and carbon monoxide emissions. The historical challenges facing HCCI are that they have lower power output compared with spark-ignited and Diesel engines, and it is difficult to control combustion timing. The research presented within this dissertation discusses strategies for increasing the power output within HCCI engines and presents solutions for using ion sensing in detecting combustion characteristics to allow inexpensive feedback control of HCCI engines. The results from these research efforts are summarized in the following sections.

9.1 Strategy for maximizing power output

Experiments were conducted on a multi-cylinder, automotive-scale HCCI engine at a wide range of different intake pressures, equivalence ratios, combustion times and exhaust backpressures with the goal of identifying the conditions that allow high power with acceptable ringing and overall stable engine performance. For all of the test points, engine efficiency and emissions were also analyzed. Although many of the results presented show only a single cylinder, similar trends were seen across all four cylinders in the study. The following results were shown in maximizing engine power output:

1) For a given intake pressure, high power output occurs with high equivalence ratios, while delayed combustion timing can be used in controlling ringing. This strategy causes the highest power output conditions near the limits of ringing, misfire and controllability.

2) For a given intake pressure, power output and efficiency are generally higher with increased equivalence ratios, but excessively advanced combustion timing can cause reduced power output and efficiency because of higher heat loss, while excessively delayed combustion timing (before misfire) can cause power output and efficiency losses because of incomplete oxidation of hydrocarbons and carbon monoxide and also thermodynamic losses.

3) At highly delayed combustion timing, higher emission of hydrocarbons and carbon monoxide are caused by very low peak in-cylinder temperatures that result in low concentrations of OH radicals which are critical in the autoignition process.

4) At a given intake pressure, ringing increases with advanced combustion timing, and the rate of this increase with advancements in combustion timing is more pronounced for higher equivalence ratios.

5) For a given intake pressure, NO_x emissions increase with higher equivalence ratios and more advanced combustion timing because of higher peak in-cylinder temperatures.

6) Power output can be increased with higher intake pressures, however at high intake pressures the range of operable combustion timings is limited by ringing and losses in controllability.

7) Efficiency and hydrocarbon and NO_x emissions are generally insensitive to higher intake pressures although mass averaged peak in-cylinder temperatures are lower with high boost pressures because of the lower intake temperatures that are utilized, while carbon monoxide emission show a slight increase with intake pressures.

8) For a fixed equivalence ratio, ringing intensity increases with increased intake pressure.

9) Using the trends identified, a high power output condition exceeding 8 bar gross IMEP was found at 2 bar intake pressure, however several other operating points showed promising power outputs with acceptable ringing intensities.

10) Indicated efficiency at the higher power output points approached 40%. At high boost pressures, concerns were identified since intake temperatures were near ambient resulting in a loss of controllability of combustion timing (lower intake temperatures are impractical while higher intake temperatures resulted in ringing).

For multi-cylinder operation of an HCCI engine, the following results were shown:

11) The importance of individual cylinder control was demonstrated through the different intake temperatures required in maintaining desired combustion timings across the different cylinders. These variations in intake temperature requirements are caused by differences in intake flow between cylinders, differences in heat transfer, variations in fuel injection and variations in geometric tolerances between cylinders. For a given intake pressure and equivalence ratio, differences in intake temperature as high as 15°C were observed in maintaining a desired combustion timing across the different cylinders.

12) Complications dealing with cylinder-cross-talk were identified for multi-cylinder thermal control of HCCI, where coupled flow dynamics between neighboring cylinders caused disturbance propagation between cylinders.

13) At high power output conditions, where stable combustion is achieved along the boundaries of misfire, peak pressure, ringing and loss of controllability, neighboring cylinders can be driven into unstable combustion regimes as a result of disturbance propagations from one cylinder.

14) These disturbance propagations can however be minimized using well designed intake manifolds that reduce the coupled flow dynamics between cylinders. Effective control of individual cylinders can also help in minimizing these disturbance propagations.

Finally, the effects of exhaust backpressure were explored because production HCCI engines would likely use turbochargers that induces backpressure in the exhaust. Different exhaust backpressures were explored for a given intake pressure where set fuel injection was maintained. The following results were identified for the effects of changing exhaust backpressure:

15) Increased exhaust backpressures cause lower intake temperature requirements in maintaining desired combustion timings

16) Exhaust backpressure has little effect on gross power output, efficiency, ringing or carbon monoxide emissions. Slight decreases in NO_x and hydrocarbon emissions were observed with increased exhaust backpressures.

For all of the tests conducted, NO_x emissions were well below the US2010 emissions regulations. The results demonstrate that high power output (sufficient for passenger vehicles) can be achieved with HCCI engines with very low levels of NO_x emission, while unburned hydrocarbons and carbon monoxide can be removed with an oxidation catalyst.

9.2 Ion sensing for characterizing and controlling HCCI combustion

Ion sensing provides an alternative in-cylinder diagnostic technique to measure combustion characteristics. This technique is significantly less expensive than using in-cylinder pressure sensors which have traditionally been used in laboratory applications of HCCI, and therefore the use of ion sensors improves the affordability of HCCI engines. Two problems with ion sensing for HCCI applications is that this technique is ineffective at lower load conditions (with low equivalence ratios), and it is unable to quantify the ringing intensity that is computed from pressure data. The research presented in this dissertation and summarized in the next two sections presents solutions to address these challenges.

9.2.1 Extending the lower equivalence ratio limits for ion sensors

KOAc is used in these experiments as a surrogate for many possible types of metal acetates. The results from this study suggest that adding small amounts of KOAc to EtOH is an effective way of increasing the ion signal-to-noise ratio. At equivalence ratios as low as ϕ=0.20, KOAc concentrations of 180 mg/L (107 ppm) were able to produce discernable ion signals. The results indicate that the ion signal saturates at high KOAC concentrations, where diminishing returns of the ion signal are seen by continuing to increase KOAc concentrations. It was found that increasing KOAc concentrations cause reduced heat release rates, and higher intake temperatures are required to offset this effect. These reduced heat release rates may be a beneficial side effect since HCCI power output is limited by excessive rates of heat release and pressure rise, however in these experiments the reduced heat release rates also contributed to a loss in power output.

9.2.2 Detecting HCCI ringing using ion sensors

Ringing intensity computed from in-cylinder pressure measurements was compared against ion current signals from a sparkplug ion sensor. The study concludes with the following findings:

1) The ringing intensity within an HCCI engine can be computed using an ion current signal using the relationship:

$$\text{Ion RI} \approx \frac{\alpha \cdot \left(\frac{P_{in}}{P_{atm}} \cdot \frac{d\text{Ion}}{dt}_{\max} \right)^2}{\sqrt{Ion_{\max}}}$$

where Ion RI is the ringing intensity (MW/m^2) as quantified by the ion current signal, P_{in} is the intake charge pressure (bar), P_{atm} is the atmospheric pressure, $dIon/dt_{max}$ is the maximum ion signal rise rate ($\mu A/s$), and Ion_{max} is the maximum of the ion current signal (μA). α is a scaling factor determined from the experimental data to convert from units of ion current into the more commonly accepted units of ringing intensity.

2) The scale factor α has a different value for each equivalence ratio. The scaling factor is measured at naturally aspirated operating conditions by comparing pressure and ion data across a wide range of combustion timings. Once measured, this value can be used at higher intake pressures.

3) On a cycle-resolved basis, the ion ringing intensity exhibits more noise than the pressure-based ringing intensity. Generally, the 300-cycle average of ion- and pressure-based ringing intensities agreed well. Thus, the ion ringing intensity produces better results if it is taken as an average over several cycles.

4) The ion ringing intensity increases as lower resistances are used in the measurement circuit. The effects of varying resistances can be corrected for by multiplying ion ringing intensity by an additional term $(R_{new}/R_{base})^2$. R_{new} is the new resistance installed in the measurement circuit and R_{base} is the original resistance at which the scaling factor α was quantified (1.029 $M\Omega$ in this study).

5) The ion ringing intensity increases as higher bias voltages across the sparkplug electrodes are used.

9.3 Further areas for improvement and future research

The research summarized in sections 9.1 and 9.2 discusses methods for increasing the power output of HCCI engines, and solutions for using ion sensing in detecting important combustion parameters for use in feedback control. The following steps are recommended in improving and extending upon the research presented in this dissertation:

Improving HCCI Power Output:

1) Investigate the use of EGR for avoiding the low temperature limits (discussed in section 6.5) which constrain the maximum power output with gasoline in HCCI engines at boosted intake pressure conditions

2) Investigate the use of mixture stratification through direct injection to allow more gradual heat release (discussed in section 4.1.2) to avoid the ringing limits constraining maximum power output

Enabling Ion Sensing at Low Equivalence Ratios using Fuel Additives:

1) Investigate whether different metal acetate additives allow the same benefits in improved ion sensing at low equivalence ratios

2) Investigate how different metal acetates influence the heat release process

3) Investigate whether the reduced peak heat release rate from introducing small amounts of KOAc additive can be used to extend the ringing limits and improve the power output from HCCI engines

Quantifying Ringing Intensity using Ion Sensing

1) Validate the ringing intensity correlation developed in section 8.3 for different fuels

2) Develop a greater understanding of whether localized effects may be causing the disagreements in ion-based versus pressure-based ringing intensity at elevated intake pressures (discussed in section 8.3.2)

3) Investigate whether using a lower resistance in the ion sensing circuit will allow oscillations in the ion signal to become apparent under ringing conditions, similar to how a pressure signal shows oscillations under ringing conditions.

10 References

1. Onishi, S., Jo, S.H., Shoda, K., Jo, P.D., and Kato, S., "Active Thermo-Atmosphere Combustion (ATAC) – A New Combustion Process for Internal Combustion Engines", SAE Paper 790501, 1979, doi: 10.4271/790501

2. Zhao, F., Asmus, T., Assanis, D., Dec, J.E., Eng, J., and Najt, P., "Homogeneous Charge Compression Ignition (HCCI) Engines: Key Research and Development Issues", Warrendale: SAE International, 2003.

3. Bogin, G., "Characterization of Ion Production Using Gasoline, Ethanol, and N-Heptane in a Homogeneous Charge Compression Ignition (HCCI) Engine, Ph.D Dissertation", Berkeley, 2008.

4. "How a four stroke engine works..", http://minhazchhiboo.blogspot.com/2011/04/how-four-stroke-engine-works.html, October 20, 2011.

5. Dec, J.E, "Advanced compression-ignition engines—understanding the in-cylinder processes", Proceedings of the Combustion Institute, 32 (2):2727-2742, 2009, doi: 10.1016/j.proci.2008.08.008.

6. NASA Glenn Research Center, "Ideal Otto Cycle", http://www.grc.nasa.gov/WWW/k-12/airplane/otto.html, October 20, 2011.

7. Stone, R., "Introduction to Internal Combustion Engines", 3rd Edition, Warrendale: SAE International, 1999.

8. McCallister, S., Chen, J-Y, and Fernandez-Pello, C., "Fundamentals of Combustion Processes", Berkeley, 2009.

9. Zhao, F., Lai, M-C., and Harrington, D.L., "Automotive spark-ignited direct-injection gasoline engines", Progress in Energy and Combustion Science, 25(5): 437-562, 1999, doi: 10.1016/S0360-1285(99)00004-0.

10. MIT, Unified Engineering Course, "Diesel Cycle", http://web.mit.edu/16.unified/www/SPRING/propulsion/notes/node26.html, October 20, 2011.

11. Schäfer, A., Heywood, J.B., Jacoby, H.D., and Waitz, I.A., "Transportation in a climate-constrained world", MIT Press, Cambridge, 2009.

12. Ford Motor Company, "Diesel Engine Aftertreatment: How Ford Knocks Out the NO_x", http://media.ford.com/images/10031/SD_Diesel_Aftertreatment.pdf, May 2011.

13. Sandia National Laboratory, "Engine Combustion Network", http://www.sandia.gov/ecn, June 2011.

14. Dec, J.E., and Yang, Y., "Boosted HCCI for High Power Output without Engine Knock and with Ultra-Low NOx Emissions – using Conventional Gasoline", SAE Paper 2010-01-1086, 2010, doi: 10.4271/2010-01-1086.

15. Dec., J.E., and Sjöberg, M., "Isolating the Effects of Fuel Chemistry on Combustion Phasing in an HCCI Engine and the Potential for Fuel Stratification for Ignition Control," SAE Paper 2004-01-0557, 2004, doi: 10.4271/2004-01-0557.

16. Yang, Y., Dec, J., Dronniou, N., and Simmons, B., "Characteristics of Isopentanol as a Fuel for HCCI Engines", SAE Paper 2010-01-2164, 2010, doi: 10.4271/2010-01-2164.

17. Saxena, S., Chen, J-Y, and Dibble, R., "Maximizing power output in an automotive scale multi-cylinder homogeneous charge compression ignition (HCCI) engine", SAE Paper 2011-01-0907, 2011, doi: 10.4271/2011-01-0907.

18. Bedoya, I.D., Saxena, S., Cadavid, F.J., and Dibble, R.W., “Exploring Strategies for Reducing High Inlet Temperature Requirements and Allowing Optimal Operating Conditions in a Biogas Fueled HCCI Engine for Power Generation”, ASME IC Engine Conference, Morgantown, WV, Oct. 2011, ICEF2011-60198.

19. Sjöberg, M., and Dec, J.E., Babajimopoulos, A., Assanis, D., “Comparing Enhanced Natural Thermal Stratification against Retarded Combustion Phasing for Smoothing of HCCI Heat-Release Rates,” SAE Paper 2004-01-2994, 2004, 10.4271/2004-01-2994.

20. Sjöberg, M., and Dec, J.E., “Ethanol Autoignition Characteristics and HCCI Performance for Wide Ranges of Engine Speed, Load and Boost,” SAE Paper 2010-01-0338, 2010, 10.4271/2010-01-0338.

21. Yang, Y., Dec, J., Dronniou, N., Sjöberg, M., and Cannella, W., “Partial Fuel Stratification to Control HCCI Heat Release Rates: Fuel Composition and Other Factors Affecting Pre-Ignition Reactions of Two-Stage Ignition Fuels”, SAE Paper 2011-01-1359, 2011, doi: 10.4271/2011-01-1359.

22. Kokjohn, S.L., Hanson, R.M., Splitter, D.A., and Reitz, R.D., “Fuel reactivity controlled compression ignition (RCCI): a pathway to controlled high-efficiency clean combustion”, International Journal of Engine Research, 12(3): 209-226, 2010, doi: 10.1177/1468087411401548.

23. Bedoya, I.D., Arrieta, A.A., and Cadavid, F.J., “Effects of mixing system and pilot fuel quality on diesel-biogas dual fuel engine performance”, Bioresource Technology, 100(24): 6624-6629, 2009, doi: 10.1016/j.biortech.2009.07.052

24. Yun, H., Kang, J-M., Chang, M-F., and Najt, P., “Improvement on Cylinder-to-Cylinder Variation Using a Cylinder Balancing Control Strategy in Gasoline HCCI Engines,” SAE Paper 2010-01-0848, 2010, doi: 10.4271/2010-01-0848.

25. Bedoya, I.D., Saxena, S., Cadavid, F.J., Dibble, R.W., and Wissink, M., “Experimental evaluation of strategies to increase the operation range of a biogas HCCI engine for power generation”, Applied Energy Journal (in press).

26. Bedoya, I.D., Saxena, S., Cadavid, F.J., and Dibble, R.W., “Numerical Analysis of the Effects of Biogas Composition in Combustion Parameters and Emissions in Biogas Fueled HCCI Engines for Power Generation”, ASME IC Engine Conference, Morgantown, WV, Oct. 2011, ICEF2011-60120.

27. Bedoya, I.D., Saxena, S., Cadavid, F.J., Dibble, R.W., and Wissink, M., “Experimental study of biogas combustion characteristics and emissions in a HCCI engine for power generation”, Energy Conversion and Management, 53(1): 154-162, 2011, doi: 10.1016/j.enconman.2011.08.016.

28. Lawler, B., Ortiz-Soto, E., Gupta, R., Peng, H., and Filipi, Z., “Hybrid electric vehicle powertrain and control strategy optimization to maximize the synergy with a gasoline HCCI engine”, SAE Paper 2011-01-0888, 2011, doi: 10.4271/2011-01-0888.

29. Delorme, A., Rousseau, A., Wallner, T., Ortiz-Soto, E., Babajimopoulos, A., Assanis, D., “Evaluation of Homogeneous Charge Compression Ignition (HCCI) Engine Fuel Savings for Various Electric Drive Powertrains”, The 25th World Battery, Hybrid and Fuel Cell Electric Vehicle Symposium & Exhibition, Shenzhen, China, Nov, 2010.

30. GE Transportation, “Hybrid Locomotive”, http://www.getransportation.com/rail/rail-products/locomotives/hybrid-locomotive.html, September 4, 2011.

31. Borman, G.L, and Ragland, K.W., “Combustion Engineering”, McGraw-Hill, 1998

32. Warnatz, J., Maas, U, and Dibble, R.W., “Combustion: Physical and Chemical Fundamentals, Modeling and Simulation, Experiments, Pollutant Formation”, 4th Edition, Springer, 2006.

33. Westbrook, C.K, Pitz, W.J., and Curran, H.J., “Auto-ignition and chemical kinetic mechanisms of HCCI combustion”, “HCCI and CAI engines for the automotive industry”, Chapter 17, Woodhead Publishing, Boca Raton, 2007, pp. 433-445.

34. Law, C.K., “Combustion Physics”, Cambridge University Press, New York, 2006, pp. 106-108.

35. Aceves, S.M., Flowers, D.L., Dibble, R.W., and Babajimopoulous, A., “Overview of modeling techniques and their application to HCCI/CAI engines”, “HCCI and CAI engines for the automotive industry”, Chapter 18, Woodhead Publishing, Boca Raton, 2007, pp. 456-474 .

36. Eng, J. A., “Characterization of Pressure Waves in HCCI Combustion”, SAE 2002-01-2859, 2002, doi: 10.4271/2002-01-2859.

37. Sjöberg, M., and Dec, J.E., “An Investigation of the Relationship between Measured Intake Temperature, BDC Temperature, and Combustion Phasing for Premixed and DI HCCI Engines,” SAE Paper 2004-01-1900, 2004, doi: 10.4271/2004-01-1900.

38. Sjöberg, M., and Dec, J.E., “Combined Effects of Fuel-type and Engine Speed on Intake Temperature Requirements and Completeness of Bulk-gas Reactions for HCCI Combustion,” SAE Paper 2003-01-3173, 2003, 10.4271/2003-01-3173.

39. Johansson, T., Johansson, B., Tunestål, P., and Aulin, H., “The Effect of Intake Temperature in a Turbocharged Multi Cylinder Engine operating in HCCI Mode”, SAE Paper 2009-24-0060, 2009, doi: 10.4271/2009-24-0060.

40. Haraldsson, G., Tunestål, P., Johansson, B., and Hyvönen, J., “Transient Control of a Multi Cylinder HCCI Engine During a Drive Cycle,” SAE Paper 2005-01-0153, 2005, doi: 10.4271/2005-01-0153.

41. Tanaka, S., Ayala, F., Keck, J.C., and Heywood, J.B., “Two-stage ignition in HCCI combustion and HCCI control by fuels and additives,” Combustion and Flame, 132 (1-2): 219-239, 2003, doi: 10.1016/S0010-2180(02)00457-1.

42. Silke, E.J, Pitz, W.J., Westbrook, C.K., Sjöberg, M., and Dec, J.E., “Understanding the Chemical Effects of Increased Boost Pressure under HCCI Conditions,” SAE Paper 2008-01-0019, 2008, doi: 10.4271/2008-01-0019.

43. Sjöberg, M., and Dec, J.E., “Comparing Late Cycle autoignition stability for single- and two-stage ignition fuels in HCCI engines,” Proceedings of the Combustion Institute, 31 (2): 2895-2902, 2007, doi: 10.1016/j.proci.2006.08.010

44. Christensen, M., Johansson, B., Amnéus, P., and Mauss, F., “Supercharged Homogeneous Charge Compression Ignition,” SAE Paper 980787, 1998, doi: 10.4271/980787.

45. Christensen, M. and Johansson, B., “Supercharged Homogeneous Charge Compression Ignition (HCCI) with Exhaust Gas Recirculation and Pilot Fuel,” SAE Paper 2000-01-1835, 2000, doi: 10.4271/2000-01-1835.

46. Olsson, J-O., Tunestål, P., Haroldsson, G., and Johansson, B., “A Turbo-Charged Duel Fuel HCCI Engine,” SAE Paper 2001-01-1896, 2001, doi: 10.4271/2001-01-1896.

47. Olsson, J-O, Tunestål, P, and Johansson, B., “Boosting for High Load HCCI,” SAE Paper 2004-01-0940, 2000, doi: 10.4271/2004-01-0940.

48. Au, M.Y, Girard, J.W., Dibble, R.W., Flowers, D., Aceves, S.M., Martinez-Frias, J., Smith, R, Seibel, C., and Maas, U., “1.9-Liter Four-Cylinder HCCI Engine Operation with Exhaust Gas Recirculation”, SAE Paper 2001-01-1894, 2001, doi: 10.4271/2001-01-1894.

49. Aceves, S.M., Flowers, D.L., Westbrook, C.K., Smith, J.R., Pitz, W, Dibble, R., Christensen, M. and Johansson, B., "A Multi-Zone Model for Prediction of HCCI Combustion and Emissions", SAE Paper 2000-01-0327, 2000, doi: 10.4271/2000-01-0327.

50. Aceves, S.M., Flowers, D.L., Martinez-Frias, J., Smith, J.R., Westbrook, C.K., Pitz, W. J., Dibble, R., Wright, J.F., Akinyemi, W.C., and Hessel, R.P., "A Sequential Fluid-Mechanic Chemical-Kinetic Model of Propane HCCI Combustion", SAE Paper 2001-01-1027, 2001, doi: 10.4271/2001-01-1027.

51. Bedoya, I.D., Saxena, S., Aceves, S., Flowers, D., Dibble, R., "A sequential Chemical Kinetics-CFD-Chemical Kinetics methodology to predict HCCI combustion and main emissions", SAE Paper 12PFL-0840, in review for 2012 SAE World Congress.

52. Dec, J.E., Yang, Y., Dronniou, N., "Boosted HCCI – Controlling Pressure-Rise Rates for Performance Improvements using Partial Fuel Stratification with Conventional Gasoline", SAE Paper 2011-01-0897, 2011, doi: 10.4271/2011-01-0897.

53. Yang, Y., Dec, J.E., Dronniou, N., Sjöberg, M., "Tailoring HCCI heat-release rates with partial fuel stratification: Comparison of two-stage and single-stage-ignition fuels", Proceedings of the Combustion Institute, 33(2):3047-3055, 2011, doi: 10.1016/j.proci.2010.06.114.

54. Hyvonen, J., Haraldsson, G., and Johansson, B., "Operating Range in a Multi Cylinder HCCI Engine Using Variable Compression Ratio," SAE Paper 2003-01-1829, 2003, doi: 10.4271/2003-01-1829.

55. Hyvönen, J., Haraldsson, G., and Johansson, B., "Balancing Cylinder-to-Cylinder Variations in a Multi-Cylinder VCR-HCCI Engine," SAE Paper 2004-01-1897, 2004, doi: 10.4271/2004-01-1897.

56. Martinez-Frias, J., Aceves, S.M., Flowers, D., and Smith, J.R., "HCCI Engine Control by Thermal Management," SAE Paper 2000-01-2869, 2000, doi: 10.4271/2000-01-2869.

57. Haraldsson, G., Tunestål, P., Johansson, B, and Hyvönen, J., "HCCI Combustion Phasing in a Multi Cylinder Engine Using Variable Compresion Ratio", SAE Paper 2002-01-2858, 2002, doi: 10.4271/2002-01-2858.

58. Yamaoka, S., Kakuya, H., Nakagawa, S., Okada, T., Shimada, A., and Kihara, Y., "HCCI Operation Control in a Multi-Cylinder Gasoline Engine," SAE Paper 2005-01-0120, 2005, doi: 10.4271/2005-01-0120.

59. Franz, J., Schwarz, F., Guenthner, M., Reissing, J., Mueller, A., and Donn, C., "Closed Loop Control of an HCCI Multi-Cylinder Engine and Corresponding Adaption Strategies," SAE Paper 2009-24-0079, 2009, doi: 10.4271/2009-24-0079.

60. Najt, P.M., and Foster, D.E., "Compression Ignited Homogeneous Charge Combustion", SAE Paper 830264, 1984, doi: 10.4271/830264.

61. Heywood, J.B., Internal Combustion Engine Fundamentals, McGraw-Hill, New York, 1988. pp. 930.

62. Kong, S.C., and Reitz, R.D., "Application of detailed chemistry and CFD for predicting direct injection HCCI engine combustion and emissions", Proceedings of the Combustion Institute, 29(1): 663-669, 2002, doi: 10.1016/S1540-7489(02)80085-2.

63. Kong, S.C., Marriott, C.D., Reitz, R.D., and Christensen, M., "Modeling and Experiments of HCCI Engine Combustion Using Detailed Chemical Kinetics with Multidimensional CFD", SAE Paper 2001-01-1026, 2001, doi: 10.4271/2001-01-1026.

64. Savitzky, A., and Golay, M.J.E, "Smoothing and differentiation by simplified least-squares procedures", Anal. Chem. 36(8): 1627-1639, 1964, doi: 10.1021/ac60214a047

65. Dec, J.E., and Hwang, W., “Characterizing the Development of Thermal Stratification in an HCCI Engine Using Planar-Imaging Thermometry”, SAE Paper 2009-01-0650, 2009, doi: 10.4271/2009-01-0650.

66. Snyder, J., Dronniou, N., Dec, J.E., and Hanson, R.K., “PLIF Measurements of Thermal Stratification in an HCCI Engine Under Fired Operation”, SAE Paper 2011-01-1291, 2011, doi: 10.4271/2011-01-1291.

67. Fric, T.F., “Effects of air-fuel unmixedness on NOx emissions”, Journal of Propulsion and Power, 9(5): 708-713, 1993.

68. Dec, J.E., Davisson, M.L., Sjöberg, M., Leif, R.N., and Hwang, W., “Detailed HCCI Exhaust Speciation and the Sources of Hydrocarbon and Oxygenated Hydrocarbon Emissions,” SAE Paper 2008-01-0053, 2008, doi: 10.4271/2008-01-0053.

69. Heywood, J.B., Internal Combustion Engine Fundamentals, McGraw-Hill, New York, 1988. pp. 251-254

70. Bogin, G.E., Mack, J.H., and Dibble, R.W., “Homogeneous Charge Compression Ignition (HCCI) Engine”, SAE Paper 2009-01-1805, 2009, doi: 10.4271/2009-01-1805.

71. Strandh, P., Christensen, M., Bengtsson, J., Johansson, R., Vressner, A., Tunestål, P, and Johansson, B., “Ion Current Sensing for HCCI Combustion Feedback”, SAE Paper 2003-01-3216, 2003, doi: 10.4271/2003-01-3216.

72. Mehresh, P., Souder, J., Flowers, D., Riedel, U, and Dibble, R.W., “Combustion Timing in HCCI engines determined by ion-sensor: experimental and kinetic modeling”, Proceedings of the Combustion Institute, 30(2): 2701-2709, 2005, doi:10.1016/j.proci.2004.08.135.

73. Tanaka, T., Narahara, K., Tabata, M., Yoshiyama, S., and Tomita, E., “Ion current measurement in a homogeneous charge compression ignition engine”, Int. Journal of Engine Research, 6: 453-463, 2005, doi: 10.1243/146808705X3041.

74. Larsson, M, Denbratt, I, and Koopmans, L., “Ion Current Sensing in an Optical HCCI Engine with Negative Valve Overlap”, SAE Paper 2007-01-0009, 2007, doi: 10.4271/2007-01-0009

75. Bogin, G., Chen, J-Y, and Dibble, R.W., “The effects of intake pressure, fuel concentration, and bias voltage on the detection of ions in a Homogeneous Charge Compression Ignition (HCCI) engine”, Proceedings of the Combustion Institute, 32(2): 2877-2884, 2009, doi: 10.1016/j.proci.2008.08.012.

76. Henein, N.A, Bryzik, W., Abdel-Rehim, A., and Gupta, A., “Characteristics of Ion Current Signals in Compression Ignition and Spark Ignition Engines”, SAE Paper 2010-01-0567, 2010, doi: 10.4271/2010-01-0567.

77. Giglio, V., Police, G., Rispoli, N., di Gaeta, A., Cecere, M., and Della Ragione, L., “Experimental Investigation on the Use of Ion Current on SI Engines for Knock Detection”, SAE Paper 2009-01-2745, 2009, doi: 10.4271/2009-01-2745.

78. Huang, Y., and Mehta, D., “Investigation of an In-Cylinder Ion Sensing Assisted HCCI Control Strategy”, SAE Paper 2005-01-0068, 2005, doi: 2005-01-0068.

79. Vressner, A., Strandh, P., Hultqvist, A., Tunestål, P, and Johansson, B., “Multiple Point Ion Current Diagnostics in an HCCI Engine”, SAE Paper 2004-01-0934, 2004, doi: 10.4271/2004-01-0934.

80. Daniels, C.F., Zhu, G.G., and Winkelman, J., “Inaudible Knock and Partial-Burn Detection Using In-Cylinder Ionization Signal”, SAE Paper 2003-01-3149, 2003, doi: 10.4271/2003-01-3149.

81. Yoshimura, K., Tokunaga, Y., Hashimoto, D., and Sakurai, H., “Knock and Misfire Detection using Ion Current Measurement for Ultra Lean Burn Medium Speed Gas Engine”, SAE Paper 2007-01-2078, 2007, doi: 10.4271/2007-01-2078.

82. Panousakis, D., Gazis, A., Paterson, J., Chen, R., Turner, J., Milovanovic, N., and Blundel, D., “Using Ion-current Sensing to Interpret Gasoline HCCI Combustion Processes”, SAE Paper 2006-01-0024, 2006, doi: 10.4271/2006-01-0024.

83. Panousakis, D., Gazis, A., Paterson, J., Chen, W-H, Chen, R., Turner, J., and Milovanovic, N., “Ion Current Signal Interpretation via Artificial Neural Networks for Gasoline HCCI Control”, SAE Paper 2006-01-1088, 2006, doi: 10.4271/2006-01-1088.

84. Aulin, H., Bentioulis, P., Tunestål, P, Hyvönen, J., and Johansson, B., “Improving Ion Current Feedback for HCCI Engine Control”, SAE Paper 2007-01-4053, 2007, doi: 10.4271/2007-01-4053.

85. Vressner, A., Hultqvist, A., Johansson, B. and Hasegawa, R., “Fuel Effects on Ion Current in an HCCI Engine”, SAE Paper 2005-01-2093, 2005, doi: 10.4271/2005-01-2093.

86. Saxena, S., Chen, J-Y, and Dibble, R.W., “Increasing the signal-to-noise ratio of sparkplug ion sensors through the addition of a potassium acetate fuel additive”, Proceedings of the Combustion Institute, 33(2): 3081-3088, 2011, doi: 10.1016/j.proci.2010.07.046.

87. Mehresh, P., Dibble, R.W., and Flowers, D., “EGR effect on Ion Signal in HCCI Engines”, SAE Paper 2005-01-2126, 2005, doi: 10.4271/2005-01-2126.

88. Jensen, D.E., and Jones, G.A., “Theoretical Aspects of Secondary Combustion in Rocket Exhausts”, Combustion and Flame, 41: 71-85, 1981, doi: 10.1016/0010-2180(81)90040-7.

89. Day, M.J., Stamp, D.V., Thompson, K., and Dixon-Lewis, G., “Inhibition of hydrogen-air and hydrogen-nitrous oxide flames by halogen compounds”, Proceedings of the Combustion Institute, 13(1): 705-712, 1971, doi: 10.1016/S0082-0784(71)80073-5.

90. Lide, D.R., “Ionization potentials of atoms and atomic ions” in “Handbook of Chem. And Phys.”, 1992, 10-211.

11 Appendix

11.1 List of Acronyms and Symbols

α	Scaling factor in ion ringing correlation
β	Scaling factor in ringing intensity correlation
ΔH_x	Enthalpy of formation of species x
γ	Ratio of specific heats, c_p/c_v
θ	Crank angle degree
θ_K	Activation temperature
ϕ	Fuel-air equivalence ratio
η_{th}	Thermal efficiency
η_{comb}	Combustion efficiency
$\eta_{ind,g}$	Gross indicated thermal efficiency
ABDC	After bottom dead center
AC	Alternating current
AFR	Air-fuel ratio
AFR_{stioch}	Stoichiometric air-fuel ratio
ATDC	After top dead center
BBDC	Before bottom dead center
BDC	Bottom dead center

BTDC	Before top dead center
c_p	Specific heat at constant pressure
c_v	Specific heat at constant volume
CAD	Crank angle degree
CAxx	Crank angle for xx% of total heat release, i.e. CA50 is the crank angle for 50% heat release
CFD	Computational fluid dynamics
CR	Compression ratio
DME	Dimethyl ether
E	Activation energy for a reaction
EGR	Exhaust gas recirculation
EVC	Exhaust valve close
EVO	Exhaust valve open
FTM	Fast thermal management
GND	Ground
HC	Hydrocarbons
HCCI	Homogeneous charge compression ignition
HR	Heat release
HRR	Heat release rate
IMEP	Indicated mean effective pressure

$IMEP_g$	Gross indicated mean effective pressure (considering only compression and power stroke)
ION50	50% of maximum ion current signal
Ion_{max}	Maximum ion current
IRR	Ion rise rate
ITHR	Intermediate temperature heat release
IVC	Intake valve close
IVO	Intake valve open
k_0	Pre-exponential factor in Arrhenius rate equation
K_p	Equilibrium constant
LHV	Lower heating value
LTC	Low temperature combustion
LTHR	Low temperature heat release
M	Molecular mass
m	Mass
m_{fuel}	Mass of fuel injected into cylinder
$m_{inducted}$	Mass of gas mixture inducted at the end of the intake stroke
MON	Motoring octane number
n_x	Number of moles of species x
NO_x	Nitric oxides, NO or NO_2

NTC	Negative temperature coefficient
NVO	Negative valve overlap
P	Pressure
P_{in}	Intake pressure into cylinder
P_{max}	Maximum in-cylinder pressure
PFS	Partial fuel stratification
PID	Proportional integral derivative
ppm	parts per million
PRFxx	Primary reference fuel, a mixture of iso-octane and n-heptane. i.e. PRF80 is 80% iso-octane, 20% n-heptane by volume
PV	Pressure-volume
PW	Pulsewidth
Q	Heat
Q_H	Heat addition
Q_L	Heat loss
R	Gas constant for a specific gas
r_c	Diesel cutoff ratio
R_u	Universal gas constant
RI	Ringing intensity
RON	Research octane number

RPM	Revolutions per minute
SCR	Selective catalytic reduction
SI	Spark-ignited
T	Temperature
t	Time
T_{in}	Intake temperature into cylinder
T_{max}	Maximum in-cylinder temperature
TDC	Top dead center
TDI	Turbocharged direct inject
TTL	Time to live
V	Volume
V_c	Clearance volume at TDC
V_d	Displaced volume
x_i	Mass fraction of species i